2-1-2001

Computational flow analysis of a dual chamber vortex generator for an absorption refrigeration system

Amilcar Ramos

Computational Flow Analysis of a Dual Chamber Vortex Generator for an Absorption Refrigeration System

By

Amílcar R. Arvelo Ramos

A Thesis Submitted in Partial Fulfillment of the Requirement for the Degree of

Master of Science in Mechanical Engineering

Approved by:

Dr. Ali Ogut Department of Mechanical Engineering.	Thesis Advisor
Dr. Amitabha Ghosh Department of Mechanical Engineering.	
Dr. P. Venkataraman Department of Mechanical Engineering.	
Dr. Edward Hensel Department Head of Mechanical Engineering.	

Department of Mechanical Engineering
College of Engineering
Rochester Institute of Technology
Rochester, New York 14623
February, 2001

PERMISSION TO REPRODUCE THE THESIS

Title of Thesis

Computational Flow Analysis of a Dual Chamber

Vortex Generator for an Absorption Refrigeration System

I, Amílcar R. Arvelo Ramos, hereby grant permission to the Wallace Memorial Library of Rochester Institute of Technology to reproduce my thesis in whole or in part. Any reproduction will not be for commercial use of profit.

February, 2002

DEDICATION

I would like to dedicate this work to my parents, Rafael Arvelo Medina and Aida Luz Ramos Arce, for all their love and understanding. For the education they gave me, and for giving me support and helping me in all my dreams to come true. Thank you for always being present besides through all the unforgettable years and encourage me to strive upwards.

Also, I would like to dedicate this work to my devoted wife Rebecca Ortiz for her assistance, patience and understanding.

ACKNOWLEDGMENTS

I would like to thank those people who provided assistance and support to me over the course of this project. First and foremost, I would like to thank my parents for giving me the moral support to make all this possible.

I would like to thank my cousin Gloribel Arvelo and her husband Robert Park for their availability in helping me while I was doing my Master of Science in Mechanical Engineering.

I would like to thank my thesis advisor, Dr. Ali Ogut, for his guidance and support of this thesis.

A special thanks to God, for giving me the strength to never give up and make possible my dream of getting a Master of Science degree in Mechanical Engineering.

ABSTRACT

A significant amount of low temperature (between 60°C and 99°C) heat is wasted annually in industrial processes. This wasted heat has the potential to drive absorption regrigeration systems with the penalty of lowering the COP (Coefficient of Performance) of the absorption regrigeration system. An absorption refrigeration system with a vortex generator, permits the use of low temperature waste heat as an energy source with improved generator capacity and COP. The vortex generator is a device that consists of two chambers (lower and upper chamber) and is used to separate the refrigerant from the absorbent in absorption refrigeration system by a cavitation process caused by the strong swirling flow within the chamber.

The scope of this project is to predict, by CFD analysis, the pressure drop toward the center of the chamber, and observe how the free surface area generated by the strong swirling flow is influenced by the inlet velocity and vortex chamber configuration. Also, based on the results of the investigation, determine the optimized design.

It can be concluded that the free surface area generated by the swirling flow increases when the inlet velocity increases and when the vortex chamber aspect ratio (diameter/height, D/H) decreases. Also, by placing the inlet of the vortex chamber at the mid-height of the vortex chamber will increase the size of the free surface area. The free surface area can be optimized when the vortex chamber dimensions are D = 16.12 cm , H = 16.12 cm (aspect ratio = 1), with inlet placed at the mid-height of the chamber. For optimum results, the inlet velocity of the solution should be 30 m/sec.

TABLE OF CONTENTS

LIST OF FIGURES

LIST OF TABLES

LIST OF SYMBOLS

A	Cross sectional area, area
A_x, A_y, A_z	Area of the fractional open area in each direction
AR	Aspect Ratio
D	Diameter
F	Fraction of fluid
$\vec{F}$	Force vector
f	Friction factor
F_B	Body force
F_c	Centrifugal force
F_s	Surface force
g	Gravity
H	Vortex Chamber height
K	Turbulent kinetic energy
Kc	Contraction coefficient
Kn	Nozzle coefficient
L	Pipe length
M	Mass
m	Mass flow rate
P	Pressure
q	Instantaneous value of flow variable
q'	Fluctuating componen of flow variable

$\bar{q}$	Mean component of flow variable
R, r	Radius
Re	Reynolds number
S	Modulus of mean rate of strain tensor
t	Time
t	Solution temperature
t'	Refrigerant temperature
u, v, w	Velocity component in a Cartesian system
V	Linear velocity
V_F	Fractional volume open to flow (open volume/volume of cell)
V_θ	Tangential velocity
X	Mass fraction
x, y , z	Cartesian coordinates

Greek Letters

α_k	Inverse Prandlt number for turbulent kinetic energy
α_ε	Inverse Prandlt number for turbulent kinetic energy dissipation rate
ε	Turbulent kinetic energy dissipation rate
Γ	Circulation
ρ	Density
ω	Angular velocity
μ	Absolute Viscosity
σ	Axial stress
τ	Shear stress

CHAPTER

ONE

INTRODUCTION

1.1 PROJECT BACKGROUND

Waste heat from industrial processes and power plants is widely accepted as a practical energy source for absorption heat pumps (Dorgan, 1995). Heat sources from approximately 99°C and above have proven to be practical. However, a significant amount of thermal resources in the range of 211 - 528 trillion kJ (200 and trillion 500 BTU's) per year in the form of low temperature (between 60 and 99°C) is known to be wasted (Fineblum, 1996). Figure 1.1 below shows the amount of energy source available for a wide range of temperatures. Figure 1.1 shows that 60% of the heat energy in the temperature range of interest is available in hot liquids rather than in gas. This is an advantage because liquid sources require smaller and less expensive heat exchangers. Conventional absorption refrigeration systems can use a heat source with lower temperature (temperatures below 99 °C) in the generator but with the penalty of lowering both the COP (Coefficient Of Performance) and generator capacity (Fineblum, 1996).

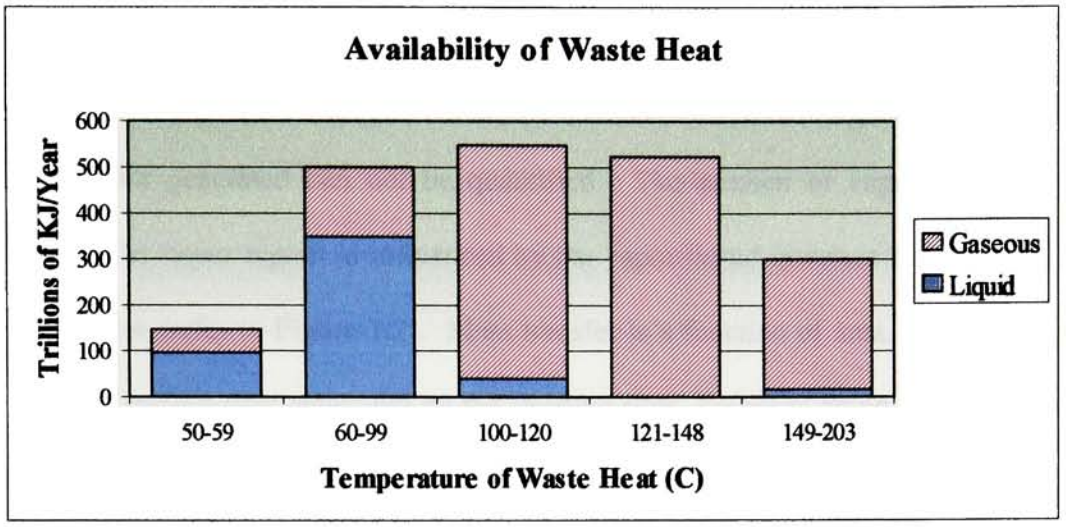

Figure 1.1. Availability of Waste Heat for a range of temperatures

An absorption refrigeration system (shown in Figure 1.4) that incorporates the dual vortex chamber generator (shown in Figure 1.3) permits generators to operate efficiently with lower temperature waste heat as an energy source with improved capacity and COP. For a description of a typical absorption refrigeration system and a dual vortex chamber generator, refer to section 1.4 and 1.3 respectively.

1.2 PROJECT OBJECTIVES AND GOALS

The purpose of this investigation is to determine how the vapor-liquid interface area generated by the strong swirling flow is influenced by the LiBr - Water refrigerant rich solution inlet velocity, and the dimensions of the vortex chamber. It is desirable to obtain an amount of

10% by mass of the refrigerant-rich solution entering the vortex chamber in vapor phase. Due to limitations in the Computational Fluid Dynamics software use, FLOW-3D, the amount of vapor generated can not be quantified. The amount of vapor generated and transferred to the vapor region is influenced by the vapor-liquid interface area generated by the swirling flow (refer to Figure 1.2). Mass transfer is a function of area. This means that the greater the surface area generated by the swirling flow, higher is going to be the amount of vapor generated and transferred to the vapor region. Also it is intended to predict the velocity and pressure distribution of the solution in the vortex chamber.

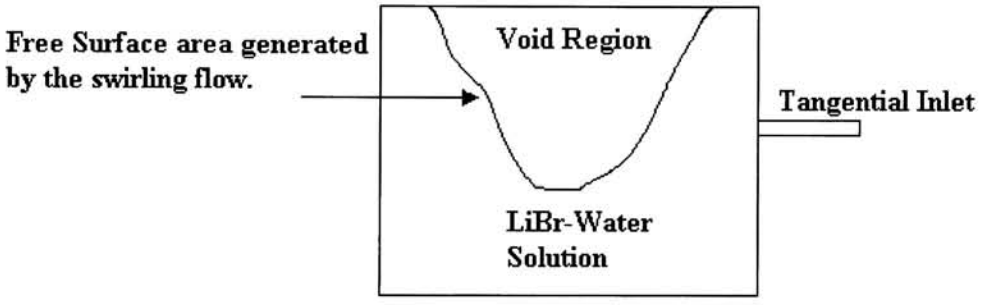

Figure 1.2 Free Surface area generated by the high tangential inlet velocity.

To prove this, FLOW-3D, Computational Fluid Dynamics (CFD) software was used. Different cases of the lower chamber vortex generator with different configurations (aspect ratios and inlet locations) and inlet velocities were studied. Simulations were run by changing one of the parameters and keeping the rest of the parameters constant with purpose of determining its effect and obtaining an optimized design.

The work involves determining conditions for separation of the refrigerant vapor from the refrigerant-rich solution. Also, verify the pressure gradient at the lower chamber. From the results of the investigation, it is hoped that there will be enough data to determine how the replacement of a conventional generator by a dual chamber vortex generator may affect the efficiency of the process and what will be the limiting factors.

1.3 DESCRIPTION OF THE DUAL VORTEX CHAMBER GENERATOR

The schematic of the vortex generator is shown in Figure 1.3. The vortex generator consists of two chambers, lower chamber and upper chamber. The lower chamber is a cylinder with a tangential inlet, a tangential outlet at the bottom of the chamber and a central outlet at the top of the chamber that connects with the upper chamber. The upper chamber has a central inlet at the bottom part and a tangential outlet at the top part. The heated refrigerant rich solution (LiBr- H_2O, fluid fraction 60% - 40% by weight of solution) enters the lower chamber tangentially at conditions close to the saturation pressure. Due to conservation of rotational momentum, the pressure is reduced toward the central portion of the lower chamber. Close to the free surface boundary, the pressure will drop below the saturation pressure of the LiBr-water solution. This will cause cavitation and as a result, the heated refrigerant-rich solution gives up some of the refrigerant as vapor.

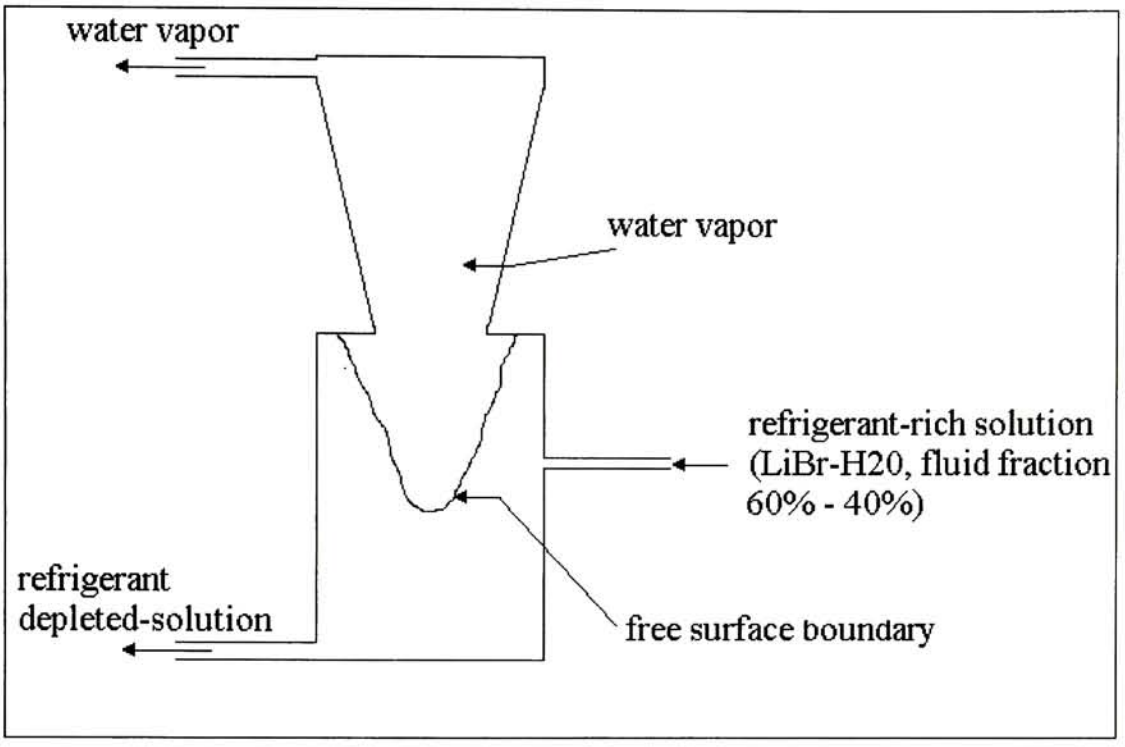

Figure 1.3. Schematic of the Vortex Chamber generator.

The refrigerant vapor will flow out of the swirling mixture toward the center and upward. The vapor will then flow through the central outlet and out of the lower chamber into the upper chamber. The upper chamber is designed as a diffuser with gradually increasing cross-sectional area. There, the swirling vapor is tangentially decelerated as a result of rotational momentum and the vapor pressure will increase prior to leaving through the tangential outlet. The deceleration of flow in the upper chamber is essentially similar to what occurs in the diffuser of a compressor (Fineblum, 1996). The refrigerant-depleted solution in the lower chamber flows outward through the bottom outlet and is conveyed to the absorber.

It is intended to replace the conventional generator in the Absorption Refrigeration Cycles by the Vortex Chamber generator. The goal of the Vortex Chamber is to obtain 10% by weight of the incoming solution in refrigerant vapor. The vortex chamber utilize the energy of the incoming LiBr-water solution to convert some of the refrigerant into water vapor. Therefore, it will required less energy from an external source to generate the same amount of vapor than in conventional generators.

1.4 ABSORPTION REFRIGERATION CYCLE

In the typical Lithium Bromide – Water absorption refrigeration cycle, as shown in figure 1.4, the refrigerant is the water and the absorbent is Lithium Bromide. The machine consists of four components that exchange energy with surroundings, one internal heat exchanger, two flow restrictors, and a pump. The four components that exchange energy with the surroundings are the condenser, generator, evaporator and absorber. The machine operates between two working pressures, the high pressure side (typically 6 KPa) and the low pressure side (typically 1 KPa). The high-pressure side is at the generator and condenser, and the low-pressure side is at the absorber and evaporator. The pressure is determined by the vapor pressure of the characteristics of the working fluids. In a 60% - 40 % Lithium Bromide – Water solution entering the condenser, the vapor pressure of the solution is 5.8 KPa. This means that the pressure at the high pressure side is 5.8 KPa.

In a typical Lithium Bromide - Water Absorption Refrigeration Cycle (see figure 1.4 for reference), the refrigerant-absorbent solution is pressurized by a pump and conveyed to the

generator through an internal heat exchanger. In the generator the refrigerant and absorbent are partially separated. Separation in conventional generators is possible when heat is supplied by a heat source. For a typical aqueous lithium bromide machine, the

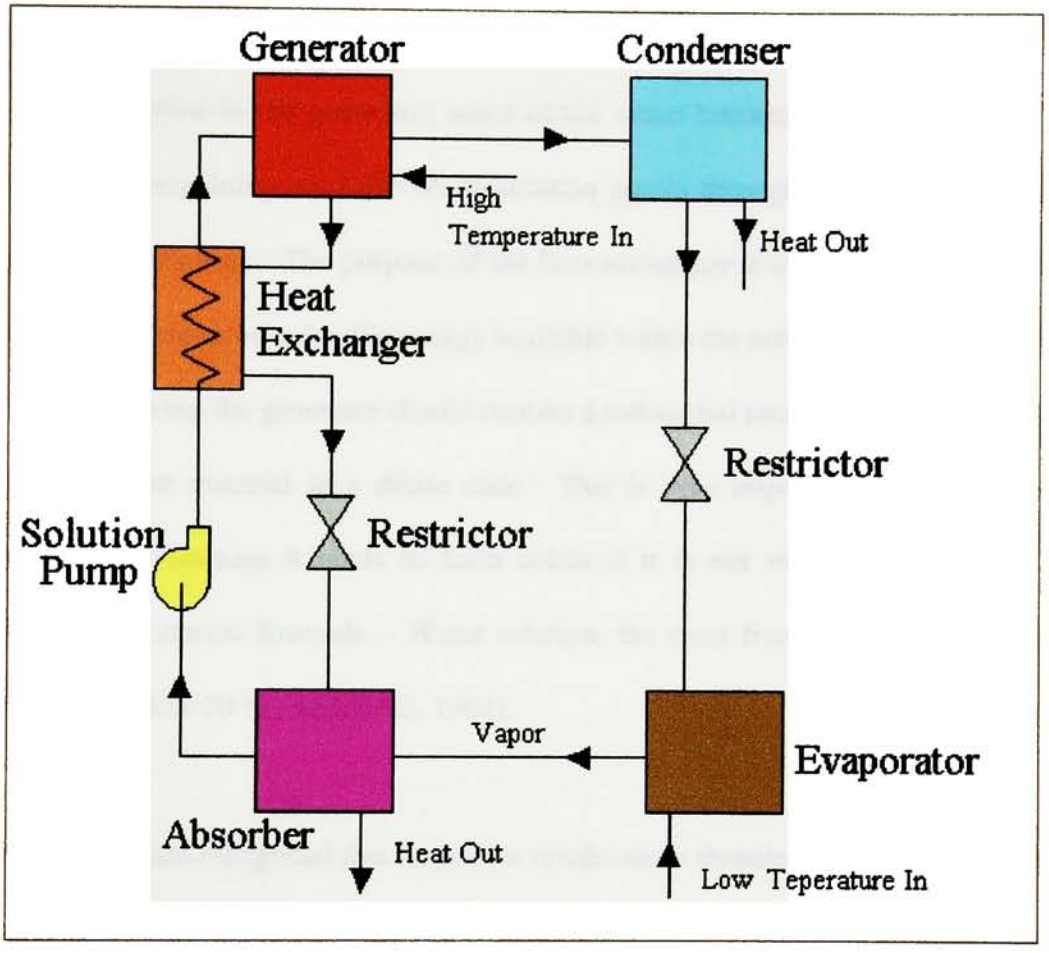

Figure 1.4. Typical Absorption Refrigeration System.

generator heat must be supplied above a temperature of approximately 90 °C (Herold, 1996). The increase in temperature in the generator converts some of the refrigerant into water vapor. It is expected that some Lithium Bromide salt molecules may escape from the liquid surface and be present in the vapor. However, the escaping tendency is so small under the

conditions encountered in an absorption machine that the vapor above the liquid solution is essentially pure water vapor. This fact can be appreciated more fully by realizing that the boiling point of solid lithium bromide is 1282 °C. (Herold, 1996).

When heat is applied in the generator, some of the water becomes vapor and flows to the condenser. The remaining hot LiBr-Water solution passes through a heat exchanger and is conveyed to the absorber. The purpose of the heat exchanger is to reduce the external heat applied at the generator by using the energy available within the solution. The hot refrigerant weak solution leaving the generator should contain a substantial amount of refrigerant to keep the pure absorbent material in a dilute state. This is very important if the absorbent is Lithium Bromide because it tends to form solids if it is not well dissolved. To avoid solidification of Lithium Bromide – Water solution, the mass fraction of Lithium Bromide should be kept below 70 % (ASHRAE, 1994).

The subcooled liquid refrigerant that leaves the condenser is throttled through the restrictor to the low pressure side and then conveyed into the evaporator, where it is evaporated at low temperature and pressure with heat of the cooled space. The low pressure refrigerant vapor at the evaporator is conveyed into the absorber while still at low pressure. In the absorber, the refrigerant vapor is absorbed by the refrigerant weak solution coming from the generator. The absorption takes place because of the high affinity between the absorbent and the refrigerant molecules. Thermal energy is released during the absorption process.

When the Vortex Chamber incorporates to the absorption refrigeration cycle, the system will remain the same. The only difference is that the generator in conventional Lithium Bromide – Water absorption refrigeration system will be replaced by the dual vortex chamber. With the replacement of the conventional generator by the vortex chamber, some of the vapor will be generated due to cavitation. A strong swirling flow will create a pressure drop toward the center of the chamber. At some point, the pressure will drop below the saturation pressure of the solution and will cause cavitation. To achieve the desirable vapor amount of 10% by weight of the incoming solution with an incorporated vortex chamber, an external heat source might be needed. But the amount of heat source needed with the vortex chamber will be less than the amount of heat source needed for conventional generators to achieve the same results. This will make the vortex chamber generator more efficient than conventional generators.

1.5 VORTEX FLOW THEORY

Flow in a curved or circular path is common in nature. A vortex is a streamline in a fluid that induces a circular motion in the surrounding fluid. Consider the flow between two concentric streamlines at an infinitesimal distance apart, as shown in the figure 1.5 below.

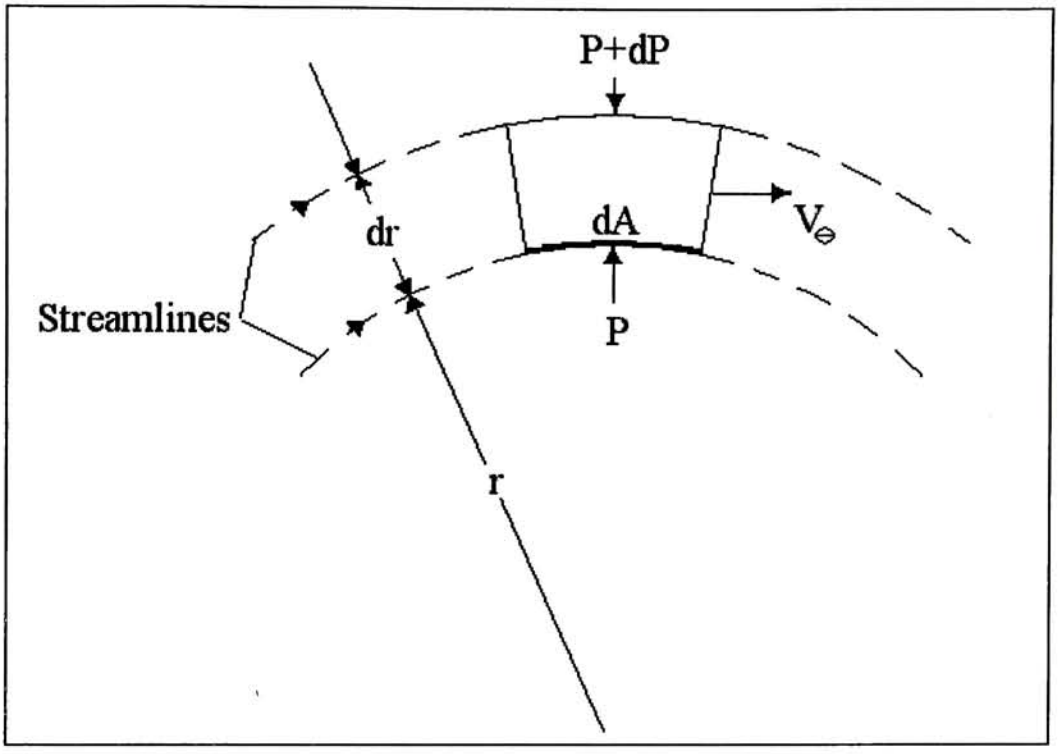

Figure 1.5. Flow in a curved path.

The radius of curvature of the path is r, and the tangential linear velocity is V_θ. The infinitesimal element is of height dr, and the average area along the curved surface is dA. The mass for this element will be

$$dm = \rho \cdot dr \cdot dA \tag{1.1}$$

The radial acceleration is defined as V_θ^2/r. The centrifugal force acting on the element has the magnitude of

$$Fc = \rho \cdot dr \cdot dA \cdot (V_\theta^2/r) \tag{1.2}$$

The pressure varies from P to P + dP as the radius varies from r to r + dr. The centrifugal force on the fluid element is just balanced by the resultant force due to the pressures over the surfaces. A force balance in the radial direction gives

$$dP = \rho(V_0^2/r) \cdot dr \tag{1.3}$$

Equation 1.3 indicates that the pressure increases with radius in curved flow and there is a fall in pressure toward the center of curvature or center of the vortex chamber by an amount of $\rho(V_0^2/r) \cdot dr$. The pressure gradient will be $dP/dr = \rho(V_0^2/r)$. The equation 1.3 above is a simplified equation of the Euler's equation and is only applicable for situations of steady state and inviscid flows. LiBr-Water solution is a very viscuos fluid. Therefore, the use of this equation to calculate the pressure drop toward the center in the vortex chamber will not give accurate results. The CFD code being used to simulate the behavior of the LiBr-Water solution inside the vortex chamber includes the effects of shear stress.

Two different types of idealized vortex flows exist. These are the forced vortex and the free vortex. A forced vortex is a line that induces a flow in the surrounding fluid, which moves in cocentric circles about the vortex core and in which the fluid tangential velocity (V_θ) increases linearly with radius. Figure 1.6 below illustrates a forced vortex flow.

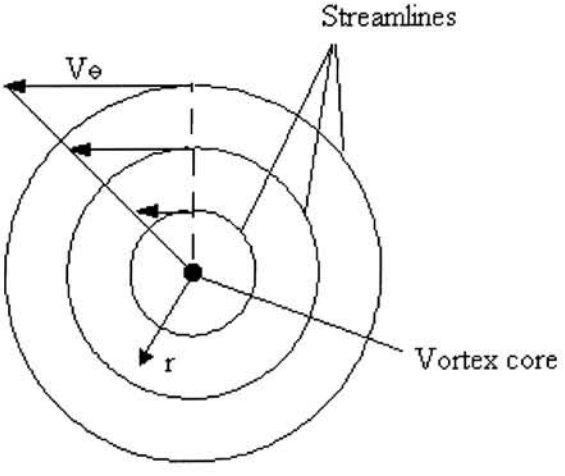

Figure 1.6. Force vortex flow.

The vortex core is perpendicular to the paper, and the fluid tangential velocity is

$$V_\theta = \omega * r \tag{1.4}$$

where ω is the fluid angular velocity and r is the radius.

The second type of vortex flow is the free vortex. A free vortex is a line that induces a flow in the surrounding fluid, which moves in cocentric circles about the vortex core and in which the fluid velocity decreases inversely with radius. Figure 1.7 illustrates a free vortex flow.

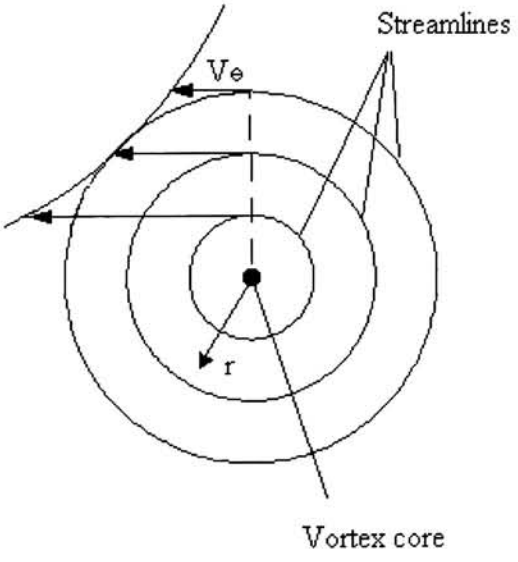

Figure 1.7. Free vortex flow.

The vortex core is perpendicular to the paper, and the fluid velocity is

$$V_\theta = \frac{\Gamma}{2\pi r} \tag{1.5}$$

where Γ is a constant that is called the circulation. If a circular path is selected with the vortex core at its center, we may determine the circulation for both vortex flows. For a forced vortex flow, the circulation depends on the path chose through r and is expressed as

$$\Gamma = \int_0^{2\pi} \omega * r(r * d\theta) = 2\pi\omega r^2 \tag{1.6}$$

For a free vortex flow the circulation is constant for any path and can be expressed as

$$\Gamma = \int_0^{2\pi} \frac{\Gamma}{2\pi r}(r * d\theta) = 2\pi\frac{\Gamma}{2\pi} = \Gamma \tag{1.7}$$

In many applications where a fluid is injected tangentially into a chamber, the vortex flow formed is a combination of a forced vortex and a free vortex flow. This is common in situations where the fluid is viscous and can not be approximated as an ideal flow. When the fluid viscosity is considerable high, as in the case of the LiBr-water solution, the non slip condition at the wall of the chamber should be met. Therefore, the velocity of the fluid at the wall is zero m/sec. Figure 1.8 shows pressure and velocity distributions of a typical vortex flow. As shown in this figure, the flow is a forced vortex flow at the center portion of the chamber and once the radius passes a critical point, the flow becomes a free vortex.

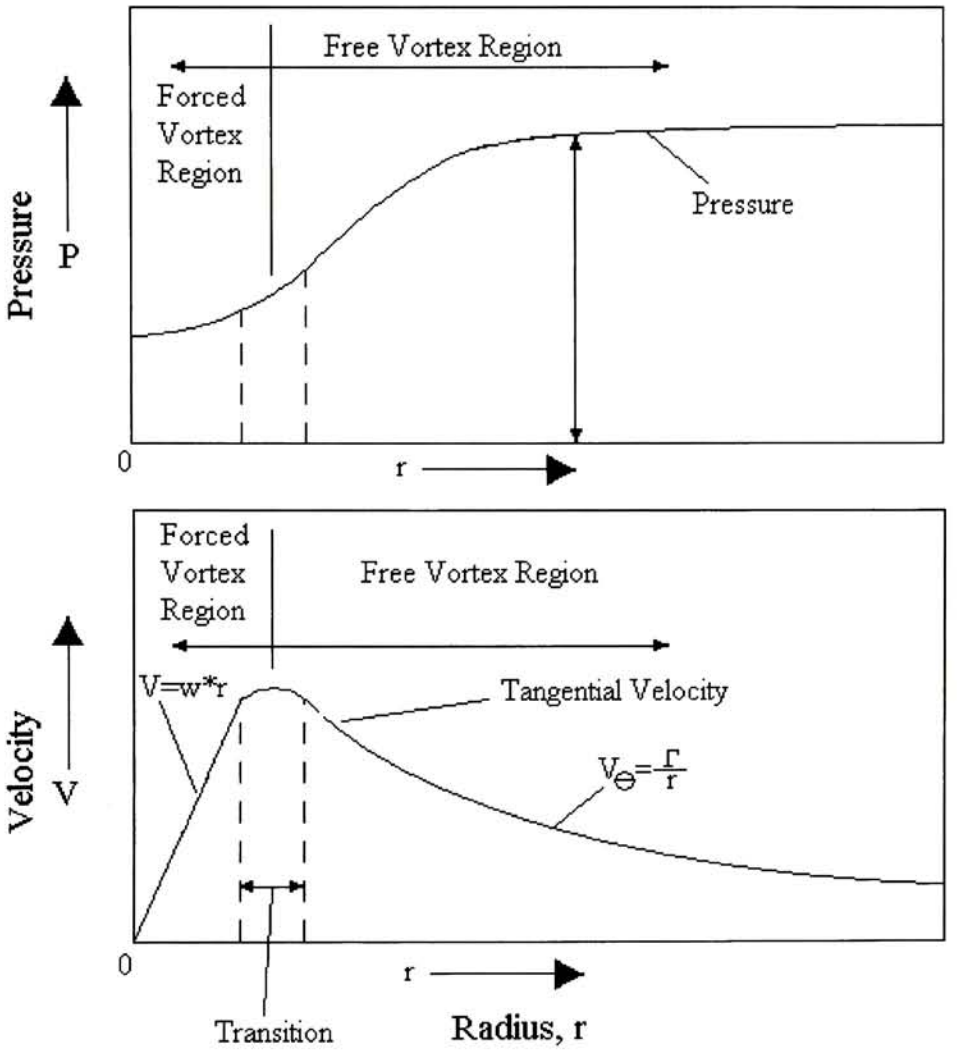

Figure 1.8. Pressure and velocity distribution in a typical vortex flow application.

In the vortex chamber, a forced vortex flow and a free vortex flow are present. In the vortex chamber the velocity increases with radius up to a critical radius. This critical radius is located very close to the vortex chamber wall. This is the forced vortex flow region. From the critical radius up to the wall, the flow is a free vortex flow. This is the free vortex flow region.

To create a vortex flow in the vortex chamber, the inlet needs to be place tangentially to the vortex chamber wall. The characteristic of the inlet velocity of the incoming fluid and the geometry of the chamber creates a strong vortical (swirling) flow field. The commonly accepted tangential inlet velocity working range to assure a strong vortex flow is from 16 – 30 m/sec (Granger, 1978).

CHAPTER

TWO

FLUID FLOW THEORY

2.1 THE MASS CONSERVATION EQUATION

Consider a control volume of infinitesimal dimensions as shown in Figure 2.1.

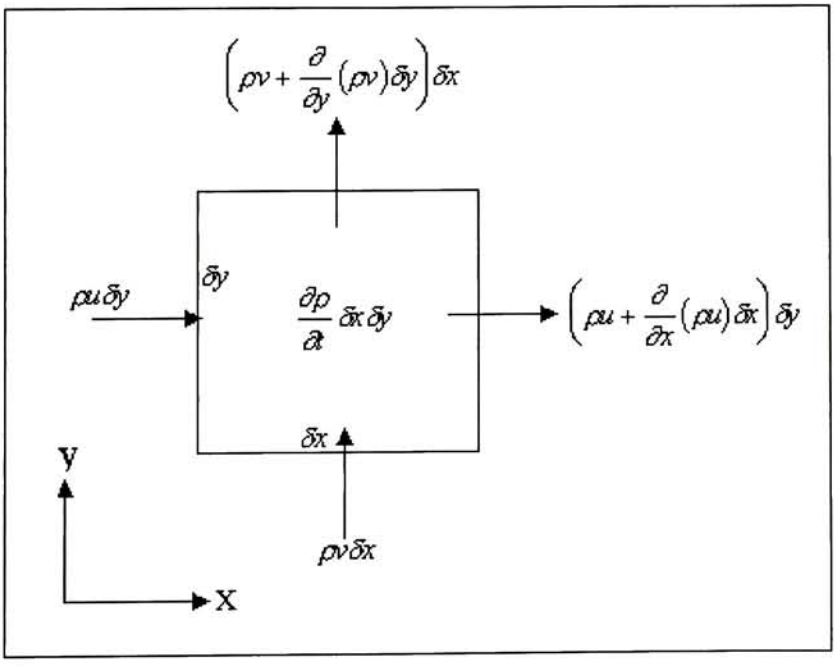

Figure 2.1. Differential element for mass balance.

A mass balance will now be made over the control volume. The application of the principle of conservation of mass yields

$$\frac{\partial}{\partial x}(\rho u)+\frac{\partial}{\partial y}(\rho v)+\frac{\partial \rho}{\partial t}=0 \tag{2.1}$$

which is the continuity equation for a two-dimensional unsteady flow in rectangular coordinates. The corresponding three-dimensional unsteady flow equation can be written as follows

$$\frac{\partial}{\partial x}(\rho u)+\frac{\partial}{\partial y}(\rho v)+\frac{\partial}{\partial z}(\rho w)+\frac{\partial \rho}{\partial t}=0 \tag{2.2}$$

Once steady state is achieved, the last term in the equation above is eliminated and if the fluid is incompressible, like the LiBr-Water solution, equation 2.2 reduce to

$$\frac{\partial}{\partial x}(u)+\frac{\partial}{\partial y}(v)+\frac{\partial}{\partial z}(w)=0 \tag{2.3}$$

When the vortex chamber starts to operate, the fluid is unsteady until a nice parabolic shape is established in the void region and is stabilized. The void region is established due the high tangential velocities. In the period of time where the void region is not stabilized, the unsteady continuity equation should be used. Once steady state is achieved, equation 2.3 can be used. However, Flow-3D is a transient code and always uses the unsteady continuity and momentum equations equation in its algorithm.

FLOW-3D also makes a small change in the continuity equation. It incorporates in the equation terms that accounts for fractional area and fractional volume area open to flow. This is applied in situations where the cell is partially filled. These terms are also added in

the momentum equations. The momentum equation, modified with the extra terms added by FLOW-3D for incompressible flows and with no mass source becomes

$$\frac{1}{V_F}\frac{\partial \rho}{\partial t} + \frac{\partial}{\partial x}(u \cdot A_x) + \frac{\partial}{\partial y}(v \cdot A_y) + \frac{\partial}{\partial z}(w \cdot A_y) = 0 \tag{2.4}$$

where, the velocity components (u, v, w) are in the coordinate directions (x, y, z). A_x is the fractional area open to flow in the x direction, and A_y and A_z are similar area fractions for flow in the y and z directions, respectively. V_F is the fractional volume open to flow. The fractional area and the fractional volume open to flow is applied in cases where the cell is partially filled. This apply in the free surface region. A pictorical representation of the fractional areas and fractional volume open to flow is shown in Figure 2.3.

2.2 THE MOMENTUM EQUATIONS

The equations of motion for real fluid, which are based on Newton's second law, permit the determination of the way the velocity varies with position. It will then be possible to find quantities such as the pressure in laminar flow. The equations, with certain modifications, can also be used for turbulent flows. For an infinitesimal system of mass dm moving in a velocity field, Newton's second law can be written

$$d\vec{F} = dm\frac{D\vec{V}}{Dt} = dm\left[u\frac{\partial \vec{V}}{\partial x} + v\frac{\partial \vec{V}}{\partial y} + w\frac{\partial \vec{V}}{\partial z} + \frac{\partial \vec{V}}{\partial t}\right] \tag{2.5}$$

There are two types of forces acting on a fluid element; body forces and surface forces. Surface forces include both normal and shear forces.

Considering the stresses that act in the x direction and making reference to Figure 2.2, to obtain the net surface force in the x direction, dF_{Sx}, we must sum the forces in the x direction.

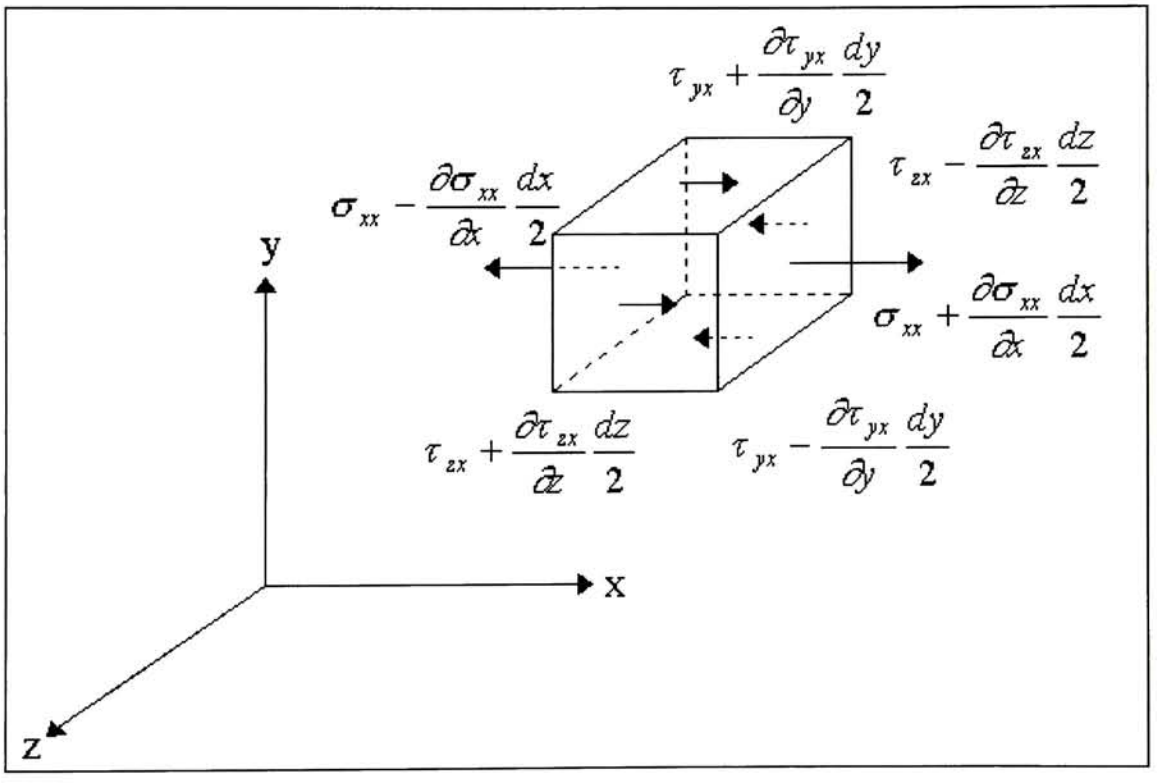

Figure 2.2. Stresses acting on a rectangular fluid particle.

The results, including the body forces, yields to

$$dF_x = dF_{S_x} + dF_{B_x} = \left(\rho g_x + \frac{\partial \sigma_{xx}}{\partial x} + \frac{\partial \tau_{yx}}{\partial y} + \frac{\partial \tau_{zx}}{\partial z} \right) dxdydz \tag{2.6}$$

Similar expressions for the force components in the y and z directions can be obtained following this procedure.

Once the expressions for the components (dF_x, dF_y, dF_z) of the force, $d\vec{F}$, acting on the element of mass dm are obtained, the force components are substitute in equation 2.5 to obtain the differential equations of motion. For the x direction result will be

$$\rho g_x + \frac{\partial \sigma_{xx}}{\partial x} + \frac{\partial \tau_{yx}}{\partial y} + \frac{\partial \tau_{zx}}{\partial z} = \rho\left(u\frac{\partial u}{\partial x} + v\frac{\partial u}{\partial y} + w\frac{\partial u}{\partial z} + \frac{\partial u}{\partial t}\right) \tag{2.7}$$

Similar results are obtain for y and z directions. To get the equations of motion called Navier-Stokes equations, the stresses may be expressed in terms of velocity gradients and fluid properties.

$$\tau_{xy} = \tau_{yx} = \mu\left(\frac{\partial v}{\partial x} + \frac{\partial u}{\partial y}\right) \tag{2.8}$$

$$\tau_{yz} = \tau_{zy} = \mu\left(\frac{\partial w}{\partial y} + \frac{\partial v}{\partial z}\right) \tag{2.9}$$

$$\tau_{xz} = \tau_{zx} = \mu\left(\frac{\partial u}{\partial z} + \frac{\partial w}{\partial x}\right) \tag{2.10}$$

$$\sigma_{xx} = -p - \frac{2}{3}\mu\nabla\cdot\vec{V} + 2\mu\frac{\partial u}{\partial x} \tag{2.11}$$

$$\sigma_{yy} = -p - \frac{2}{3}\mu\nabla\cdot\vec{V} + 2\mu\frac{\partial v}{\partial y} \tag{2.12}$$

$$\sigma_{zz} = -p - \frac{2}{3}\mu\nabla\cdot\vec{V} + 2\mu\frac{\partial w}{\partial z} \tag{2.13}$$

Combining equations 2.7 with equations 2.8 – 2.13 results in the Navier-Stokes equation for the x direction.

$$\rho\frac{Du}{Dt}=-\frac{\partial p}{\partial x}+\frac{\partial}{\partial x}\left[\mu\left(2\frac{\partial u}{\partial x}-\frac{2}{3}\nabla\cdot\vec{V}\right)\right]+\frac{\partial}{\partial x}\left[\mu\left(\frac{\partial v}{\partial x}+\frac{\partial u}{\partial y}\right)\right]+\frac{\partial}{\partial z}\left[\mu\left(\frac{\partial u}{\partial z}+\frac{\partial w}{\partial x}\right)\right] \tag{2.14}$$

Similarly, the Navier-Stokes equations for the y and z directions and assuming gravity is present only in the z direction yields to

$$\rho\frac{Dv}{Dt}=-\frac{\partial p}{\partial y}+\frac{\partial}{\partial x}\left[\mu\left(\frac{\partial v}{\partial x}+\frac{\partial u}{\partial y}\right)\right]+\frac{\partial}{\partial y}\left[\mu\left(2\frac{\partial v}{\partial y}-\frac{2}{3}\nabla\cdot\vec{V}\right)\right]+\frac{\partial}{\partial z}\left[\mu\left(\frac{\partial v}{\partial z}+\frac{\partial w}{\partial y}\right)\right] \tag{2.15}$$

$$\rho\frac{Dw}{Dt}=\rho g_z-\frac{\partial p}{\partial z}+\frac{\partial}{\partial x}\left[\mu\left(\frac{\partial w}{\partial x}+\frac{\partial u}{\partial z}\right)\right]+\frac{\partial}{\partial y}\left[\mu\left(\frac{\partial v}{\partial z}+\frac{\partial w}{\partial y}\right)\right]+\frac{\partial}{\partial z}\left[\mu\left(2\frac{\partial w}{\partial z}-\frac{2}{3}\nabla\cdot\vec{V}\right)\right] \tag{2.16}$$

These equations are non-linear, there are more dependent variables than governing equations, and no general method of solution exist. The only method to solve them is by CFD analysis.

With the addition of fractional area open are open to flow, the momentum equations are represented by FLOW-3D as follows

$$\frac{\partial u}{\partial t}+\frac{1}{V_F}\left\{uA_x\frac{\partial u}{\partial x}+vA_y\frac{\partial u}{\partial y}+wA_z\frac{\partial u}{\partial z}\right\}=-\frac{1}{\rho}\frac{\partial p}{\partial x}+G_x+f_x \tag{2.17}$$

$$\frac{\partial v}{\partial t}+\frac{1}{V_F}\left\{uA_x\frac{\partial v}{\partial x}+vA_y\frac{\partial v}{\partial y}+wA_z\frac{\partial v}{\partial z}\right\}=-\frac{1}{\rho}\frac{\partial p}{\partial y}+G_y+f_y \tag{2.18}$$

$$\frac{\partial w}{\partial t}+\frac{1}{V_F}\left\{uA_x\frac{\partial w}{\partial x}+vA_y\frac{\partial w}{\partial y}+wA_z\frac{\partial w}{\partial z}\right\}=-\frac{1}{\rho}\frac{\partial p}{\partial z}+G_z+f_z \tag{2.19}$$

In these equations, (G_x, G_y, G_z) are body accelerations and (f_x, f_y, f_z) are viscous accelerations. The vicous accelerations are also functions of the fractional areas and volume open to flow. They can be expressed as follows

$$\rho V_F f_x = wsx - \left\{ \frac{\partial}{\partial x}\left(A_x \tau_{xx}\right) + \frac{\partial}{\partial y}\left(A_y \tau_{xy}\right) + \frac{\partial}{\partial z}\left(A_z \tau_{xz}\right) \right\} \tag{2.20}$$

$$\rho V_F f_y = wsy - \left\{ \frac{\partial}{\partial x}\left(A_x \tau_{xy}\right) + \frac{\partial}{\partial y}\left(A_y \tau_{yy}\right) + \frac{\partial}{\partial z}\left(A_z \tau_{yz}\right) \right\} \tag{2.21}$$

$$\rho V_F f_z = wsz - \left\{ \frac{\partial}{\partial x}\left(A_x \tau_{xz}\right) + \frac{\partial}{\partial y}\left(A_y \tau_{yz}\right) + \frac{\partial}{\partial z}\left(A_z \tau_{zz}\right) \right\} \tag{2.22}$$

In the above expressions the terms wsx, wsy and wsz are wall shear stresses. The fractional areas (A_x, A_y, A_z) and the volume open to flow (V_F) are applied in the cells that are partially filled.

2.3 TURBULENT FLOW

The majority of flows are turbulent in nature. The turbulence model to be used is the Renormalization Group (RNG) k-ε model. This model belongs to the k-ε family of models. It falls in the category of "two-equation" turbulence models based on an isotropic eddy-viscosity concept. The major differences between the RNG and the standard k-ε models, stemming from the fact that the RNG model was derived using more rigorous statistical technique, with model constants that are derived "analytically". The RNG model

has an additional term in its ε equation that significantly improves the accuracy for rapidly strained flows. Also the effect of swirl on turbulence is included in the RNG model, which enhance the accuracy of swirling flows. Unlike the standard k-ε model that is based on Reynolds averaging, the RNG-based k-ε turbulence model is derived from the instantaneous Navier-Stokes equations, using rigorous mathematical technique called Renormalization Group (RNG) Methods(Fluent, 1996).

In Flow-3D, the following two transport equations are used in the RNG turbulent model

$$\frac{\partial k}{\partial t}+\frac{1}{V_F}\left(u\cdot A_x\frac{\partial k}{\partial x}+v\cdot A_y\frac{\partial k}{\partial y}+w\cdot A_z\frac{\partial k}{\partial z}\right)=\frac{1}{V_F}\{\frac{\partial}{\partial x}(a_k\frac{\mu_{eff}}{\rho}A_x\frac{\partial k}{\partial x})+\frac{\partial}{\partial y}(a_k\frac{\mu_{eff}}{\rho}A_y\frac{\partial k}{\partial y})+\frac{\partial}{\partial z}(a_k\frac{\mu_{eff}}{\rho}A_z\frac{\partial k}{\partial z})\}+C_\mu\frac{k^2}{\varepsilon}S^2-\rho \qquad (2.23)$$

and

$$\frac{\partial \varepsilon}{\partial t}+\frac{1}{V_F}\left(u\cdot A_x\frac{\partial \varepsilon}{\partial x}+v\cdot A_y\frac{\partial \varepsilon}{\partial y}+w\cdot A_z\frac{\partial \varepsilon}{\partial z}\right)=\frac{1}{V_F}\{\frac{\partial}{\partial x}(a_\varepsilon\frac{\mu_{eff}}{\rho}A_x\frac{\partial \varepsilon}{\partial x})+\frac{\partial}{\partial y}(a_\varepsilon\frac{\mu_{eff}}{\rho}A_y\frac{\partial \varepsilon}{\partial y})+\frac{\partial}{\partial z}(a_\varepsilon\frac{\mu_{eff}}{\rho}A_z\frac{\partial \varepsilon}{\partial z})\}+C_{1\varepsilon}\cdot C_\mu\cdot k\cdot S^2-C_{2\varepsilon}\frac{\varepsilon^2}{k}-R \qquad (2.24)$$

where $a_k$and $a_\varepsilon$are the inverse Prandtl numbers for k and ε. μ_{eff} is the effective viscosity. S is the modulus of the mean rate-of-strain tensor and R in the ε equation is given by

$$R=\frac{C\mu\rho\eta^3(1-\eta/\eta_o)}{1+\beta\eta^3}\frac{\varepsilon^2}{k} \qquad (2.25)$$

where $\eta = Sk/\varepsilon$, $\eta_o = 4.38$, $\beta = .012$, $C\mu = .0845$, $C_{1\varepsilon} = 1.42$ and $C_{2\varepsilon} = 1.68$.

2.4 FREE SURFACE THEORY

In the vortex chamber, the high tangential velocities will generate a vortex flow. This will create a void region in the central portion of the chamber. To simulate the interface between the void region and the Lithium Bromide - Water solution, it is necessary to turn on the free surface model.

An interface between a gas and liquid is often referred to as a free surface. The reason for the "free" designation arises from the large difference in the densities of the gas and liquid. A low gas density means that that inertia can generally be ignored compared to that of the liquid. The only influence of the gas is the pressure it exerts on the liquid surface. Free surfaces require the introduction of special methods to define their location, their movement and their influence on a flow. Regardless the method employed, there are three essential features needed to model free surfaces (Flow-3D, 1999):

1. A scheme is needed to describe the shape and location of a surface,
2. An algorithm is required to evolve the shape and location with time, and
3. Free-surface boundary conditions must be applied at the surface.

Flow-3D uses the Volume-of-Fluid (VOF) method to track the free surface. The idea for this approach originated as a way to have the powerful volume-tracking feature of the Marker-and-Cell (MAC) method without its large memory and CPU cost.

If the amount of fluid in each cell is known, it is possible to locate surfaces and determine the slopes and surface curvatures. Surfaces are easy to locate because they lie in cells partially filled with fluid or between cells full of fluid and cells that have no fluid. Slopes and curvatures are computed by using the fluid volume fraction in neighboring cells. The essential element in this process is to remember that the volume should be a step function, example, having a value of either one or zero. Knowing this, the volume fractions in neighboring cells can then be used to locate the position of fluid within a particular cell.

Free surface boundary condition must be applied as in the MAC method. Finally, to compute the time evolution of surfaces, a technique is needed to move volume fractions through a grid in such a way that the step-function nature of the distribution is retained. The basic kinematic equation for fluid fractions is similar to that for the height-function method, where F is the fraction of fluid function.

$$\frac{\partial F}{\partial t}+\frac{\partial F}{\partial x}+\frac{\partial F}{\partial y}+\frac{\partial F}{\partial z}=0 \tag{2.26}$$

The vortex chamber as shown in Figure 1.2 presents a free surface in the region between the Lithium Bromide-Water solution and the water vapor. The region occupied by the water vapor is known as the void region. For the simulation of the lower chamber, the software does not solve the dynamics of the gas in the void region. Instead, it treats them as regions of uniform pressure. This pressure is used as a boundary condition on the Lithium Bromide - Water / water vapor interface. Since in this case, the void region is adjacent to a pressure boundary (the top of the lower chamber), the pressure in the void region is going to be the same as in the boundary.

In Flow-3D, the fluid configurations at the void region volumes and interfacial area are defined in terms of a volume of fluid (VOF) function of F(x,y,z,t). This function represents the volume of Lithium Bromide - Water per unit volume and satisfies the equation

$$\frac{\partial F}{\partial t}+\frac{1}{V_F}\left[\frac{\partial}{\partial x}\left(F\cdot A_x\cdot u\right)+\frac{\partial}{\partial y}\left(F\cdot A_y\cdot v\right)+\frac{\partial}{\partial z}\left(F\cdot A_z\cdot w\right)\right]=FDIF \tag{2.27}$$

where

$$FDIF=\frac{1}{V_F}\left[\frac{\partial}{\partial x}\left(\nu_F\cdot A_x\cdot\frac{\partial F}{\partial x}\right)+\frac{\partial}{\partial y}\left(\nu_F\cdot A_y\cdot\frac{\partial F}{\partial y}\right)+\frac{\partial}{\partial z}\left(\nu_F\cdot A_z\cdot\frac{\partial F}{\partial z}\right)\right] \tag{2.28}$$

In this equation:

V_F = the fractional volume open to flow

= open volume / volume of cell

A_x, A_y, A_z = area of the fractional open area in each direction

Refer to the figure below for better understanding

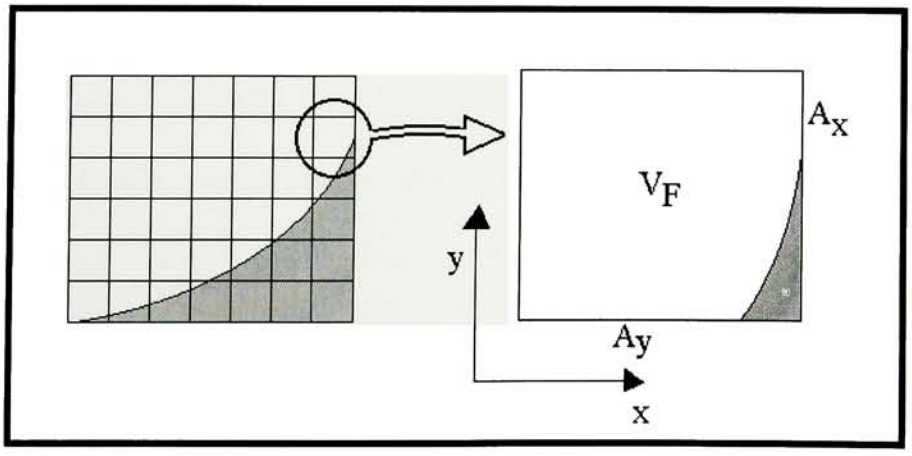

Figure 2.3. Partially filled cell.

The diffusion coefficient is defined as $\nu_F = C_F \mu/\rho$. Where C_F is a constant whose reciprocal is referred to as a turbulent Schmidt number.

The interpretation of F depends on the type of problem being solved. F has values between 0 and 1. If no LiBr –Water solution is in the cell, F = 0. If the cell is completely filled with LiBr – Water, then F = 1.

CHAPTER

THREE

Computational Fluid Dynamics Analysis

3.1 CFD Code Introduction

The Computational Fluid Dynamics (CFD) software package FLOW-3D was used for flow analysis. This code is a tool for the investigation of the dynamic behavior of liquid and gases. Because the software is based on the fundamental laws of mass, momentum and energy conservation, it is capable of simulating a wide variety of fluid flows. The specialty of this package is the simulation of free surface flows. FLOW-3D is a transient CFD code. This means that the program has been constructed in such a way that the problems are solved in a time dependent manner. Steady state results are computed as the limit of a time transient (FLOW-3D, 1996). Steady state is achieved when the mean kinetic energy and the volume of fluid does not change with time.

FLOW-3D differs from the other CFD programs in several ways. It uses a fixed (Eulerian) grid of rectangular control elements because these are simpler to generate, increase the accuracy in the results, requires less memory and simple numerical approximations. A

special technique called FAVOR (Fractional-Area-Volume-Obstacle-Representation) method is used to define general geometric regions within the rectangular grid. This method has a great advantage over grid methods that deforms their elements to fit geometry. The biggest advantage is that geometry and grids are completely independent of one to another. This feature is called Free Gridding, and it eliminates the tedious task of generating body fitted or finite-elements grids. FAVOR method uses partial control volumes to give users the advantages of a body-fitted grid but retains the construction simplicity of an ordinary rectangular grid.

Another feature that differs FLOW-3D from other CFD codes is the Volume of Fluid (VOF) technique. This is the preferred feature for many applications that involve free surface boundaries. The VOF method consists of three elements: a volume of fluid function for defining surfaces, a special advection method that maintains a sharp definition of surfaces as they move and deform within a computational grid, and the application of normal and tangential stress boundary conditions at the surfaces. The VOF method also allows for the breakup and coalescence of fluid surfaces.

Finally, relaxation and convergence parameters that are needed in all Computational Fluid Dynamics programs, are determined by FLOW 3D as it is running. This allows the program to maintain solution accuracy.

3.2 MODEL GENERATION

Any problem on CFD simulation requires a mathematical model formulation in order to be run. A mathematical model consists of the boundary conditions, initial conditions and the governing equations.

The purpose of the CFD simulation of the vortex chamber is to study the behavior of the fluid dynamics (pressure gradients and velocity vectors) of the LiBr-Water solution within the chamber. In this thesis, a model will be generated for the lower chamber and only the incompressible region of it will be study. The incompressible region of the lower chamber is the region occupied by the LiBr-Water solution. Parameters of inlet velocity and aspect ratio (chamber diameter / chamber height) will be modify in the model to obtain the optimized design.

3.3 INITIAL CONDITIONS

Initially the lower chamber is partially filled. The chamber has one tangential inlet and two outlets. One of the outlets is at the center of the top wall of the lower chamber and connects the lower chamber with the upper chamber. The other outlet is a tangential outlet located at the bottom of chamber. Refrigerant-rich solution enters the chamber through the tangential inlet, the depleted solution leaves the chamber through the tangential outlet and vapor leaves the chamber through the outlet at the center of upper boundary. Since no

evaporation takes place in the vortex chamber, all the incoming solution exits the vortex chamber through the bottom outlet.

At the inlet, the composition of the solution is 60% LiBr and 40% water and the solution temperature is 80°C. With these conditions, the saturation vapor pressure of the refrigerant (vapor) and the refrigerant temperature can be determine. The vapor saturation pressure for these conditions is 5.8 KPa. This is a typical value in the high-pressure shell of absorption refrigeration cycles. These parameters can be determined by using Equilibrium Chart for Aqueous Lithium Bromide Solution from ASHRAE (Appendix D). Also can be determined by using the following formulas (ASHRAE, 1993):

$$t = \sum_0^2 B_n X^n + t' \sum_0^2 A_n X^n \tag{3.1}$$

$$t' = \left(t - \sum_0^2 B_n X^n\right) / \left(\sum_0^2 A_n X^n\right) \tag{3.2}$$

$$LogP = C + D / (t'+459.72) + E / (t'+459.72)^2 \tag{3.3}$$

$$t' = \frac{-2E}{D + \left[D^2 - 4E(C - \log P)\right]^{.5}} - 459.72 \tag{3.4}$$

where:

$A_0 = -2.00755$	$B_0 = 321.128$	$C = 6.21147$
$A_1 = 0.16976$	$B_1 = -19.332$	$D = -2886.373$

A_2 = -3.133336 E-3 B_2 = 0.374382 E = -337269.46

A_3 = 1.97668 E-5 B_2 = -2.0637 E-3

t' = Refrigerant temperature, °C Range: 0< t' < 230°F

t = Solution temperature, °C Range: 40 < t < 350°F

X = Percent of LiBr, % Range: 45 < X < 70%

P = vapor saturation pressure, psia

Also from the initial conditions, the properties of the solution such as density and dynamic viscosity can be determined by using ASHRAE charts (Appendix E and F).

For the inlet conditions of the solution, the saturation pressure of the refrigerant is 5.8 KPa. The pressure at the inlet should be very close to saturation pressure. For this reason the pressure of the liquid portion of the partially filed chamber was set to 6 KPa.

Also to reduce computing time in the simulation, an initial tangential velocity was applied to the solution within the vortex chamber. The initial tangential velocity was set to increase linearly in the radial direction with a maximum velocity at the wall of the vortex chamber. At the wall it was set to have a velocity equal to the inlet velocity.

3.4 MODEL MESHING AND BOUNDARY CONDITIONS

3.4.1 Meshing

Due to the geometry of the chamber, cylindrical coordinates seems to be the best coordinate system for meshing. But in Computational Fluid Dynamics analysis, cylindrical coordinates are used only for axisymmetric or annular domain calculations. The Vortex Chamber generator is not axisymmetric. Therefore, rectangular coordinates are going to be used for the meshing. Also, at the inlet of the chamber, the results of the simulation will not be good if cylindrical coordinates are used. This is because at the inlet, the diameter is very small and it will be very difficult to capture the details in this area with a cylindrical mesh. The rectangular mesh in the inlet section is going to be very dense to capture the behavior of the fluid dynamics in that section.

3.4.2 Boundary Conditions

Two different types of boundary conditions were used in the model (velocity and pressure boundaries). A velocity boundary condition was set at the inlet of the vortex chamber. A pressure boundary was set to the bottom outlet of the vortex chamber. Also a pressure boundary was used at the void region of the vortex chamber.

Figure 3.1 below, shows the symbols used for each boundary conditions.

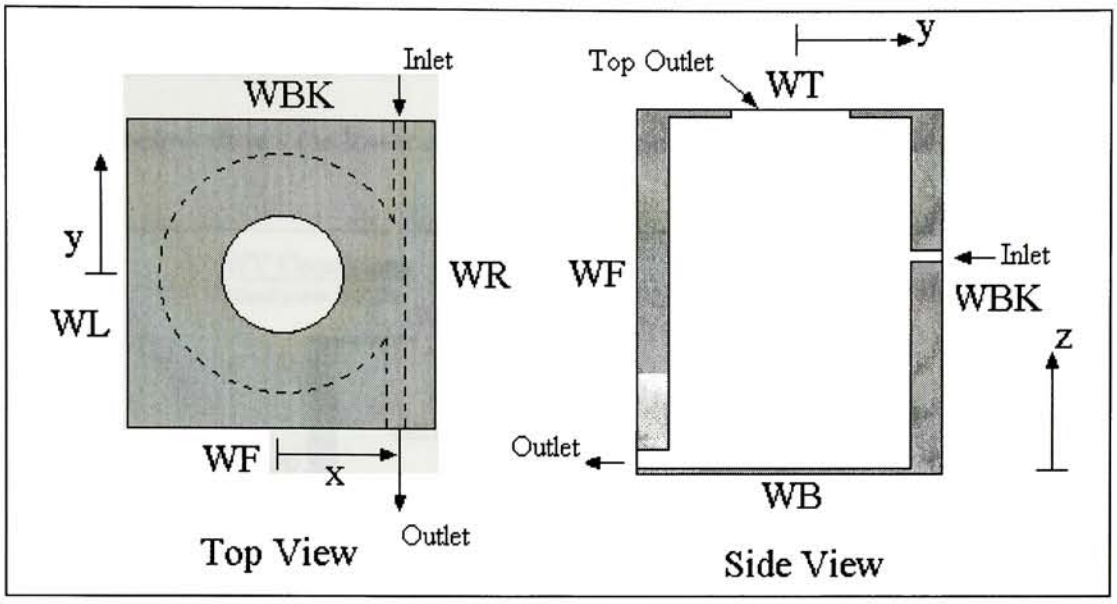

Figure 3.1. Vortex Chamber schematic with boundary conditions symbols.

Where:

WB = boundary condition type at minimum z side (bottom) of mesh.

WBK = boundary condition type at maximum y side (back) of mesh.

WF = boundary condition type at minimum y side (front) of mesh.

WL = boundary condition type at minimum x side (left) of mesh.

WR = boundary condition type at maximum x side (right) of mesh.

WT = boundary condition type at maximum z side (top) of mesh.

The boundaries at the left (WL), right (WR) and bottom (WB) are treated as rigid walls. No fluid flow across these boundaries. The back boundary (WBK) is where the Lithium-Bromide/Water solution enters the chamber. This is a constant velocity boundary

because the fluid enters the chamber at a specified velocity. The inlet velocities of the solution to the chamber are 15, 20 and 30 m/sec. The top (WT) and front (WF) boundaries are pressure boundaries and were set to a pressure of 5 KPa and 4.5 KPa respectively. The figure below shows the lower chamber schematic with the boundary conditions.

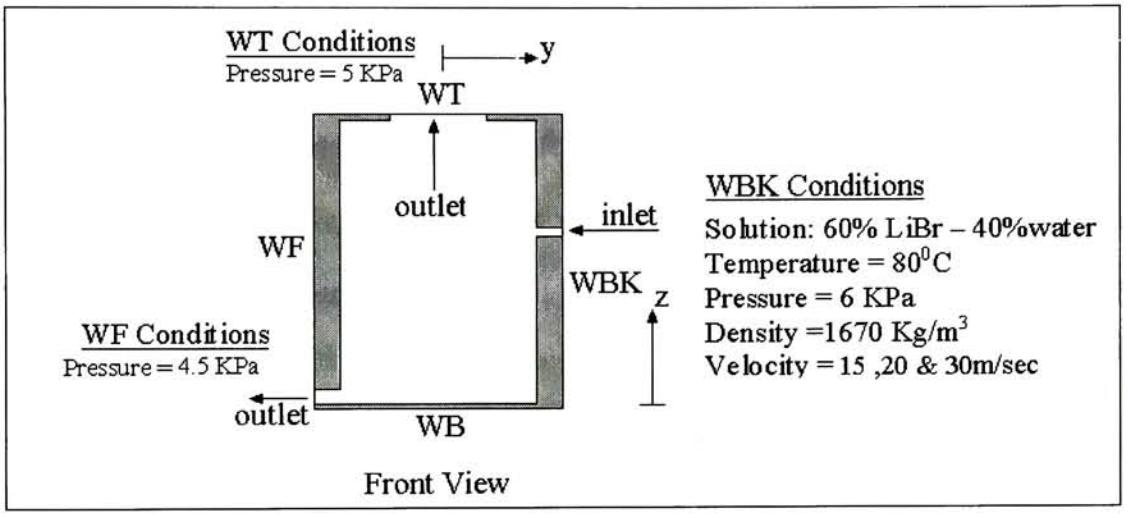

Figure 3.2. Lower Chamber Schematic with boundary conditions.

3.5 MODEL STUDY

Different Vortex Chamber configurations and inlet velocities were studied. Parameters such as the vortex chamber aspect ratio (diameter/height), inlet location and inlet velocities where changed in the model. The purpose of this was to determine how the vapor-liquid interface area is influenced by these parameters. It also will help to determine the optimized vortex chamber design. Also the void pressure was changed in the model to determine the effect of it.

In the model studied, the LiBr-Water was treated as an incompressible fluid and a turbulent flow model was activated. This was determined by calculating the Reynolds number at the inlet of the chamber. Since the Reynolds number at the inlet is significantly high, a turbulent model should be run. The turbulent model used was the RNG model. The RNG model is the best turbulent model to simulate swirling flows (Fluent, 1996). Also because the vortex chamber is partially filled, a free surface model had to be activated. The purpose of the free surface model is to activate an auxiliary equation that helps to define the free surface shape accurately.

In the vortex chamber, when the LiBr-water solution pressure drops below its saturation pressure, water becomes vapor. The phenomena of liquid to gas phase change due to pressure drop is called cavitation. FLOW-3D does not has an evaporation model, therefore when cavitation occurs, the software interprets that as a void region that opens up in the fluid. In reality what should happen is convert the water portion of the solution in vapor. To model this situation an evaporation model is required.

The model studied was started with a partially filled chamber. The purpose of this is to save time in the simulation process. An initial tangential velocity was given to the solution in the vortex chamber. The tangential velocity was set to increase linearly with radius. Also, the initial pressure of the solution in the vortex chamber was set to 6 KPa.

The model studied was solved using an implicit scheme (ADI). The reason of selecting implicit scheme and not explicit scheme is because of the bad aspect ratio of the mesh. In the inlet region, a fine mesh had to be used to model the small inlet. At the chamber, a coarser mesh is used. This makes small cells adjacent to bigger cells. When sudden change in cell size is present, implicit algorithm is a better solver. Also, because the problem is unstable by nature, an implicit scheme is needed to solve it accurately.

All the cases where run until steady state was achieved. Flow 3D is a transient code and steady state solution is achieved when the mean kinetic energy and the volume of solution in the chamber remain constant.

3.6 MODEL PARAMETERS

In the model, several parameters where fixed, and several where changed. The parameters that where changed are aspect ratio (diameter/height), inlet velocity and inlet location. The purpose of changing the parameters is to predict the optimized design to the vortex chamber.

The inlet velocity was set to 15, 20 and 30 m/sec. In order to achieve a strong swirling flow and enough pressure reduction toward the center of the chamber to generate water vapor, the inlet velocity should be 15 m/sec or higher. The higher the inlet velocity is, more pressure reduction toward the center is obtained.

The vortex chamber was modeled for different aspect ratios (diameter/height). The vortex chamber aspect ratios selected for modeling where 1, 1.5 and 2. The diameter and height of the vortex chamber for each aspect ratio were set in such a way that the vortex chamber volume remains the same for all the aspect ratios. The vortex chamber volume was set to be 1297 cm^3. Also the inlet location was changed in the model to determine its effect in the surface area. The inlet was placed in two different locations; the top and the mid-height of the vortex chamber.

Among the fixed parameters in the model are the pressure at the void region and the pressure at the bottom and top outlets. The high-pressure side on an absorption refrigeration typically range between 6 and 10 KPa and is determined by the mass fraction of the LiBr-Water solution. For a 60-40% LiBr–Water solution the saturation vapor pressure is 5.8 KPa. Therefore, the pressure in the vortex chamber has to be less than 5.8 KPa to generate water vapor. A void pressure of 5 KPa was selected for the void region. This pressure was selected by assuming a pressure in the high pressure side of the system of 6 KPa and a pressure recovery in the upper chamber of 1 KPa.

The pressure at the bottom outlet of the chamber was selected to be 4.5 KPa. This pressure was set to a pressure below the void pressure to ensure that the chamber does not fill up completely. There is no analytical mean to calculate the pressure at this boundary. But even if the boundary pressure of 4.5 KPa is not the correct one, the outlet pipe is long enough and this pressure boundary will not affect the results in the chamber.

3.7 CASES STUDIED

A total of 14 model variations where studied to determine the optimized vortex chamber design base on the size of the vapor-liquid interface area. The bigger the free surface area , the better the design. The study was focused in finding the optimized design in a particular range of dimensions, inlet locations, and inlet velocity.

Three different aspect ratios where considered for analysis purposes. Where aspect ratio is defined as

$$AR = D/H \tag{3.5}$$

Where

D = chamber diameter

H = chamber height

The three different aspect ratios considered were 1, 1.5 and 2. The dimensions of the chamber for the three different aspect ratios were selected in such a way that the total volume of the chamber remains the same. For each chamber with different aspect ratio, also the inlet location and the inlet velocity were changed. The purpose of this was to determine the effect of the inlet location and inlet velocity in the surface area. Finally, two simulations with the same mass flow rate but with different inlet velocity where studied to determine if it is more important to have a high inlet velocity or a higher mass flow rate to generate the free surface area. The table below shows a list of the cases studied.

Case	Aspect Ratio	Diameter (cm)	Height (cm)	Inlet Location	Inlet Vel. (m/s)	Mass Flow Rate (g/sec)
1	1	16.12	16.12	Center	30	910
2	1	16.12	16.12	Center	20	607
3	1	16.12	16.12	Center	15	455
4	1.5	18.44	12.29	Top	20	607
5	1.5	18.44	12.29	Center	30	910
6	1.5	18.44	12.29	Center	20	607
7	1.5	18.44	12.29	Center	15	455
8	2	20.32	10.16	Top	30	910
9	2	20.32	10.16	Center	30	910
10	2	20.32	10.16	Top	20	607
11	2	20.32	10.16	Center	20	607
12	2	20.32	10.16	Center	15	455
13	1.5	18.44	12.29	Center	20	607
14	1.5	18.44	12.29	Center	20	607

Case 13. Void Pressure = 15KPa

Case 14. Higher Mass flow rate (910 g/sec @ 20m/sec)

Table 3.1. List of the cases studied.

3.8 VORTEX REYNOLDS NUMBER

The importance of the Reynolds Number is that is going to determine if the flow is turbulent or laminar. If the Reynolds Number is higher than 4000, then the flow in the chamber is turbulent (Gerhart 1992).

The Reynolds Number is calculated at the inlet of the chamber and is defined as

$$\Re e = \frac{\rho * V * D}{\mu} \tag{3.6}$$

where

ρ = density of the solution

V = Inlet velocity of the solution

D = Inlet diameter

μ = Absolute viscosity of the solution

For a 60-40% LiBr-H_2O solution, the density ρ = 1670 Kg/m^3 and the absolute viscosity is μ = .0029 Kg/m-sec.

The inlet diameter is D = .191 in or 0.485 cm and is fixed.

To establish a good swirling flow, the inlet velocity has to be in the range of 16 to 30 m/sec. For a 16 m/sec inlet the velocity, the Reynolds Number is,

$$\Re e = \frac{\left(1670 Kg / m^3\right) \cdot \left(16 m / \sec\right) \cdot \left(.00485 m\right)}{\left(.0029 Pa - \sec\right)} = 44686$$

The value obtained in the Reynolds Number establishes that the flow inside the chamber is turbulent. For the cases studied the inlet velocity is equal or higher than 15 m/sec. Therefore, the flow is going to be turbulent. A Renormalization Group (RNG) model is going to be used to model turbulent flow.

3.9 PRESSURE DROP

3.9.1 Inlet

To calculate the pressure drop at the inlet, the theory of analysis of fully developed flow in pipes can be applied. For the CFD models, the inlet was modeled as a long pipe with a very small diameter. This is not the right configuration. The right configuration of the inlet should be like the figure 3.3.

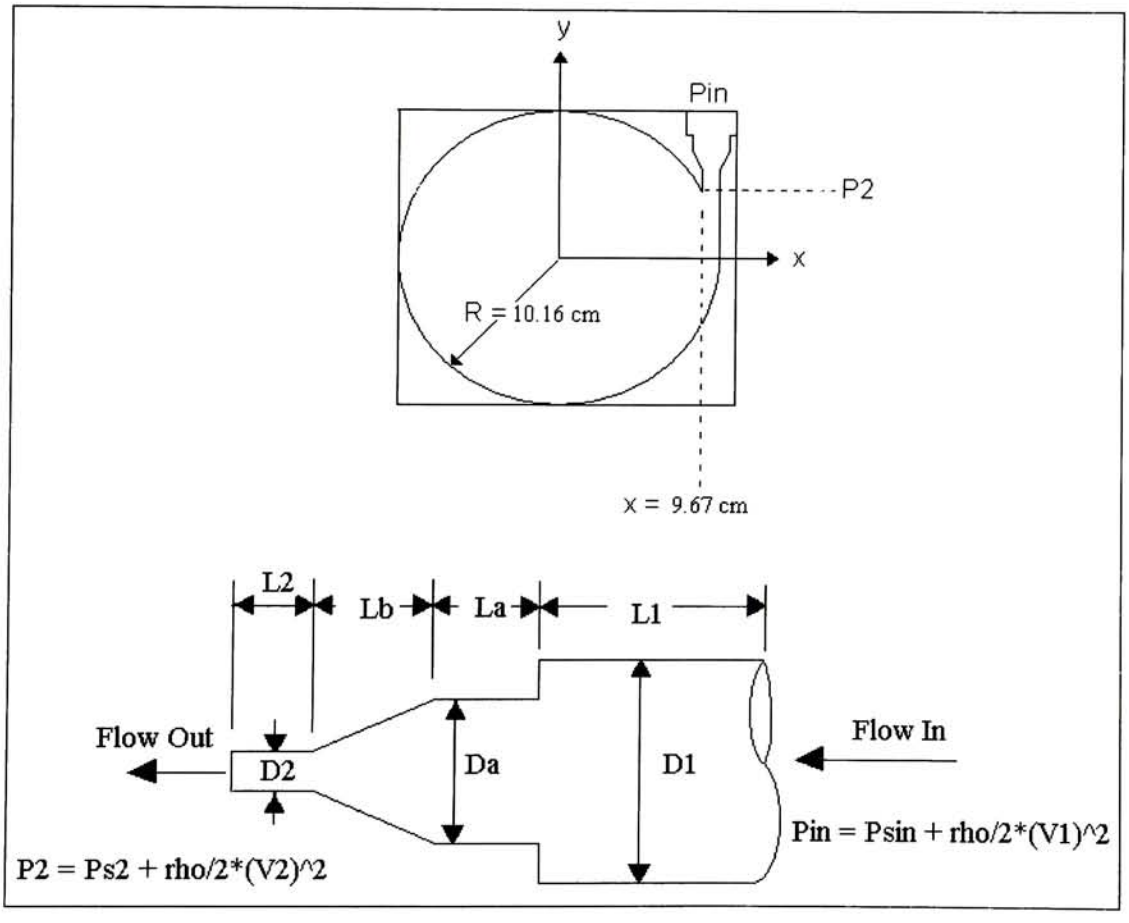

Figure 3.3. Detail of inlet pipe and fittings.

The simulations were modeled as a long tube because FLOW 3D can not model the behavior of high speed fluid through a set of fittings with a sudden reduction in the cross sectional area. The reason for that is because the flow field is undergoing a substantial change in velocity at a short period of time and when this happens, it gives convergence problem.

Modeling the inlet as a long pipe will not affect the results. From the results, the pressure at P2 in figure 3.4 can be obtained and once P2 is known, an analysis of fully developed flow in pipes can be done going backwards to obtain the pressure at the inlet of vortex chamber for its real configuration.

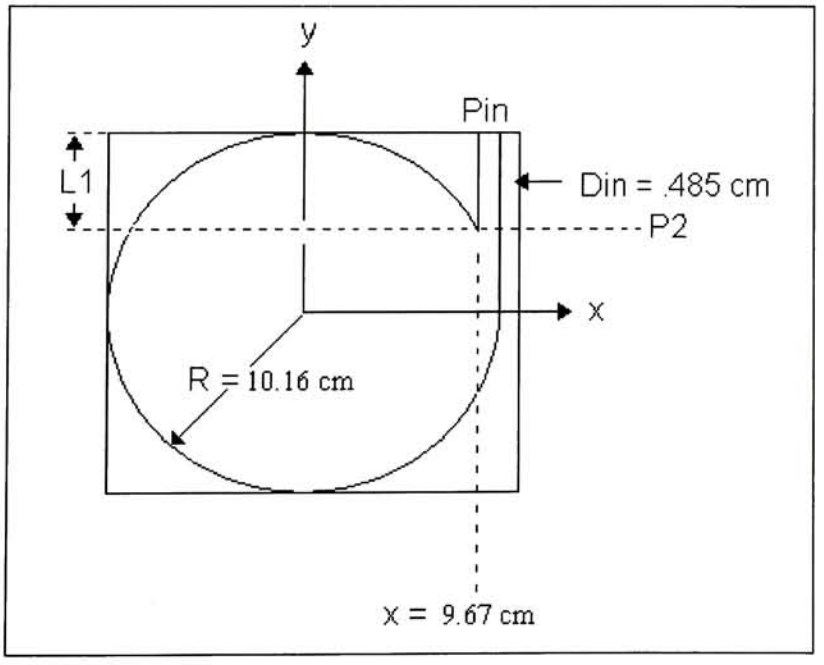

Figure 3.4. Detail of modified inlet.

To calculate the pressure drop in the inlet the Bernoulli equation with extra terms that considers the energy losses from fittings and losses from pipe friction is utilized. The equation becomes.

$$P_{in} + \frac{\rho(V_{in})^2}{2} = P_2 + \frac{\rho(V_2)^2}{2} + f_1\left(\frac{L_1}{D_1}\right)\frac{\rho(V_1)^2}{2} + f_a\left(\frac{L_a}{D_a}\right)\frac{\rho(V_a)^2}{2} + f_2\left(\frac{L_2}{D_2}\right)\frac{\rho(V_2)^2}{2} +$$

$$Kc\frac{\rho(V_a)^2}{2} + Kn\frac{\rho(V_a)^2}{2} \qquad (3.7)$$

Where the third, forth and fifth terms of the right hand side of the equation are the major losses (losses due to pipe friction) and the last two terms are the minor losses (losses due to fittings). In this equation, f is the friction factor and is a value that depends on the roughness of the pipe and the Reynolds number in the section of interest. The value of f can be obtained from the Colebrook formula

$$f = \frac{.25}{\left\{\log\left[\left(\frac{\varepsilon}{D}\right)/3.7 + 2.51/\left(\Re e\cdot\sqrt{f}\right)\right]\right\}^2} \qquad (3.8)$$

or from the Moody Chart for friction factors. This chart is in page 116, Appendix I.

Also the continuity equation is needed to calculate the velocity at each section of the pipes.

$$\dot{m} = \rho\cdot V\cdot A \qquad (3.9)$$

for constant density the continuity equation can be rewritten as

$$V_{in} \cdot D_{in}^{\ 2} = V_a \cdot D_a^{\ 2} = V_2 \cdot D_2^{\ 2} \tag{3.10}$$

Knowing the velocity at P2, ant the diameters of each section, the velocities can be calculated and therefore the pressure drop at the inlet section.

3.9.2 Bottom Outlet

The pressure drop at the outlet can be calculated following the same procedure used to calculate the pressure drop at the inlet. The only difference is that the outlet is a pipe with no change in the cross sectional area (see figure 3.5 below).

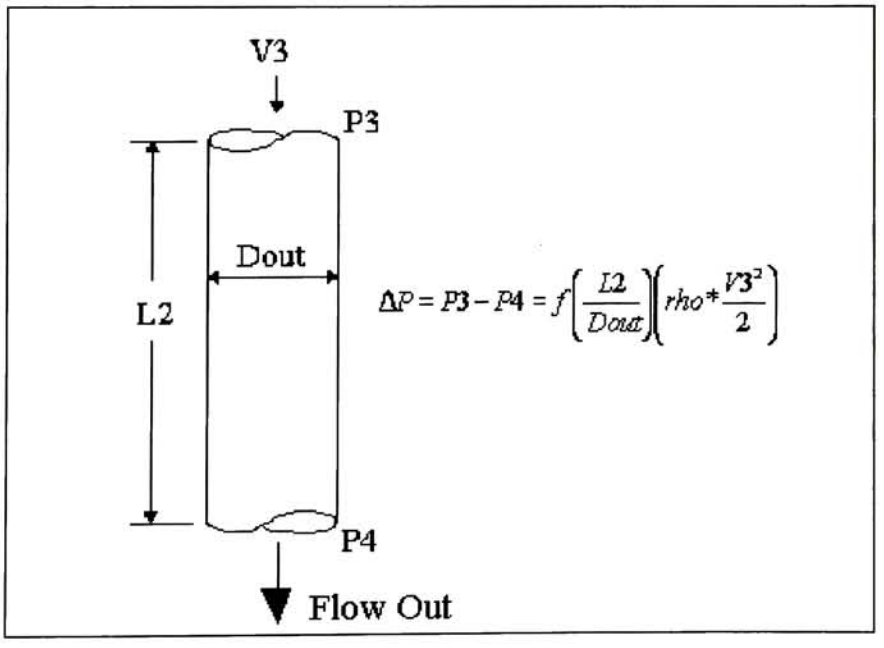

Figure 3.5. Detail of bottom outlet pipe.

Since there is no change in the cross sectional area of the pipe at the outlet, equation 4.3 can be reduced to

$$P_3 = P_4 + f\left(\frac{L_2}{D_{out}}\right)\frac{\rho(V_3)^2}{2} \tag{3.11}$$

Also at the outlet, the velocity is not known but this can be obtained from the results of the simulation.

3.10 CACULATION OF FREE SURFACE AREA

Unfortunately, the amount of vapor generated can not be calculated with the program used for the CFD flow analysis. The reason for this is because Flow 3D does not have an evaporation model. Even the amount of vapor can not be quantified, the vapor generated is going to be influenced by the free surface area. Due to mass transfer, a bigger free surface area will generate mode vapor.

The vapor-liquid interface surface area can not be directly calculated by the software because it is not capable to perform that operation. A manual procedure to calculate the vapor-liquid interface surface area is going to be used. To calculate the surface area, a function that approximates the free surface geometry has to be develop. Then, the solid of revolution technique is a applied over the axial vortex chamber axial axis to calculate the vapor-liquid interface surface area. The limits of integration are obtained from Flow 3D results. To get the surface area the following formula was used

$$Surface\_Area = \int_a^b 2\pi\sqrt{1+(\frac{\partial}{\partial x}f(x))^2}\,dx \tag{3.12}$$

where a and b are the are the limits of integration and f(x) is the function that represents the vapor-liquid interface.

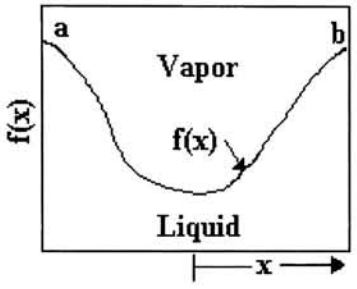

Figure 3.6. Graph of the vapor-liquid interface function and its limits.

CHAPTER

FOUR

RESULTS AND DISCUSSION

4.1 INTRODUCTION

In this chapter a discussion of the results of the cases studied is presented. Different cases where studied to determine the optimized design. The analysis will include pressure distributions in the vortex chamber, pressure drop at the inlet and outlet, and velocity vectors plots. The optimized design was selected based on the size of the free surface area. The amount of vapor generated can not be calculated. But the generation of vapor is going to be influenced by the free surface area created by the strong vortex. The bigger the free surface area, higher is going to be the mass transfer rate of vapor from the LiBr-water solution to the vapor region in the lower chamber. The result of the vortex chamber with the optimized design is going to be presented in more detail. The parameters changed to determine the optimized design where inlet velocity, inlet location and vortex chamber aspect ratio (diameter/height). Also a discussion of the mesh and initial conditions is going to be presented and discussion of steady state solutions as well.

4.2 MODEL MESH

In this section, an example on how the vortex chamber was meshed is presented. A rectangular grid is used to mesh the domain of the vortex chamber. With the exception of the optimized design, the total number of cells for each simulation is approximately 10,000 cells. For the optimized design, a dense mesh was applied and the total number of cells for this case was 100,000 cells.

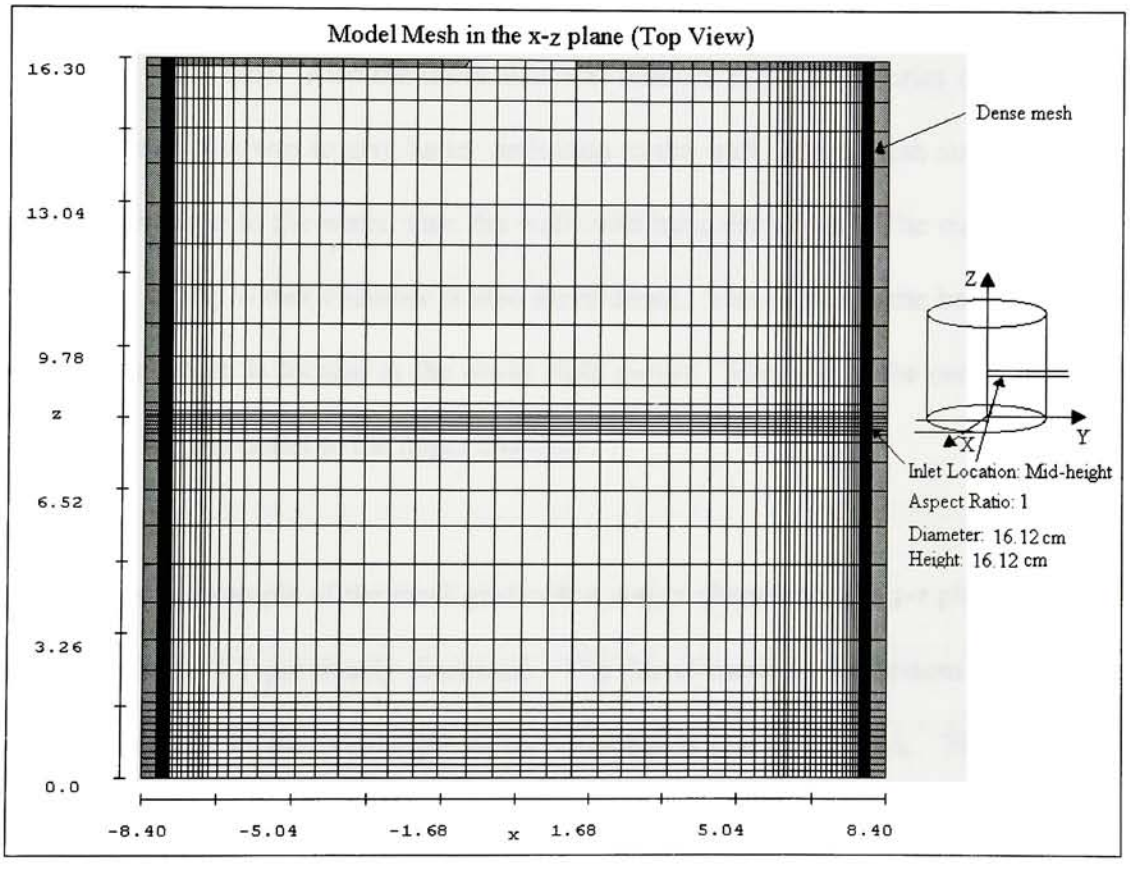

Figure 4.1 Mesh example in the x-z plane for the optimized chamber design.

In figure 4.1, the inlet is located at z = 8.1 cm, x = 8.1 cm and the gray portion at the boundaries of the domain are the wall of the vortex chamber. The bottom of the domain is a wall boundary. That is why the wall was not modeled in that section.

Since the diameter of the inlet pipe is very small, the mesh in that area has to be very fine to capture the effect of a non-slip condition in a viscous solution. A good practice is that at least 3 cells on each direction (from wall to wall of the pipe) should be present. To achieve this, the mesh size was reduced in the right side (x = 8.1 cm) and in the mid-height of the chamber (z = 8.1 cm). Also the mesh size was reduced at the boundaries of the domain. The purpose of this was to give better definition to the wall. If the mesh size is increased in the region close to the walls, then the walls will have distortions. The mesh size at the bottom part of the vortex chamber is also more dense. This is due to the bottom outlet of the chamber which is located at the lower right corner. The hole at the center of the top boundary is the top outlet to the upper chamber.

Figure 4.2 is an example of the mesh grid of the vortex chamber in the y-z plane. It is very similar to figure 4.1 previously discussed. The dense mesh in the bottom is due to the bottom outlet and in the mid-height of the chamber is due to the inlet. The hole at the center of the top boundary is the top outlet to the upper chamber

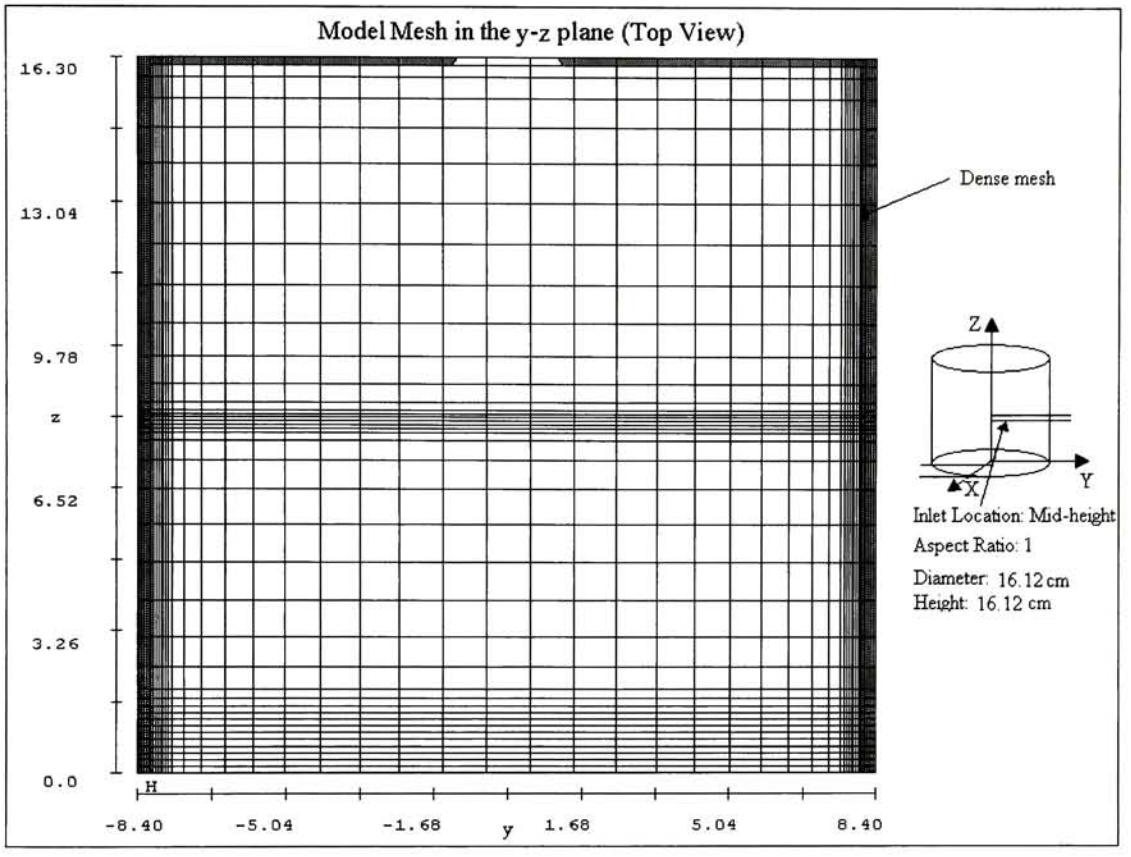

Figure 4.2 Mesh example in the y-z plane for the optimized chamber design.

Figure 4.3 is an example of the mesh grid of the vortex chamber in the x-y plane. This figure shows the inlet pipe. It can be appreciated how dense is the mesh in this section. As discussed before, there should be at least three cells in the inlet pipe from wall to wall to obtain good results in the simulation due to the boundary layer effects.

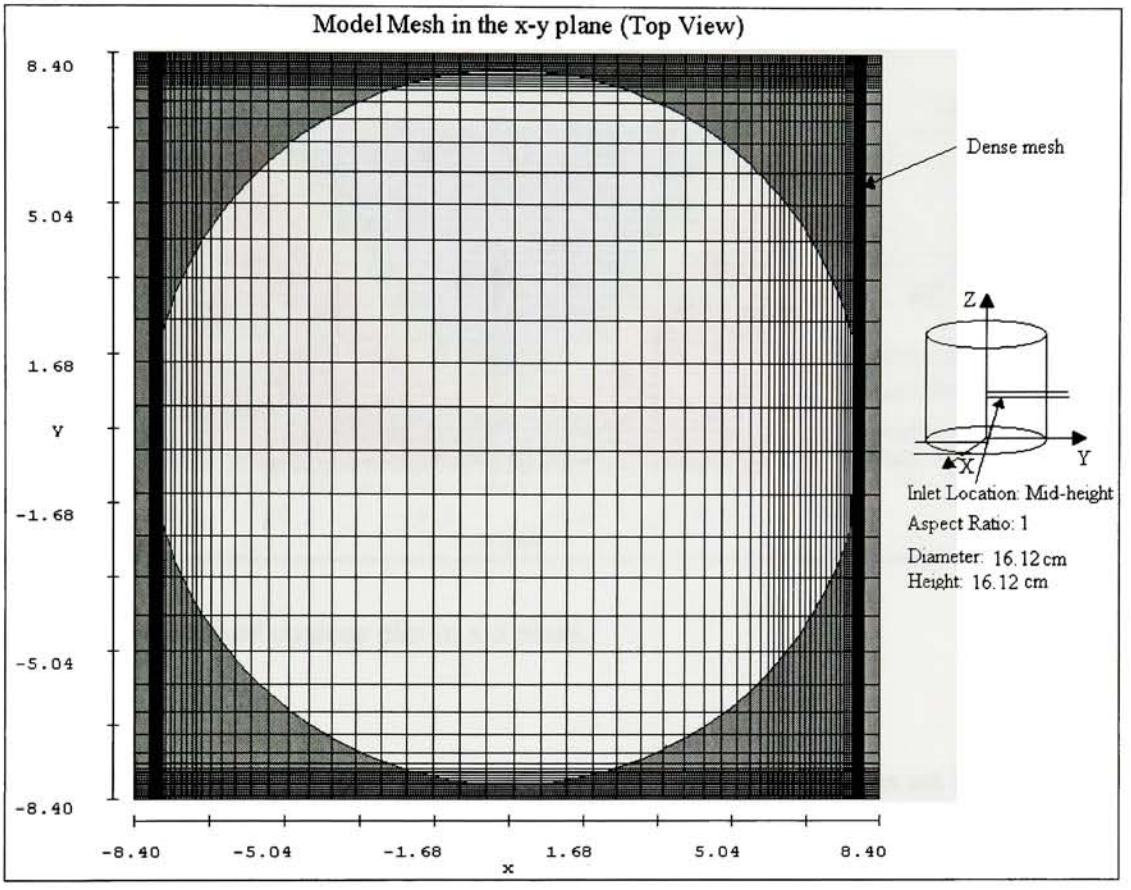

Figure 4.3 Mesh example in the x-y plane for the optimized design.

4.3 INITIAL CONDITIONS

4.3.1 INITIAL FLUID DISTRIBUTION

The next two figures show how the LiBr-water solution was set initially in the vortex chamber. The initial fluid configuration was set in such a way to save time in running the simulations.

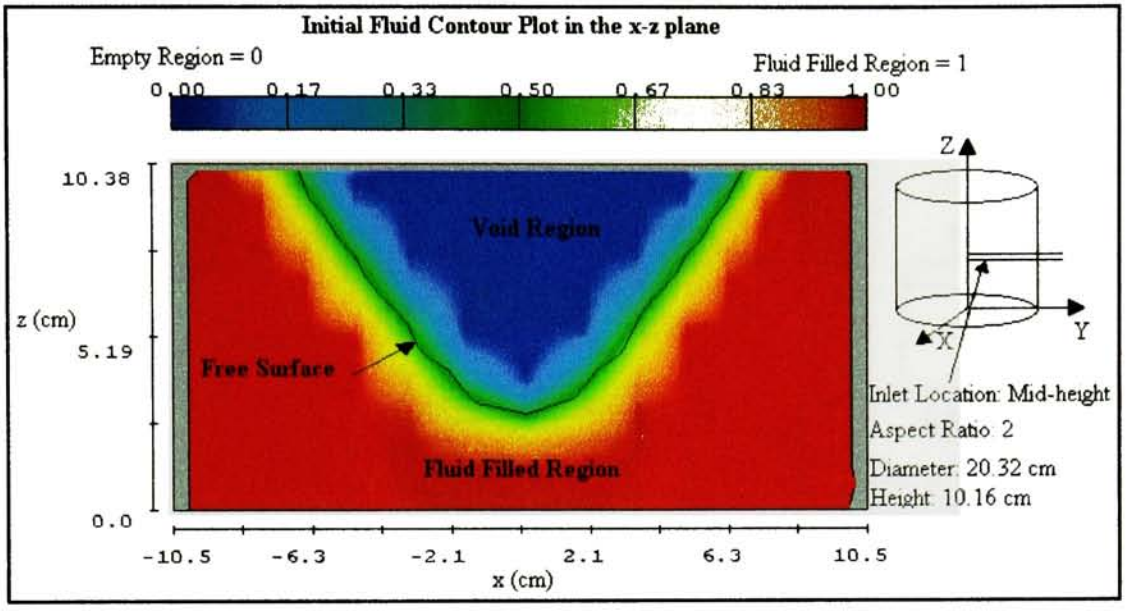

Figure 4.4 Initial fluid contour plot in x-z plane.

Figure 4.4 is a contour plot that shows how the LiBr-water solution was set initially in the vortex chamber. It was expected that the high tangential velocities were going to generate a strong vortex flow and therefore a void region at the central portion of the chamber. For this reason, the fluid in the vortex chamber initially was set in such a way that the void region will have a conical shape. The void region is the empty space where no fluid is present. Figure 4.4 shows the void region in color blue. The red color in figure 4.4 shows the section that is initially filled with the LiBr-water solution. The green section in the figure above shows the interface between the LiBr-water solution and the void region.

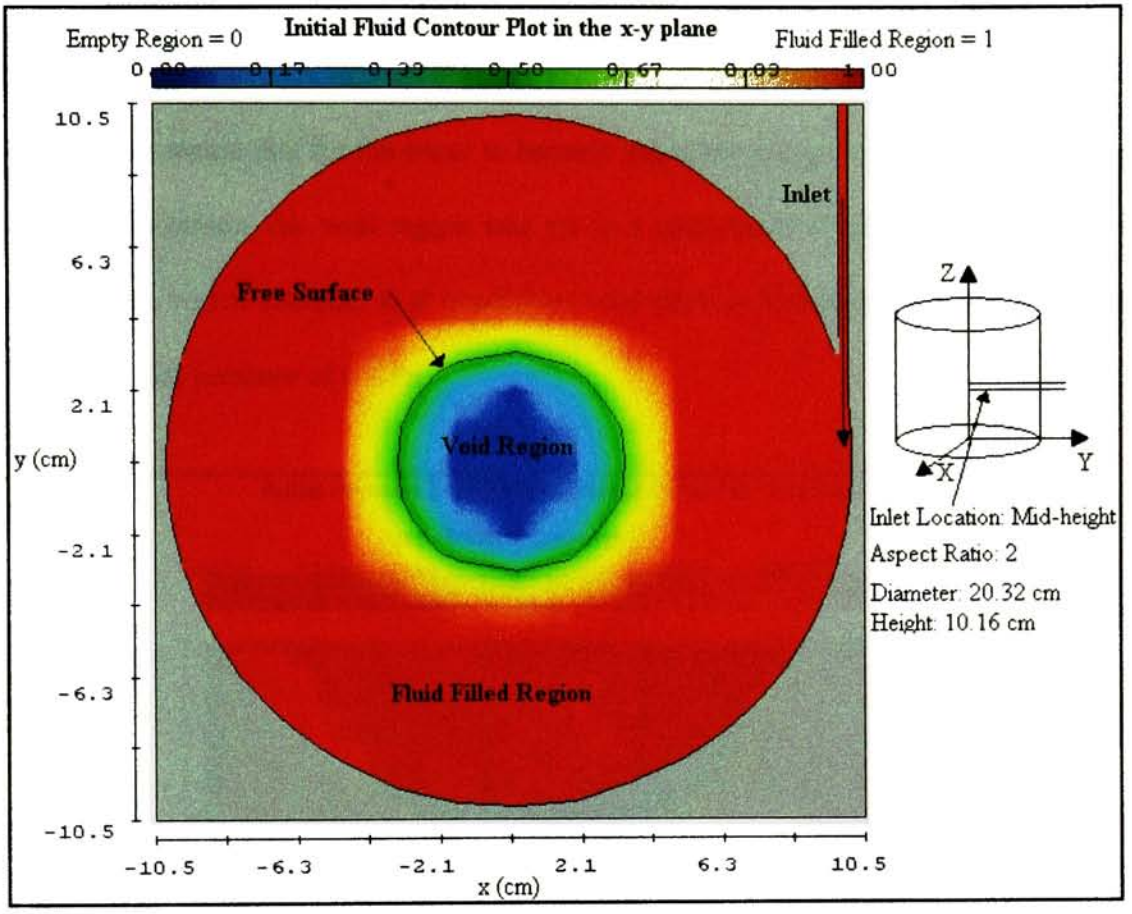

Figure 4.5 Initial fluid contour plot in x-y plane.

Figure 4.5 is contour plot of the fluid in the vortex camber in the x-y plane. It shows the inlet pipe. The void region is colored with blue. The section in red is the part that is initially filled with LiBr-water solution. The green section shows the interface between the LiBr-water and the void region.

4.3.2 INITIAL PRESSURE DISTRIBUTION

In order to have vapor generation in the vortex chamber, cavitation should take place. Cavitation occurs when the pressure of a liquid drops below its saturation pressure and as a

consequence the liquid becomes a gas. The saturation pressure of the LiBr-Water solution with a composition of 60% lithium bromide and 40% of water and a temperature of 80C is 5.8 KPa. This means that for the water to become vapor the pressure should be 5.8 KPa or less. For this reason, the void region was set to a pressure of 5 KPa. The LiBr-Water solution in the vortex chamber is at conditions very close to its saturation point. It was set to have an initial pressure of 6 KPa.

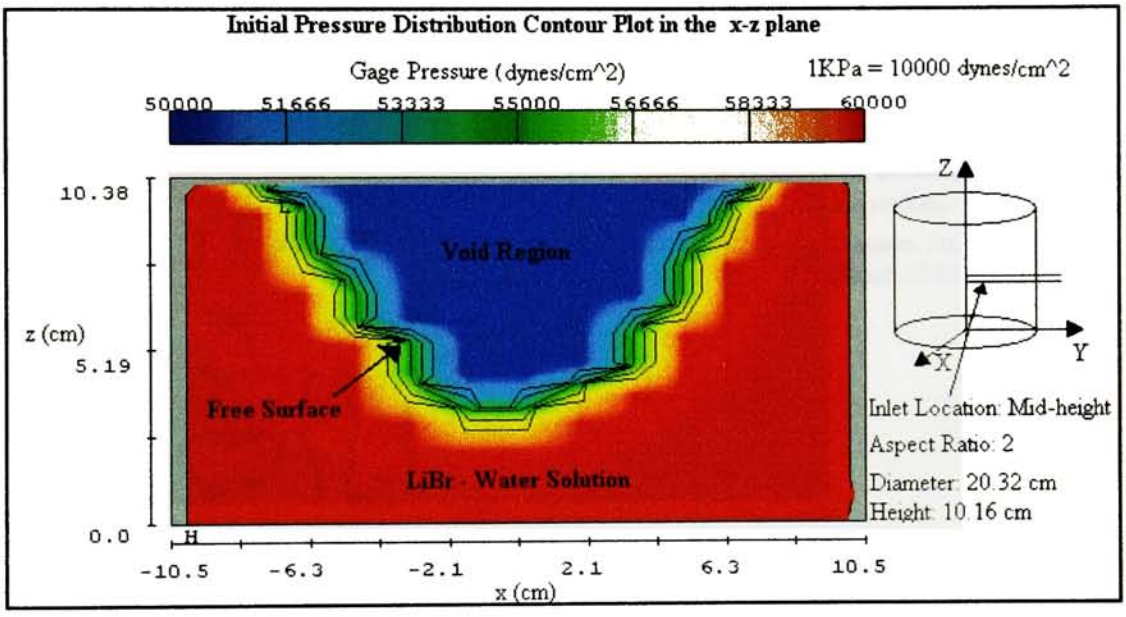

Figure 4.6 Initial pressure distribution contour plot in x-z plane.

Figure 4.6 shows the initial pressure distribution contour plot in the x-z plane. The saturation pressure of a 60% LiBr- 40% water solution at a temperature of 80 C is equal to 5.8 KPa. This means that the pressure at the void region should have a pressure equal to 5.8 KPa or less. As shown in figure 5.6 (section in blue color), it was arbitrarily set to 5

KPa (50000 dyne/cm^2). The section initially filled with LiBr-water solution was set to 6 KPa (dyne/cm^2). This is section is represented in figure 4.6 with the red color.

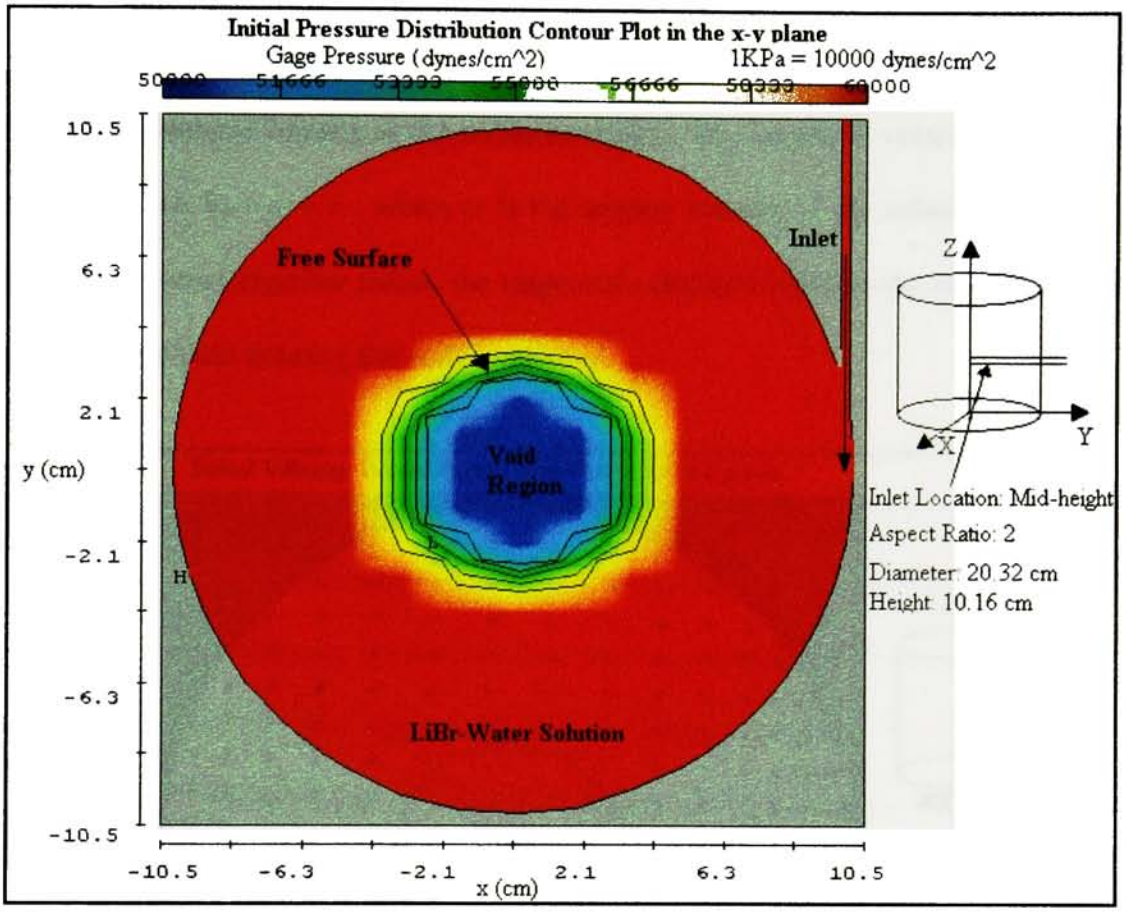

Figure 4.7 Initial pressure distribution contour plot in x-y plane.

Figure 4.7 shows the initial pressure distribution contour plot in the x-y plane. It also shows the inlet pipe. The void region is colored with blue and has an initial pressure of 5 KPa (50000 dyne/cm^2). The section in red is the part that in initially filled with LiBr-water solution and is initially set to 6 KPa (60000 dyne/cm^2).

4.3.3 INITIAL VELOCITY VECTORS DISTRIBUTION

The initial tangential velocity vector distribution is a function of the vortex chamber radius. It was set to increase linearly as the radius increases. The tangential velocity is determine by the equation $V_\theta = \omega * r$, where ω is the angular velocity of the solution. When r is equal to the vortex chamber radius, the tangential velocity is equal to the magnitude of the velocity of the fluid entering the vortex chamber.

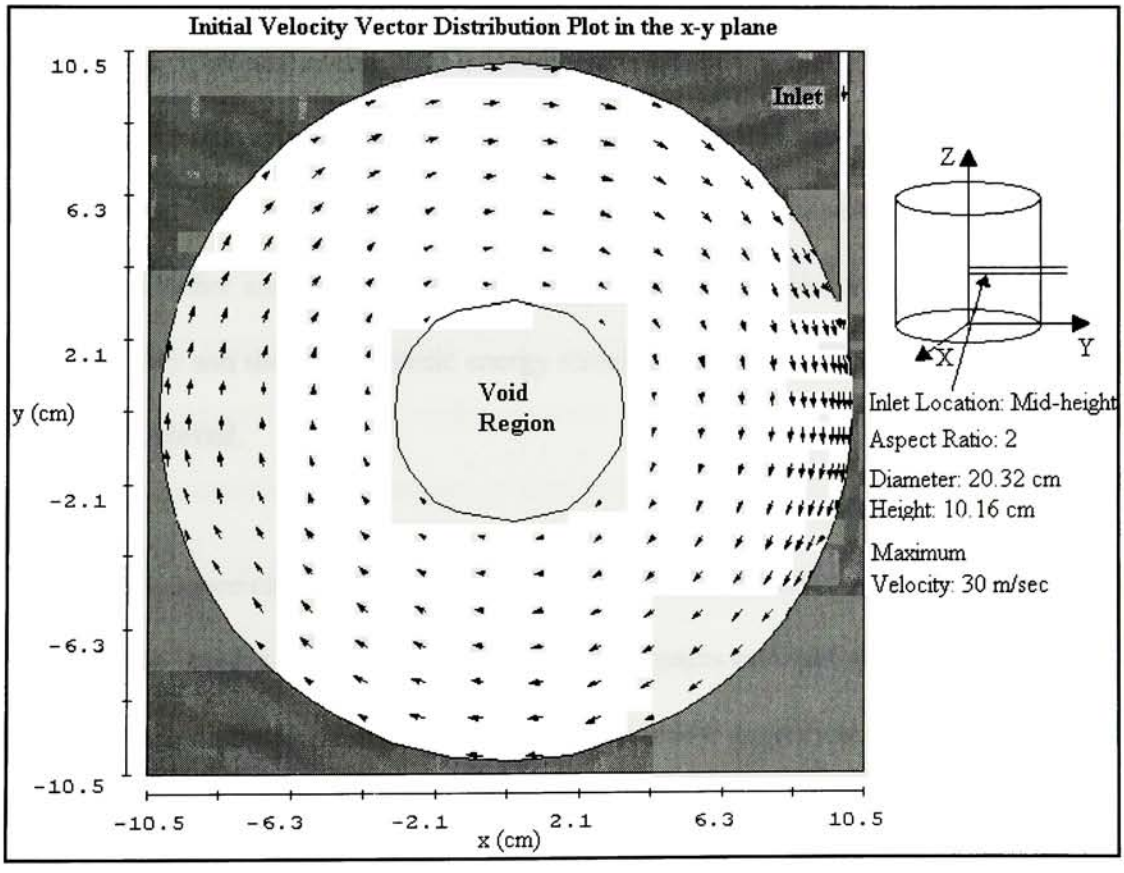

Figure 4.8 Initial velocity distribution contour plot in x-y plane.

Figure 4.8 shows an example on how the velocity distribution was set initially. The tangential velocity was set assuming a constant angular velocity. This means that at a

radius of 0 cm the tangential velocity is 0 cm/sec and at a radius equal to half the diameter, the tangential velocity has a maximum value. The value of the constant angular velocity varies on each simulation and was selected depending on the inlet velocity boundary. The tangential velocity distribution remains constant along the z axis.

4.4 STEADY STATE SOLUTION

All the simulations where run until a steady state solution was achieved. Flow 3-D is a transient code. This means that the program always run in transient mode. To determine if the solution achieved steady state, it is necessary to compare the volume rate of change in the vortex chamber and the mean kinetic energy. When the volume of solution inside the vortex chamber and the mean kinetic energy remains constant with time, then a steady state solution is achieved.

Also a mass balance can be made to determine if the solution entering the chamber is equal to the solution leaving the chamber. If these two remains constant and do not change with time, steady state solution is achieved. The figures below are typical example of the results once steady state is achieved.

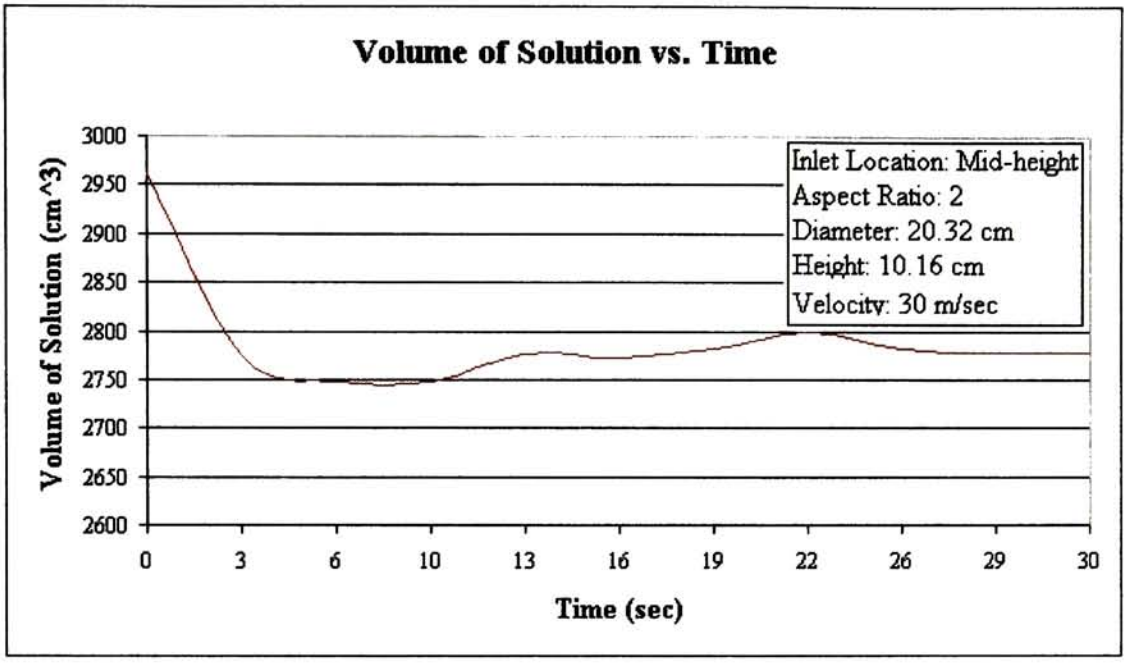

Figure 4.9 Volume of solution in the vortex chamber with time.

Figure 4.9, shows how the volume of solution in the vortex chamber is varying with time until steady state is achieved. During the first 3 seconds, the chamber starts to empty. This is happening because the initial condition of the tangential velocity distribution was set to high. As a consequence, the amount of solution leaving the chamber is bigger than the incoming solution to the chamber. After the 3 seconds, the volume of solution in the chamber goes up and down until it stabilize.

The average mean kinetic energy is another way to determine if steady state is achieved. The mean kinetic energy is defined as the product of half the mass and the sum of the square of the velocity components. Therefore, for steady state the magnitude of the

velocity components remains constant. Figure 4.10 below is a typical result for the average mean kinetic energy with time.

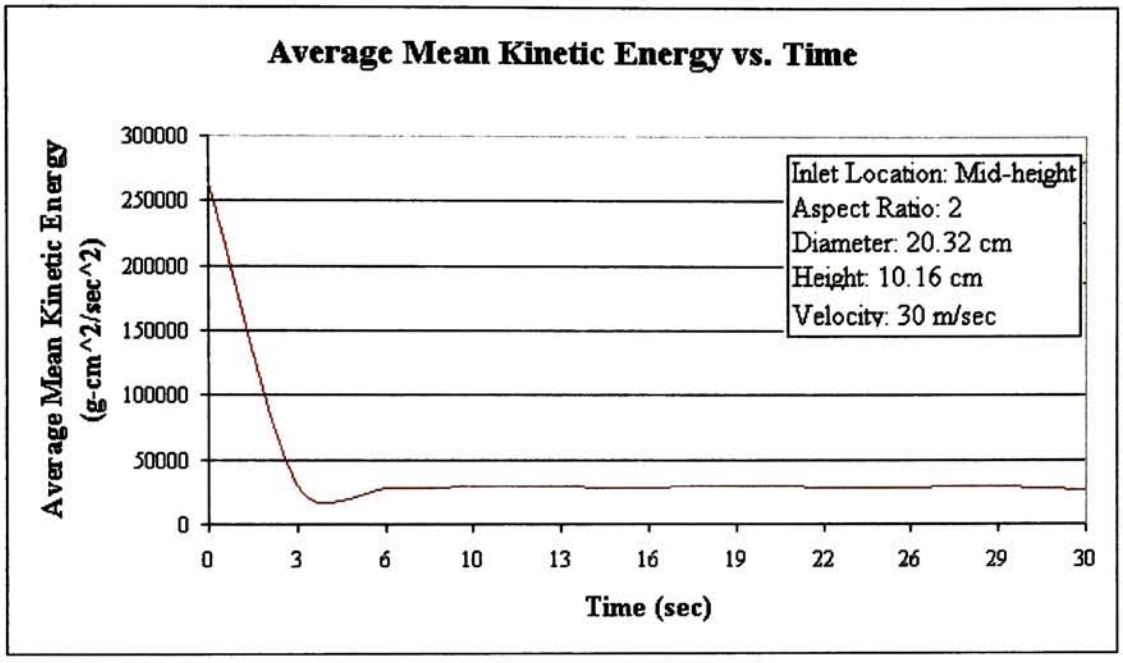

Figure 4.10 Average mean kinetic energy with time.

Once steady state is achieved, for a constant density fluid, the volume flow rate at the inlet boundary is equal to the volume flow rate at the bottom outlet boundary. Figure 4.11 shows the results of a simulation on how the volume flow rate at the inlet and outlet boundaries change with time until steady state is achieved. The inlet boundary is a velocity boundary. Therefore, the volume flow rate at this boundary will not change with time because is fixed. The bottom outlet boundary shows how volume flow rate change with time until it match the inlet boundary.

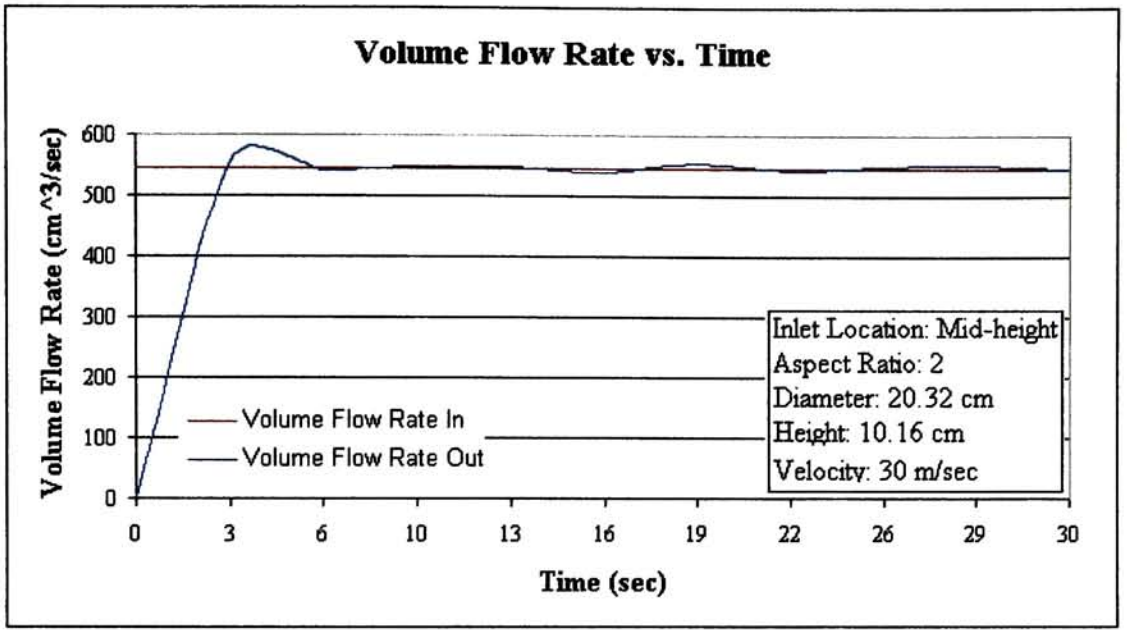

Figure 4.11 Volume flow rate with time.

4.5 RESULTS OF CASES STUDIED

The amount of vapor generated can not be determine with Flow-3D. Mass transfer is a function of area. Therefore, the amount of vapor generated is going to be directly proportional to the LiBr-water to water vapor surface area generated by the strong vortex flow. The LiBr-water to water vapor surface area can not be automatically calculated by the software. The free surface area was calculated manually with the procedure mentioned in Appendix C. Table 4.1 below shows the results of the LiBr-water to water vapor surface area.

Case	Aspect Ratio	Diameter (cm)	Height (cm)	Inlet Location	Inlet Vel. (m/s)	Surface Area (cm^2)
1	1	16.12	16.12	Center	30	391
2	1	16.12	16.12	Center	20	308
3	1	16.12	16.12	Center	15	287
4	1.5	18.44	12.29	Top	20	249
5	1.5	18.44	12.29	Center	30	309
6	1.5	18.44	12.29	Center	20	257
7	1.5	18.44	12.29	Center	15	234
8	2	20.32	10.16	Top	30	226
9	2	20.32	10.16	Center	30	279
10	2	20.32	10.16	Top	20	255
11	2	20.32	10.16	Center	20	237
12	2	20.32	10.16	Center	15	213
13	1.5	18.44	12.29	Center	20	257
14	1.5	18.44	12.29	Center	20	283

Case 13. Void Pressure = 15KPa

Case 14. Higher Mass flow rate (910 g/sec @ 20m/sec)

Table 4.1. Results of the cases studied.

The results of table 4.1 shows that the LiBr-water to vapor free surface area generated by the swirling flow is directly proportional to the inlet velocity. The higher the inlet velocity, larger is going to be the size of the surface area of the LiBr-water to vapor interface. The reason for this is because when the fluid velocity is increased, its momentum is also increased. Momentum is directly proportional to the fluid velocity. The LiBr-water solution entering the vortex chamber at 30 m/sec has a bigger momentum than when

entering at 15 m/sec and 20 m/sec. The momentum of this incoming solution will then be transferred to the solution inside the vortex chamber. The higher the momentum of the incoming solution, the greater is going to be the momentum transfer. As a consequence of this, the rotational momentum of the LiBr-water solution in the chamber will be greater. This will create a strong vortex flow and increase the free surface area between the LiBr-water solution and the water vapor.

Also results shows that the free surface area is going to be better if the inlet location is at the center of the vortex chamber. When the inlet is placed at the top of the vortex chamber, the solution entering the chamber decelerates faster than when the inlet is at the center of the chamber. When the inlet is at the top it decelerates faster because of the two walls close to the inlet. These two walls are the vortex chamber side wall and the top wall. The presence of these two walls decreases the fluid velocity due to skin friction. When the inlet is at the center of the vortex chamber, only one wall is close to the inlet. As a consequence the loss due to skin friction is going to be less.

Table 4.1 also shows that the free surface area is influenced by the dimensions of the vortex chamber. When the vortex chamber aspect ratio (diameter/height) is decreased, the LiBr-water to water vapor surface area increases. When the diameter of the vortex chamber is decreased, the fluid flow path is also decreased. When the fluid flow path is decreased, the losses in the kinetic energy are minimized. As a consequence, the LiBr-water solution velocity is going to be remain high. If the fluid path is increased, the more losses in kinetic energy will be present and therefore the LiBr-water solution velocity

will be reduced. A high solution velocity will generate a stronger forced vortex flow and therefore a bigger free surface area.

4.5.1 COMPARISON OF DIFFERENT VOID PRESSURES

A vortex chamber with an aspect ratio (diameter/height) of 2 and an inlet velocity of 20 m/sec with the inlet located at the mid height of the vortex chamber was simulated with different void pressures. The purpose of this was to determine the effect of different voids pressures to the solution domain.

Aspect Ratio	Void Pressure (KPa)	Inlet Velocity (m/sec)	Inlet Location	Surface Area (cm^2)
2	5	20	Center	257
2	15	20	Center	257

Table 4.2. Comparison of the results for different void pressures.

Results show that there is no effect in the solution when the void pressure is changed. The free surface and the velocity vectors remain unchanged. The only effect that this cause is that the fluid pressures in the solution domain are increased by 10 KPa when the void pressure is set to 15 KPa. This means that the void pressures in the solution domain are gage pressures relatives to the void pressure.

4.5.2 COMPARISON OF MASS FLOW RATES

Table 4.3 below shows the effect of different mass flow rates to the LiBr - water to vapor free surface area. Results shows that higher mass flow rates increases the free surface area. Also, in situations where the mass flow rates are the same but the velocities are different, the solution with higher inlet velocity will generate a bigger surface area. This is due to momentum.

Aspect Ratio	Mass Flow (gr./sec)	Inlet Velocity (m/sec)	Inlet Location	Surface Area (cm^2)
1.5	607	20	Center	257
1.5	910	20	Center	283
1.5	910	30	Center	309

Table 4.3. Comparison of the results for different mass flow rates and velocities

Momentum is defined as mass times velocity. Momentum is also a function of area. In the cases where the velocities are the same but the inlet mass flow rates are different, the case with higher mass flow rate generates a bigger surface area. A higher inlet mass flow rate was achieved by increasing the inlet diameter. Since momentum is a function of area, a bigger free surface area will be generated when the inlet diameter is increased without changing the inlet velocity.

4.5.3 COMPARISON OF SURFACE AREA vs. INLET VELOCITY

The LiBr-water to water vapor free surface area is influenced by the inlet velocity and the vortex chamber aspect ratio (diameter/height). Figure 4.12 and Table 4.4 below shows how the vortex chamber free surface area is related to the inlet velocity and aspect ratio. From the graph it can be determine that the free surface area increases as the inlet velocity increase. Also, for a bigger aspect ratio the free surface area is going to be less. This is because the fluid path is longer and will have more losses due to friction.

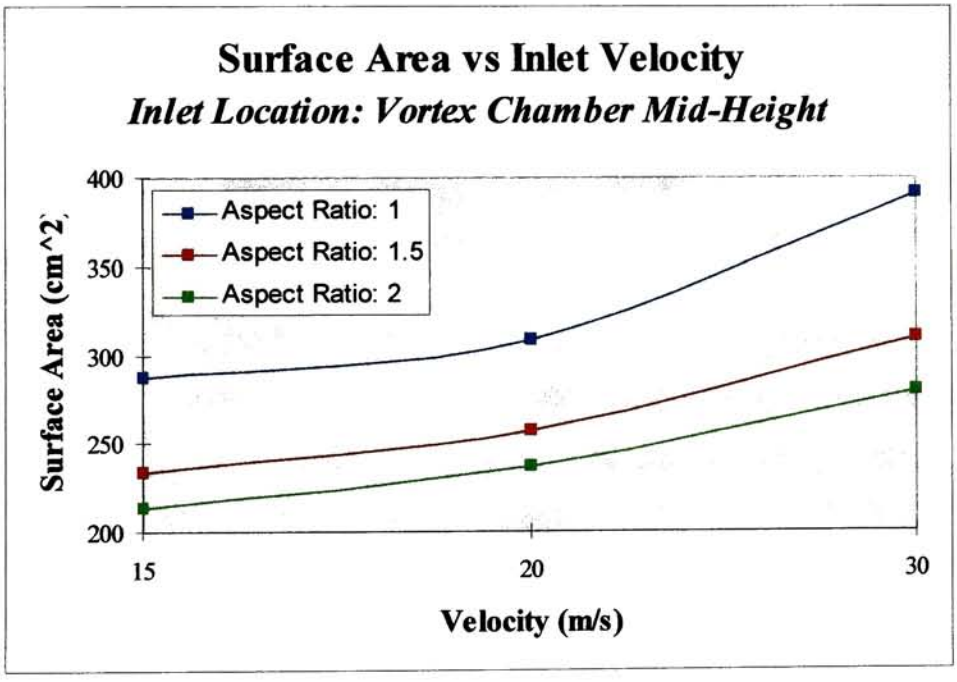

Figure 4.12 Relation of Surface Area vs. Inlet Velocity with inlet at the center of the chamber.

Inlet Location: Vortex Chamber Mid-Height

Inlet Vel. (m/s)	Free Surface Area (cm^2)		
	Aspect Ratio: 1	Aspect Ratio: 1.5	Aspect Ratio: 2
15	287	234	213
20	308	257	237
30	391	309	279

Table 4.4. Comparison of Free Surface Area vs. Inlet Velocity with inlet at the center of the chamber.

4.6 VORTEX CHAMBER PRESSURE DISTRIBUTION

4.6.1 PRESSURE DISTRIBUTION IN THE VORTEX CHAMBER

The pressure distribution in the vortex chamber will depend on the dimensions of the vortex chamber, the inlet location and the inlet velocity. The following figures are examples on how the pressure is distributed in the vortex chamber. Also the pressure distribution versus aspect ratio and inlet velocities are compared.

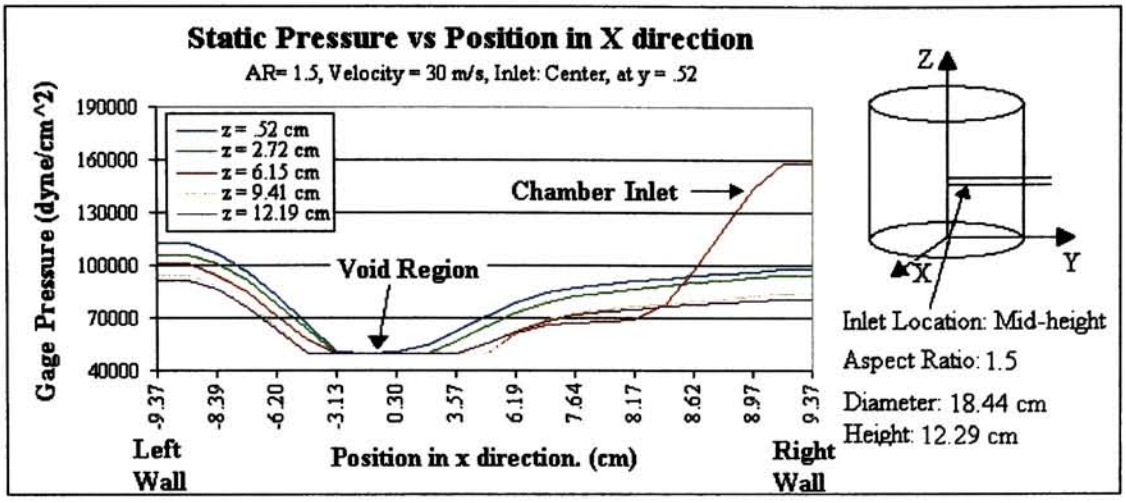

Figure 4.13 Pressure distribution in the x-plane.

Figure 4.13 shows how the pressure is distributed along the x axis of the vortex chamber at different elevations (z). The pressure is higher at the wall of the vortex chamber and decreases toward the center. This agrees with the vortex flow theory. The graph also shows that at a lower elevation, the pressure along the x axis is higher. This means that the pressure in the vortex chamber increases in direction to the bottom wall of the chamber. In figure 5.13, for z = 6.15 cm and x = 9.37 cm the corresponding pressure is very high in comparison with the rest of the location. The reason for this is because the inlet is located in that area.

Figure 4.14 below, shows the pressure distribution of the vortex chamber in the axial direction for different locations in the along the x axis. The pressure increases linearly toward the bottom of the vortex chamber. This is due to hydrostatic pressure. The abrupt change appreciated in the graph happens due to the high inlet velocity.

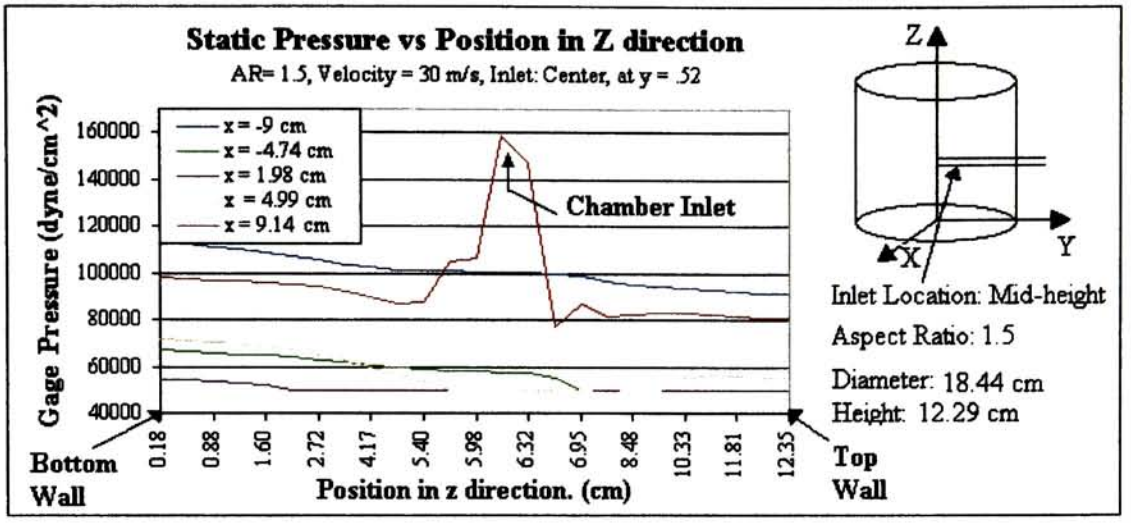

Figure 4.14 Pressure distribution in the axial direction with inlet at the center of the chamber.

The fluid particles that entering the vortex chamber have a high kinetic energy. Once the fluid particles with high inlet velocity enters the vortex chamber, they hit the wall of the chamber causing a big pressure increase. That is why the drastic change in pressure in the graph.

Figure 4.15 below is the same graph that in figure 4.14 but with the difference that the inlet location is at the top of the vortex chamber.

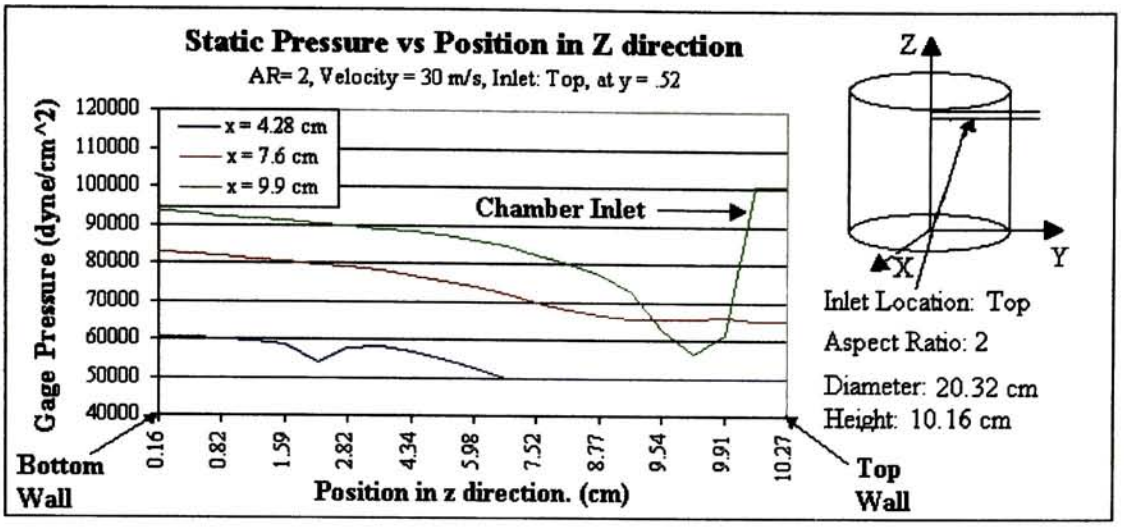

Figure 4.15 Pressure distribution in the axial direction with inlet at the top of the chamber.

4.6.2 PRESSURE DISTRIBUTION vs. INLET VELOCITY

The pressure distribution in the vortex chamber varies in the radial direction an is a function of the vortex chamber inlet velocity.

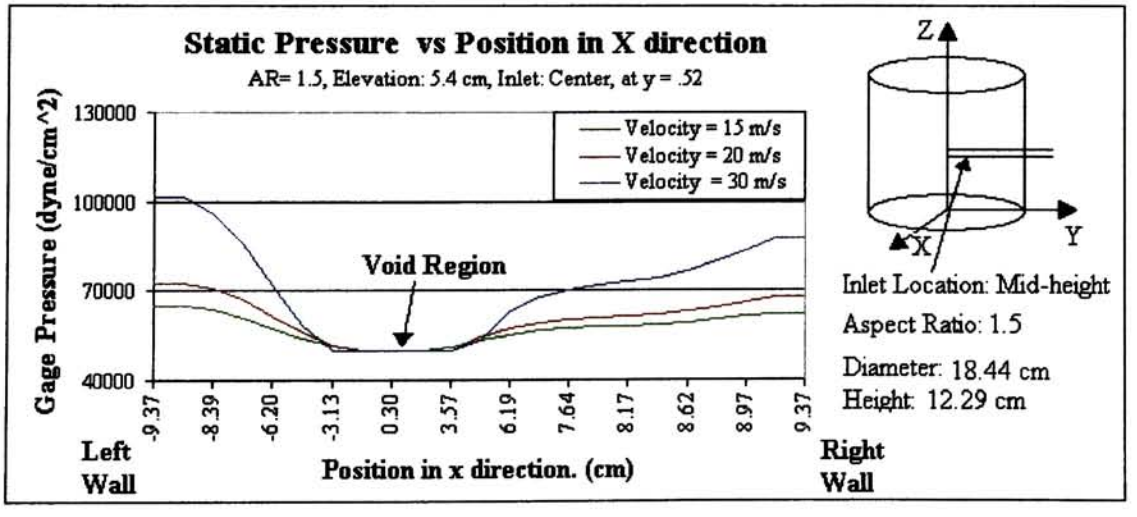

Figure 4.16 Pressure distribution along the x axis, for different inlet velocities.

Figure 4.16 above, shows an example of how the pressure varies in the radial direction (along the x axis) for different inlet velocities. As expected, a higher inlet velocity cause a bigger pressure drop toward the center of the vortex chamber.

The figure 4.17 below shows an example on how the pressure varies along the z axis of the vortex chamber for different inlet velocities.

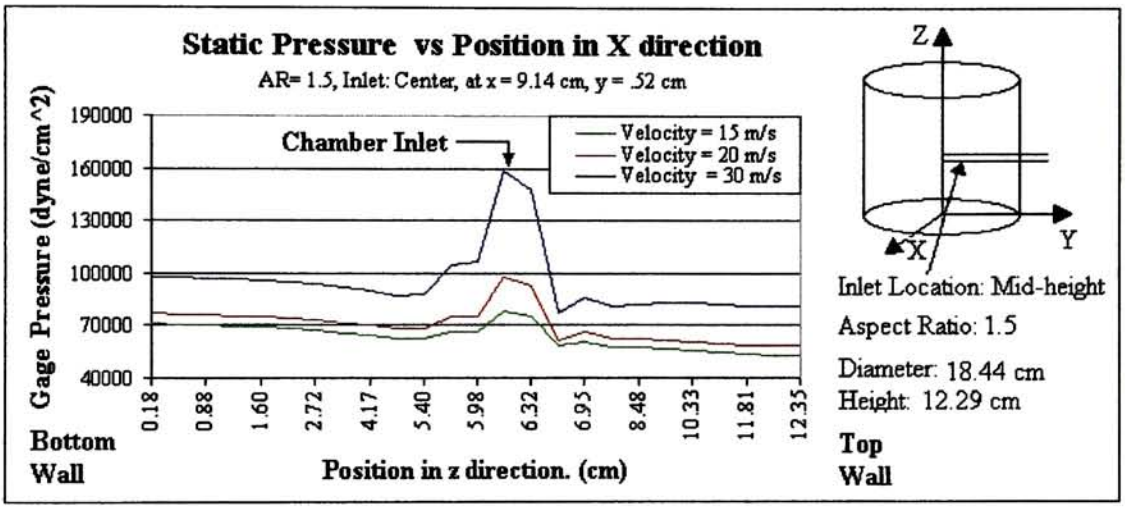

Figure 4.17 Pressure distribution in the axial direction, for different inlet velocities.

In figure 4.17, shows that the pressure distribution along the z axis will be higher for a higher inlet velocity. This is because the centrifugal force acting on the fluid will be proportional to the square of the velocity and therefore the pressure will be higher. Also from figure 4.17 it can be appreciated that the pressure increases linearly toward the bottom of the vortex chamber. The abrupt change at the center of the vortex chamber is due to the inlet. When the solution enters the vortex chamber, it hits the wall creating a high pressure point.

4.6.2 PRESSURE DROP AT THE INLET OF THE VORTEX CHAMBER

The pressure drop at the inlet portion of the vortex chamber is very high. This is due to the combination of small pipe diameter and high inlet velocity. Due to the high pressure drop at the inlet portion, a pump with a head capacity bigger than the normal pumps used for this type of application will be needed. The vortex chamber will perform the function of a conventional generator with less external energy but will require a bigger pump in order to compensate the pressure drop at the inlet and have a strong vortex flow. Table 4.5 below, shows the pressure drop at the inlet portion of the vortex chamber for different aspect ratios and inlet velocities.

	Aspect Ratio		
Inlet Velocity	**AR = 1**	**AR = 1.5**	**AR = 2**
15 m/sec	192 KPa	206.7 Kpa	219 KPa
20 m/sec	341.9 KPa	367 KPa	388 KPa
30 m/sec	769 KPa	825.6 KPa	872 KPa

Table 4.5. Pressure drop at the inlet of the vortex chamber for different aspect ratios and velocities.

An example of calculation procedures for the pressure drop at the inlet of the chamber is presented in Appendix A.

4.6.3 PRESSURE DROP AT THE VORTEX CHAMBER BOTTOM OUTLET

The pressure drop at the bottom outlet varies with inlet velocity, aspect ratio and inlet location. Table 4.6 below shows the pressure drop at the bottom outlet for the different cases studied.

Aspect Ratio	Inlet Velocity (m/s)	Inlet Location	Pressure Drop (KPa)
1	15	Center	0.473
1	20	Center	0.615
1	30	Center	1.21
1.5	15	Center	0.359
1.5	20	Top	0.394
1.5	20	Center	0.42
1.5	30	Center	0.617
2	15	Center	0.164
2	20	Top	0.332
2	20	Center	0.365
2	30	Top	0.661
2	30	Center	0.761

Table 4.6. Pressure drop across the bottom outlet for the cases studied.

From table, it can be concluded that the pressure drop across the bottom outlet is higher when the inlet velocity increases, when the aspect ratio decreases and when the inlet location is at the center of the vortex chamber. When the inlet velocity is 30 m/s, the pressure drop at the bottom outlet is higher than the cases where the inlet velocity are 15 and 20 m/s because the fluid particles have more kinetic energy. When the aspect ratio decreases and the inlet location is at the center of the vortex chamber, the pressure at the bottom outlet is higher because the path of the fluid particles to get to the bottom outlet is minimized. When the distance of the fluid path from inlet to bottom outlet is reduced, the

pressure drop in the vortex chamber due to skin friction is reduced. Therefore, the fluid particles arrive to the bottom of the vortex chamber with more kinetic energy and consequently the pressure drop across the bottom outlet will be bigger.

The diameter of the bottom outlet for the cases studied range between 1.4 cm and 1.85 cm. This diameter will depend on the inlet velocity, inlet location and aspect ratio. For a good design, a diameter of 2 cm at the bottom outlet with a valve to control the outflow should be considered.

Appendix B shows an example of the procedure to calculate the pressure drop at the bottom outlet.

4.7 PRESSURE CONTOUR AND VELOCITY VECTOR PLOTS

4.7.1 SIDE VIEW OF PRESSURE AND VELOCITY VECTOR PLOTS

A comparison of the pressure distribution, velocity vectors and a discussion of the fluid behavior for the different vortex chamber configurations and inlet velocities is presented in the following figures 4.18 to figure 4.21.

Figure 4.18 shows a contour plot of the pressure distribution in a vortex chamber of aspect ratio of 2 and a inlet velocity of 30 m/sec. The inlet is at the top of the vortex chamber. The pressure in figure 4.18 increases from center toward the wall of the vortex chamber.

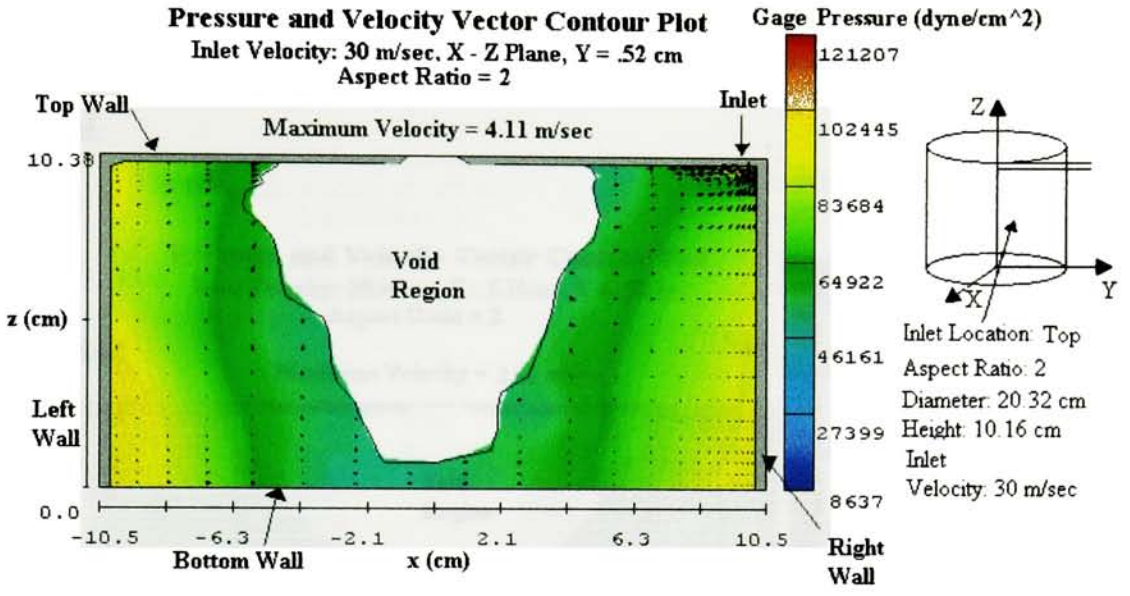

Figure 4.18 Contour Plot in the x-z plane, Aspect Ratio = 2, Inlet: Top,Velocity = 30 m/s

The vortex chamber with an aspect ratio of 2 has the bigger diameter of all the cases studied. Because of a bigger diameter, the fluid path from inlet to bottom outlet is larger than the other cases studied. As a consequence the pressure drop due to skin friction is larger for this case and the fluid particles lose more kinetic energy. Therefore the fluids particles tends to be less turbulent than in the cases with smaller aspect ratio. In a highly turbulent fluid, the instantaneous pressure will fluctuate more and the probability of getting more vapor is higher.

The inlet velocity in figure 4.18 is 30 m/sec. Figure 4.19 is the same vortex chamber with the same configuration but with an inlet velocity of 20 m/sec. Results shows that for a higher inlet velocity, larger is going to be the void region or free surface area. Therefore, the higher the inlet velocity for a vortex chamber with same dimensions and configurations, bigger is going to be the free surface area and therefore more vapor is going to be generated.

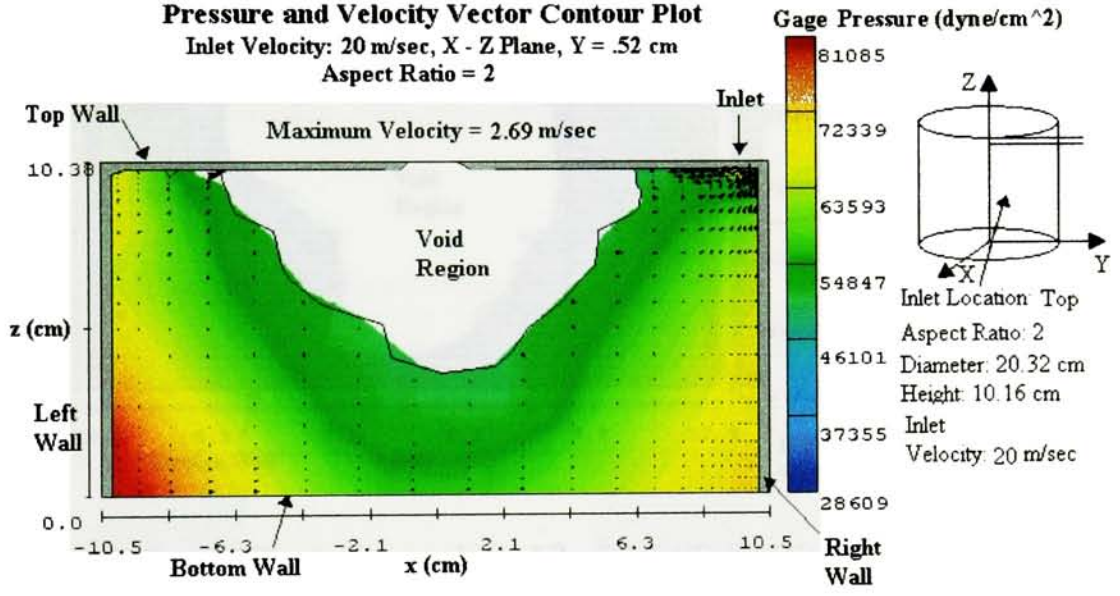

Figure 4.19 Contour Plot in the x-z plane, Aspect Ratio = 2, Inlet: Top,Velocity = 20 m/s

The vortex chamber presented in figure 4.19 has the same dimensions and configuration that the vortex chamber of figure 4.18. The only difference is that the inlet velocity is 20 m/sec instead of 30 m/sec. This is to show how the inlet velocity affect the size of the void region or the vapor volume. For this case, since the surface area is smaller, less vapor will be generated.

Also it can be appreciated that for lower inlet velocity, the pressure drop from wall to center of the vortex chamber is going to be smaller. For the case where the inlet velocity is 30 m/sec, the pressure drop from wall to center is approximately 4.5 KPa. For the case where the inlet velocity is 20 m/sec, the pressure drop from wall to center is approximately 2 KPa.

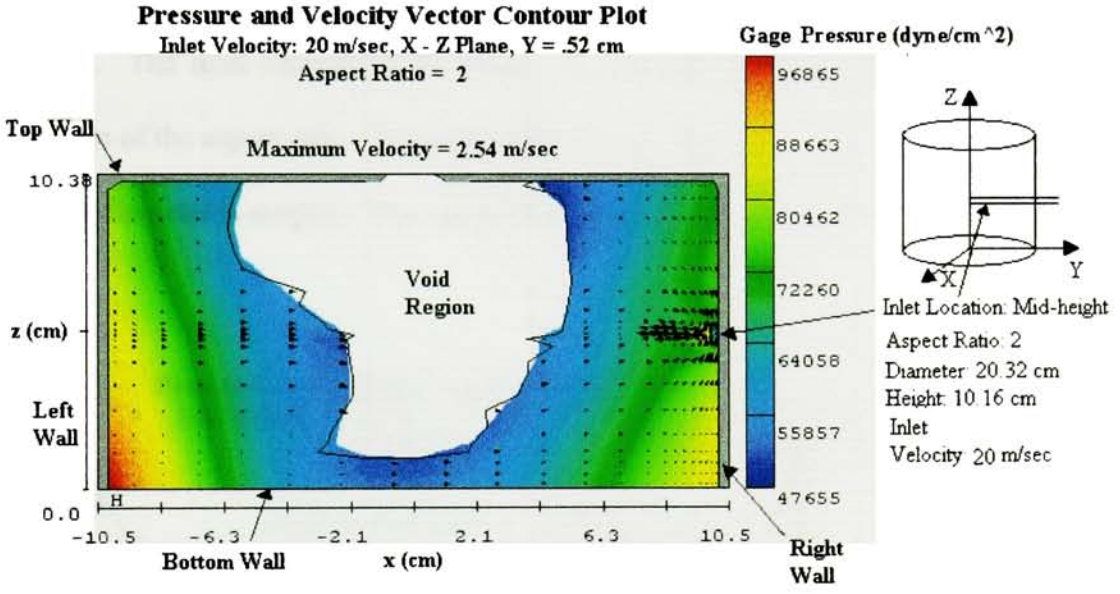

Figure 4.20 Contour Plot in the x-z plane, AR= 2, Inlet:Center,Velocity = 20 m/s

The vortex chamber in figures 4.19 and 4.20 have the same dimensions. The only difference is that the location of the inlet in figure 4.20 is at the center of the vortex chamber. The inlet velocity in both cases is the same 20 m/sec. Result shows that for the case were the inlet location is at the center of the vortex chamber, the surface area is larger. Therefore, more vapor is expected to be generated when the inlet location is at the center of the vortex chamber. The reason why more vapor is generated when the inlet location is at the center is because more advantage is taken from the momentum of the incoming solution. The mass

of fluid entering the chamber is used to push more effectively all the solution in the vortex chamber. This will generate a stronger swirl flow and therefore a bigger free surface area. A bigger surface area will generate more vapor because the mass transfer will be higher.

Figure 4.21 shows a contour plot for the pressure distribution and the velocity vectors for the case where the aspect ratio is 1.5 and the inlet location is at the center of the vortex chamber. The inlet velocity is 20 m/sec. Is basically the same as figure 4.20 with the difference of the aspect ratio. Since the aspect ratio in figure 4.21 is smaller, also the vortex chamber diameter is smaller. This means that the fluid path from inlet to bottom

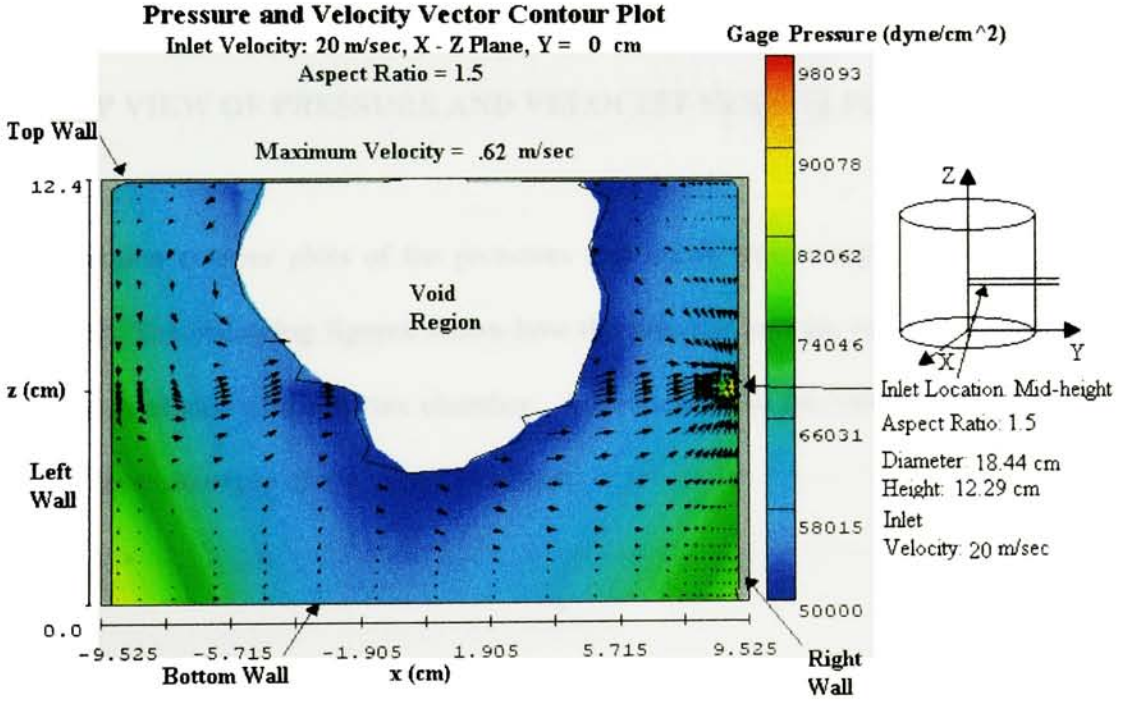

Figure 4.21 Contour Plot in the x-z plane, AR=1.5, Inlet:Center,Velocity = 20 m/s

exit is smaller than for the case where the aspect ratio is 2. As a consequence, the decrease in velocity due to friction is smaller. This will cause to generate a bigger surface area than in the case where the aspect ratio is 2 . Therefore more vapor is expected to be generated if the aspect ratio is reduced.

Also since the diameter is smaller for the case where the aspect ratio is 1.5, the velocity vectors are going to be higher and therefore the flow is more turbulent. There is more chance to generate more vapor in a turbulent flow than in a laminar flow due to the sudden changes in pressure and velocities.

4.7.2 TOP VIEW OF PRESSURE AND VELOCITY VECTOR PLOTS

In this section contour plots of the pressures and vector from a top view perspective is presented. The following figures shows how the pressure and the velocity vectors varies along the axial axis of the vortex chamber. Also shows how the void region increases in size from bottom to top of the vortex chamber.

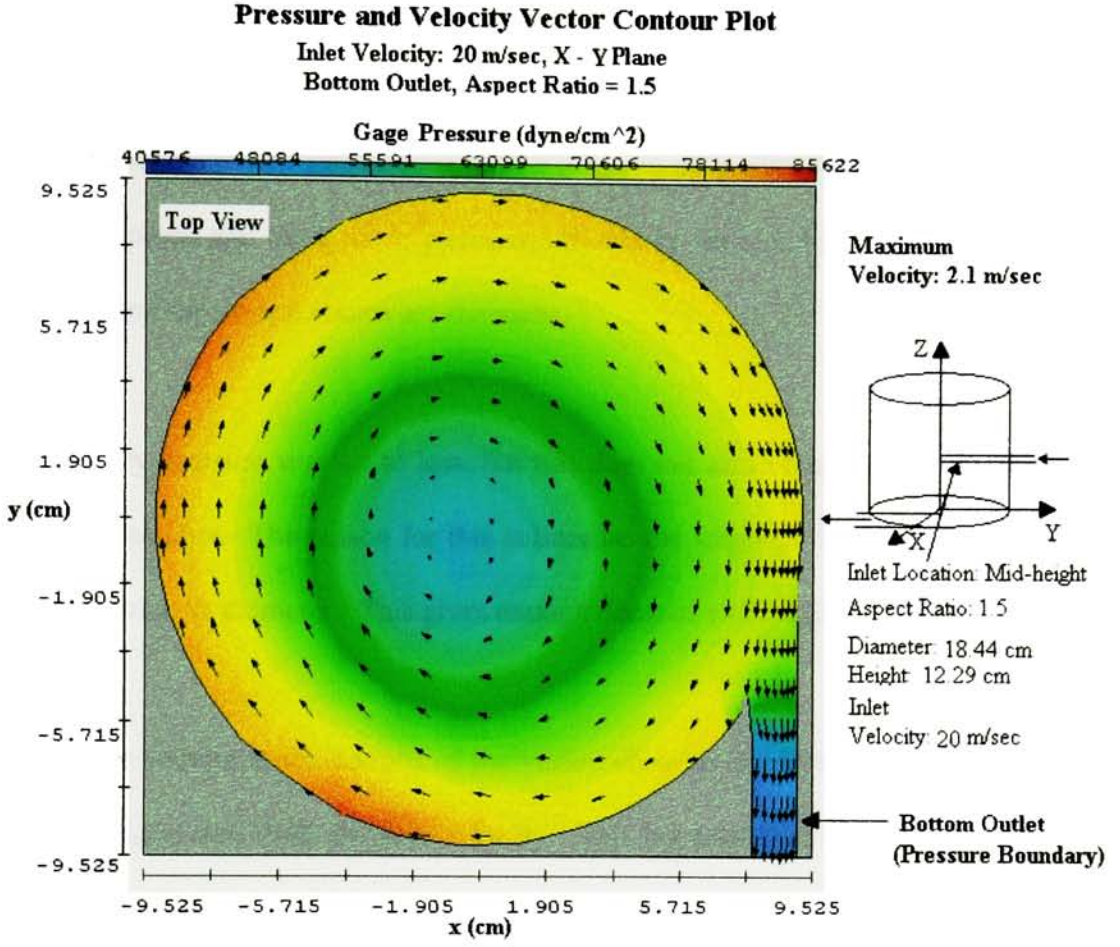

Figure 4.22 Contour Plot in the x-y plane, bottom location.

Figure 4.22 shows a contour plot of pressure and velocity vectors at the bottom of the vortex chamber. It can be seen from the figure that the highest pressure is at the wall and decreases toward the center of the vortex chamber.

At the outlet, the fluid particles accelerates. This means that the pressure boundary at the bottom outlet was set to low. The pressure drop across the outlet pipe in the simulation gave 2 KPa. Theoretical calculations gave a pressure drop across the bottom outlet of 1.2 KPa. This means that the boundary pressure should be set to 5.3 KPa so the results in the simulation and theoretical results are the same.

The boundary pressure was set to low, but this does not affect the pressure distribution in the vortex chamber. The reason for this is because the length of the bottom outlet pipe is more than twice its diameter. This gives enough distance to the fluid to recover.

The velocity vectors at the bottom of the vortex chamber are in the range of 2 to 3 m/s. This is approximately 10% the inlet velocity. This big reduction in the velocity is due to the skin friction and high viscosity of LiBr-Water solution.

The next figure 4.23 below, shows a pressure distribution and the velocity vectors at the inlet of the vortex chamber. The figure 4.23 shows a big pressure drop at the inlet. This is due to the high velocity at the inlet and the small diameter of the pipe. Also it can be appreciated how quick the inlet velocity is dissipated when the fluid particles enters the vortex chamber.

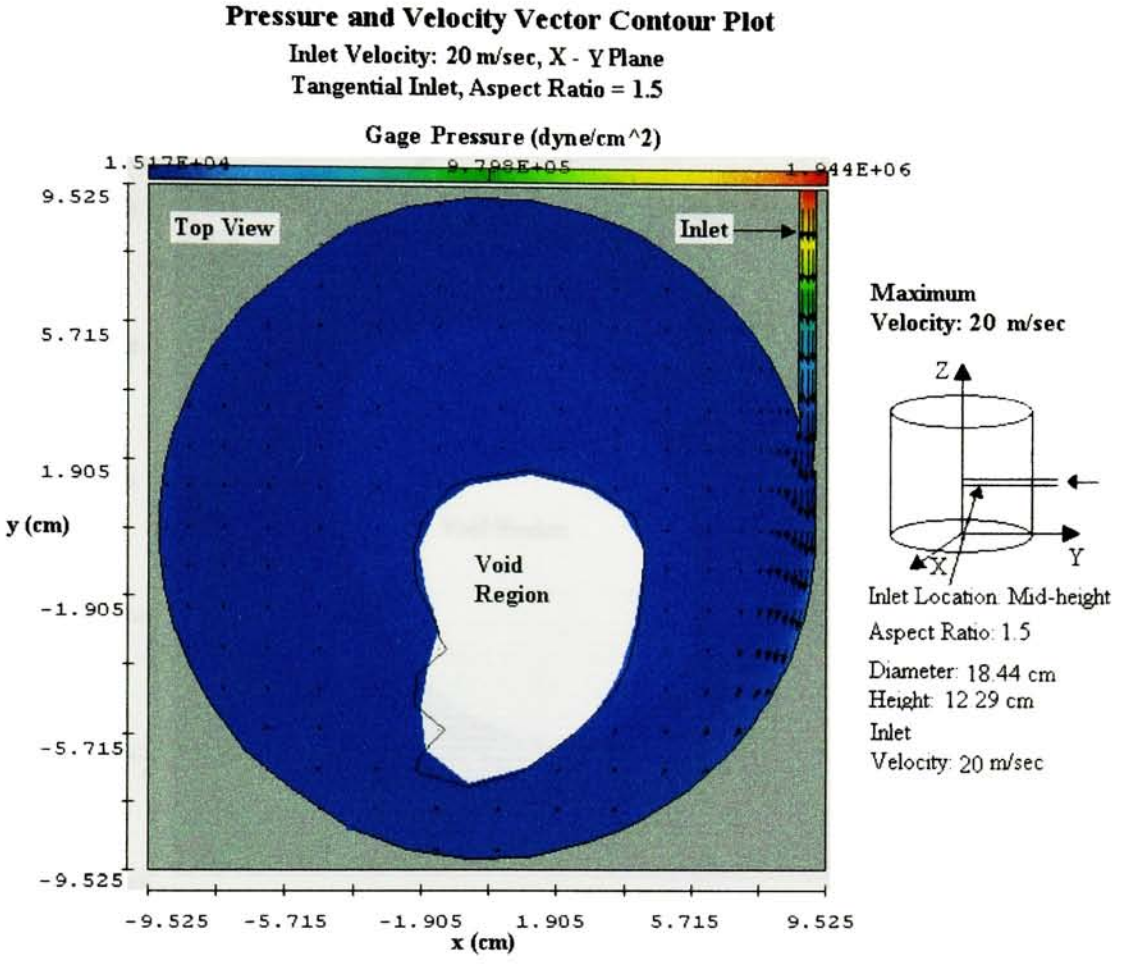

Figure 4.23 Contour Plot in the x-y plane, inlet location at center of the vortex chamber

In figure 4.23 also can be seen that the void region is shifted toward the inlet section. This is because in the inlet section the velocities of the particles are higher than in the rest of the vortex chamber and due to centrifugal force, the void region is going to be shifted to the higher velocity section. The fluid particles on the section with lower velocity tends to collapse and move toward the center of the chamber.

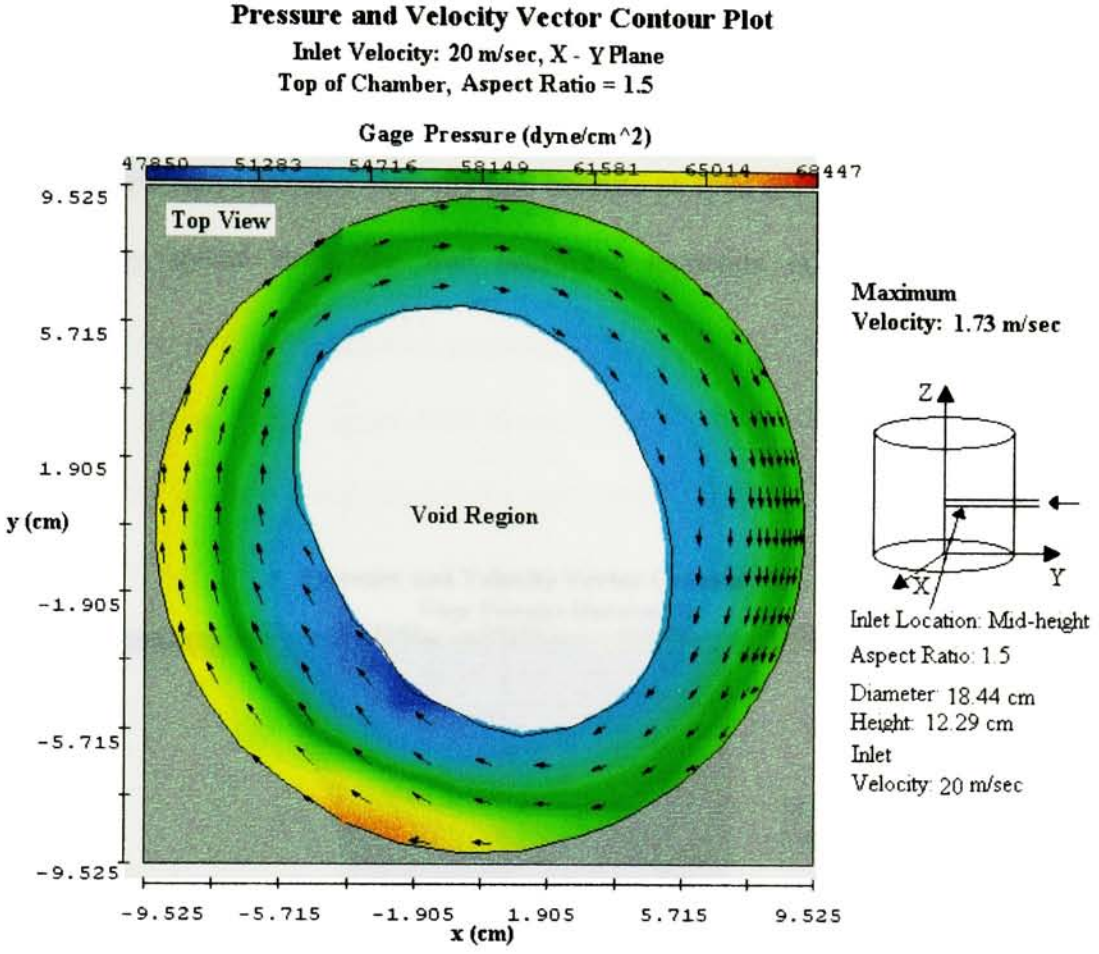

Figure 4.24 Contour Plot in the x-y plane, top of the vortex chamber

Figure 4.24 shows pressure contour plots and velocity vectors at the top of the vortex chamber. The inlet location for this case is at the center of the chamber. Again it can be appreciated the pressure drop toward the center of the vortex chamber. The velocity vectors are relatively low if compared with the inlet. This is due to the high friction at the top due to the side wall and top wall. The void region, as expected, is bigger at the top portion of the vortex chamber. Also in this figure, the void region is more centralized. This is because the velocity distribution in the radial direction is about the same in all directions.

A detail of the vortex chamber just after the inlet is presented in figure 4.25. It can be seen the fast decrease in the velocity vectors toward the center and along the wall surface. This is because LiBr-water solution viscosity and because as soon the fluid particles enters the chamber, they spread along the wall causing a reduction in velocity due to mass conservation.

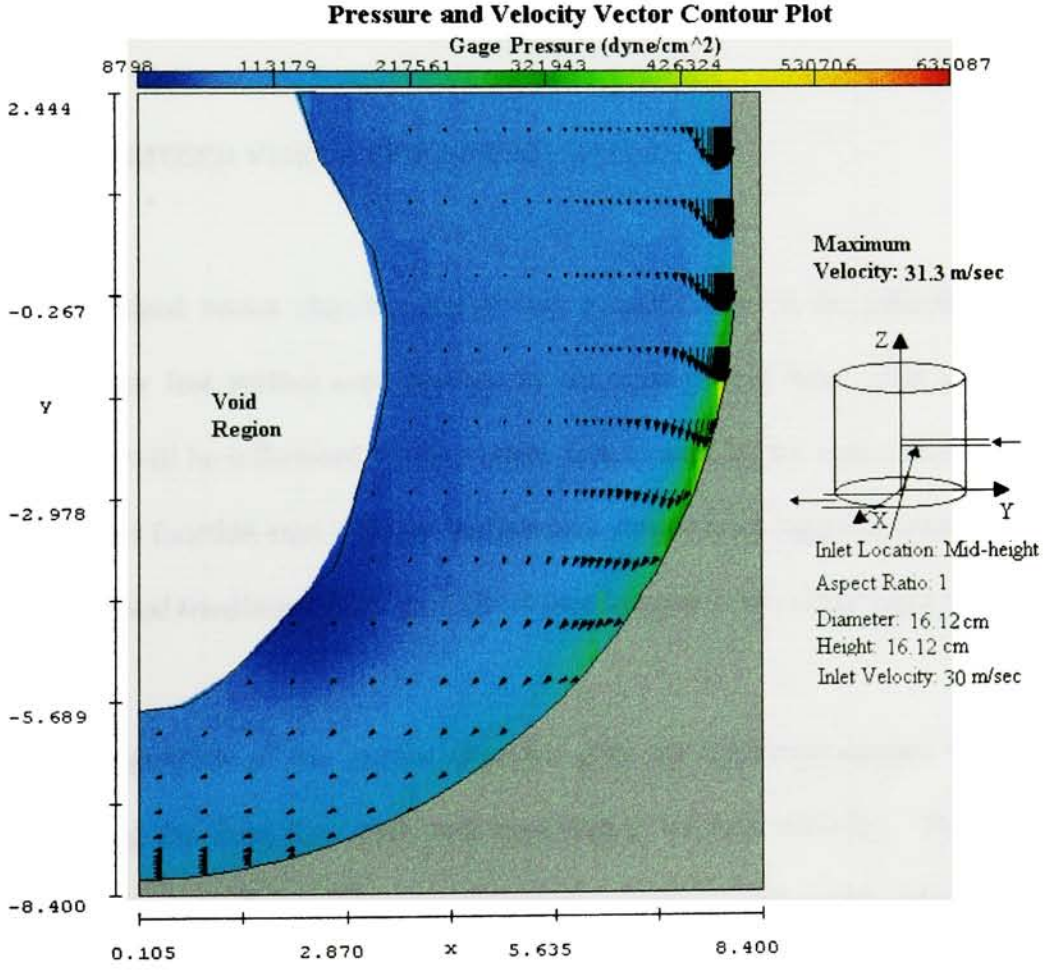

Figure 4.25 Contour Plot in the x-y plane, detail of the inlet section

This section also shows the non-slip condition at the wall of the vortex chamber. This is because the LiBr-water solution is a viscous solution. Therefore, the velocity of the fluid particles attached to the wall have to be zero m/sec. Also it can be appreciated that the velocity of the fluid particles increases from the wall toward the negative radial direction up to a certain distance from the wall of the chamber. This is the boundary layer region. After that, the tangential velocity starts to decrease with decreasing in radius. This is the forced vortex flow region. Also figure 4.25 shows the point of higher pressure in the vortex chamber. This is when the fluid entering the vortex chamber hit the wall that is right in front of the inlet.

4.8 OPTIMIZED VORTEX CHAMBER DESIGN

The optimized vortex chamber design was selected base on the LiBr-Water solution to water vapor free surface area develop by the strong swirl flow. The amount of vapor generated will be influenced by the surface area created by the vortex flow. Because mass transfer is a function area, a bigger surface area means that a bigger amount of vapor will be generated and transferred from the LiBr-Water solution to the water vapor region.

The configuration of the vortex chamber with the optimized design was obtained by minimizing the fluid flow path and maximizing the inlet velocity. This means that the optimized vortex chamber has a configuration with an aspect ratio of 1 and the inlet is located at the mid-height of the vortex chamber. The inlet velocity for the optimized design is 30 m/sec. The corresponding diameter and height for a vortex chamber with an aspect

ratio of 1 is 16.12 cm. design is 30 m/sec. The corresponding diameter and height for a vortex chamber with an aspect ratio of 1 is 16.12 cm.

4.8.1 PRESSURE DISTRIBUTION FOR THE OPTIMIZED DESIGN

Several pressure contour plots for the optimized vortex chamber design are presented to compare how the fluid flow behavior varies with location.

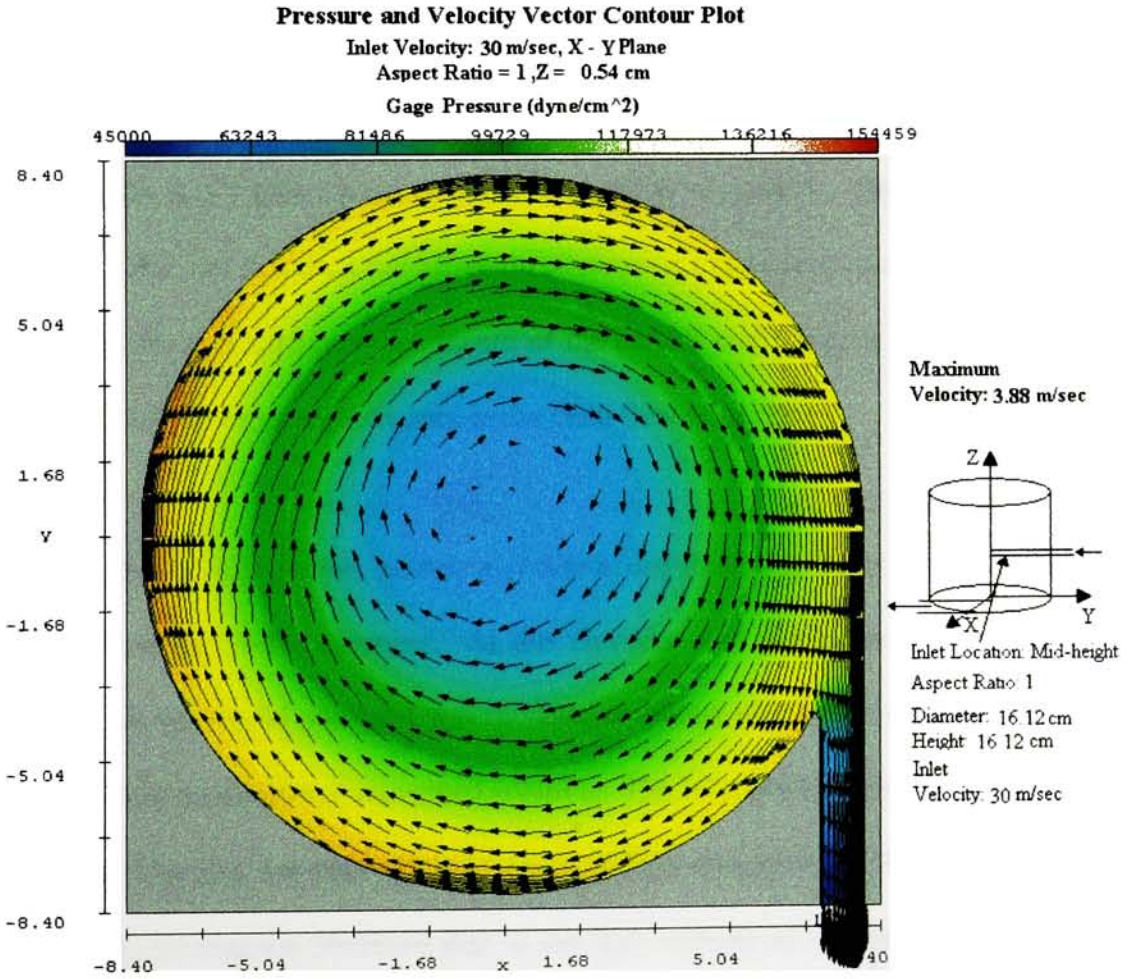

Figure 4.26. Pressure contour plot for the optimized design in the x-y plane at the bottom location of the chamber.

Figure 4.26 shows a contour plot of pressure and velocity vectors at the bottom of the optimized vortex chamber. In this figure, the highest pressure is at the wall and decreases toward the center of the vortex chamber. The tangential velocity is also higher close to the wall and decreases toward the center of the vortex chamber.

At the outlet, the fluid particles accelerates. This is because the pressure boundary at the bottom outlet was set to low. Results of the simulation shows a pressure drop across the bottom outlet pipe of 2.5 Kpa. Theoretical calculations shows that the pressure drop across the bottom outlet pipe is 1.21 KPa. From this can be concluded that the pressure at the bottom outlet is 5.7 KPa. It was initially assumed to be 4.5KPa. The boundary pressure was set to low, but this does not affect the pressure distribution in the vortex chamber. The reason for this is because the length of the bottom outlet pipe is more than twice its diameter. This gives enough distance to the fluid flow to recover.

The next figure 4.27 below, shows a pressure distribution and the velocity vectors at mid-height of the vortex chamber. At this elevation was placed the inlet of the vortex chamber. In the model, the inlet was modeled as a long pipe with a diameter of .49 cm. This was done to achieve a converged solution. The inlet configuration should looks like figure 3.3. The inlet was not modeled using a configuration similar to figure 3.3. because it was giving convergence problems due to the high velocity of the fluid particles and the drastic changes in cross sectional area.

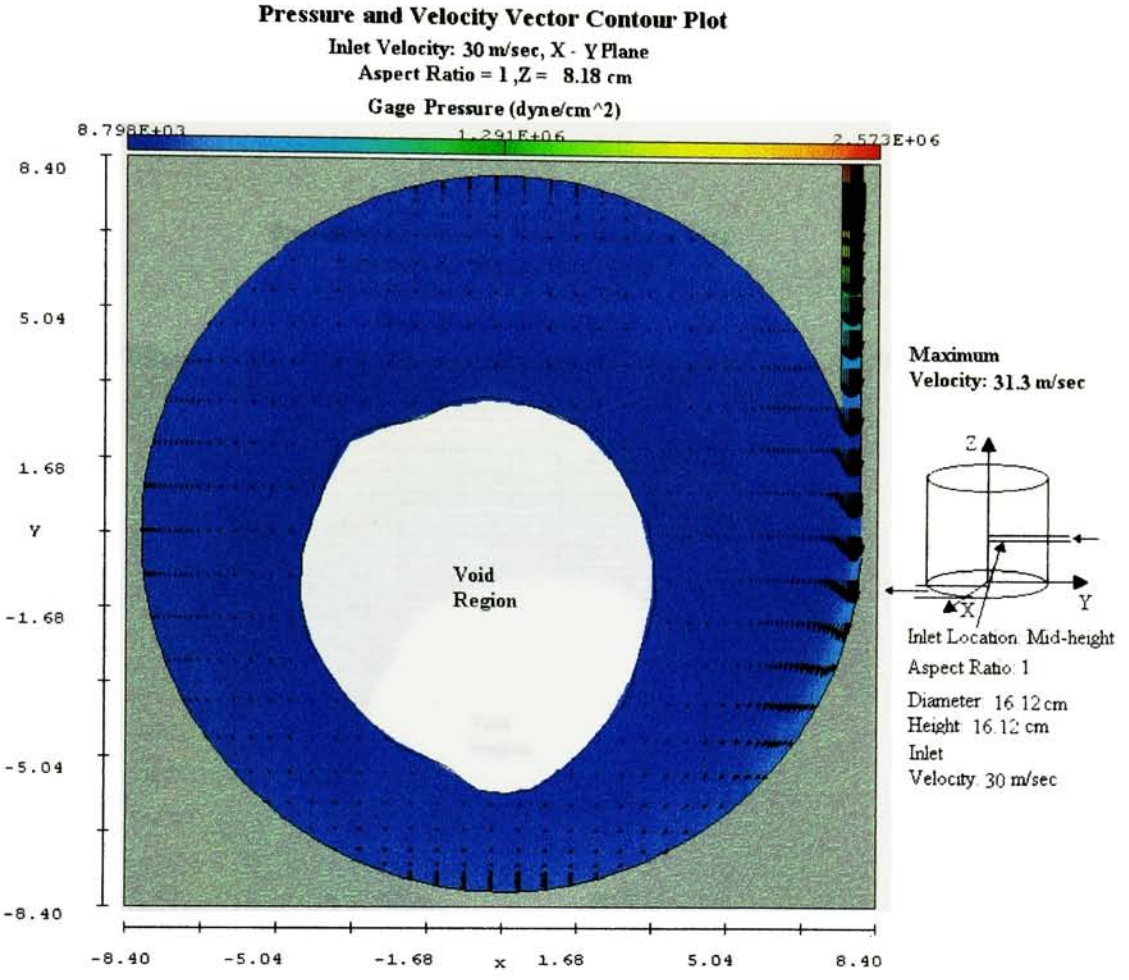

Figure 4.27 Pressure contour plot for the optimized design in the x-y plane at the mid-height elevation of the chamber.

In Figure 4.27, the high pressure drop at the inlet is due to the high velocity of the fluid particles and the small diameter of the pipe. Also it can be appreciated how fast the inlet velocity is dissipated when the fluid particles enters the vortex chamber. The velocity of the fluid particles entering the vortex chamber decrease due to mass conservation. The reason for this is because the vortex chamber space is very big if compared with the inlet diameter.

Figure 4.28 below shows a pressure distribution and velocity vector plot at the top of the optimized vortex chamber.

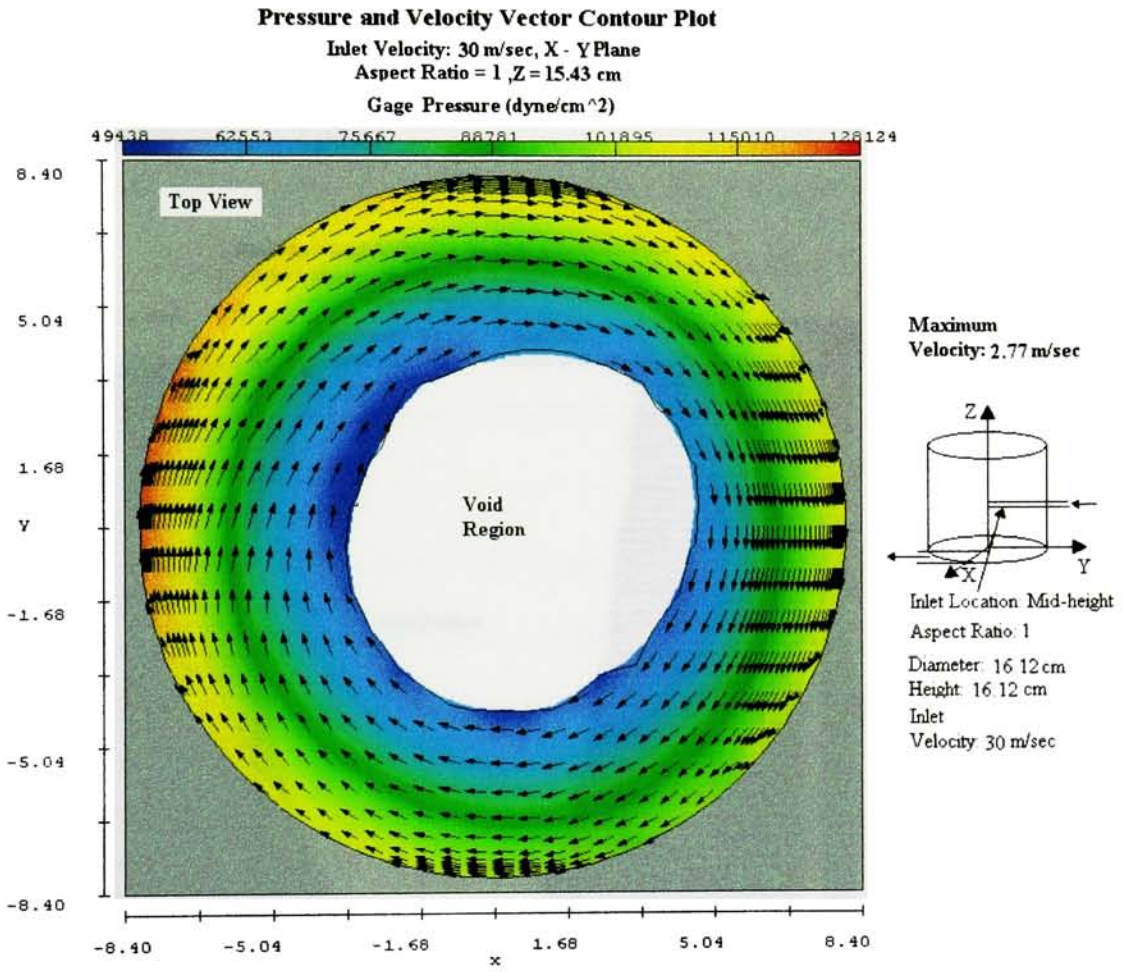

Figure 4.28. Pressure contour plot for the optimized design in the x-y plane at the top location of the chamber.

In this figure it can be appreciated the pressure drop from wall to center of the vortex chamber. Also it shows how the void region is shifted toward the right side of the vortex chamber. The shift of the void region is because the inlet is located at the right side of the

chamber. Therefore, the high velocity region is at the right side. This makes the centrifugal force bigger in magnitude toward the right side of the chamber and will create the shift of the void region.

Figure 4.29 below shows a pressure contour and velocity vector plot of the optimized vortex chamber in the x-z plane.

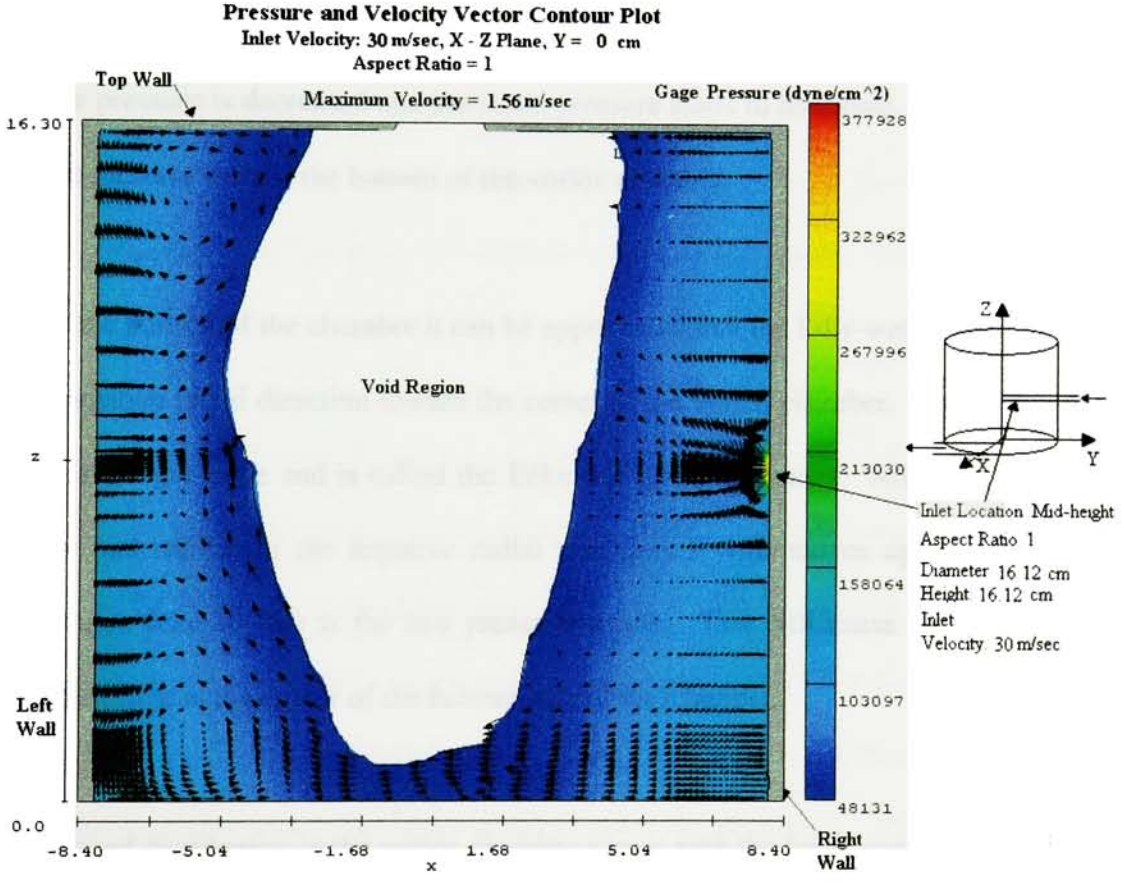

Figure 4.29. Pressure contour plot for the optimized design in the x-z

In figure 4.29 it can be appreciated how the pressure is reduced toward the center of the vortex chamber. This agrees with the theory of vortex flows. In the top section of the

figure, the solution tends to move toward the void region because of the top wall obstruction. The top wall will force the solution to move to the central portion of the chamber. It also generates a friction force to the solution. As a consequence the fluid particles will reduce in velocity causing a decrease in the centrifugal force. This will make the fluid particles to fall in the void region. The figure also shows that the pressure increases toward the bottom of the vortex chamber. This is because once the fluid particles enter the vortex chamber the velocity is reduced drastically. As a consequence, the dynamic pressure is decreased and the static pressure starts to dominate. This will cause a pressure increase toward the bottom of the vortex chamber.

Also at the bottom of the chamber it can be appreciated that the LiBr-water solution moves in the negative radial direction toward the center of the vortex chamber. This is due to the weak centrifugal force and is called the Eckman layer phenomena. After the LiBr-water solution had moved in the negative radial direction, it will moves up toward the free surface area because this is the low pressure region. This will cause the generation of circulating flow at the center of the bottom part of the chamber.

The pressure distribution in the vortex chamber agrees with the force vortex flow theory. It decreases with decreasing in radius.

4.8.2 VELOCITY MAGNITUDE AND VECTORS FOR THE OPTIMIZED DESIGN

The following figures shows velocity magnitude contours and vector plots for the optimized vortex chamber design at different elevations.

Figure 4.30 below shows the velocity magnitude and vector plots at the bottom of the optimized vortex chamber design. LiBr-water is a viscous solution. Therefore, the non-slip condition should be met. This means that the velocity of the fluid particles adjacent to the wall should be zero m/sec. That is why close to the wall of the vortex chamber, the tangential velocity of the fluid particles decreases as they approach to the wall.

At the bottom outlet, because LiBr-water solution is a viscous fluid, a velocity profile with a parabolic shape and maximum velocity at the center of the pipe should be appreciated. Because at the outlet, the LiBr-water solution is not a fully developed flow, the velocity profile with the parabolic shape is not well defined. But if the outlet pipe is extended, the fluid will turn to a fully developed flow and the velocity profile will be well defined. Also at the bottom outlet, the LiBr-water solution starts to accelerate. This means that the pressure boundary at the bottom outlet was set too low.

In general, it can be seen in figure 4.30, that the tangential velocity increases linearly with radius up to a critical radius. This critical radius, with the exception of the bottom and top part of the vortex chamber, is 7.5 cm. At the bottom and top of the vortex chamber, this critical radius is smaller (7 cm) due to the resistance offered to the flow by the bottom and

top walls. This agrees with the forced vortex flow theory. From that critical radius up to the wall, the tangential velocity starts to decrease until at the wall it becomes zero. This is the boundary layer region and can be observed in figure 4.32.

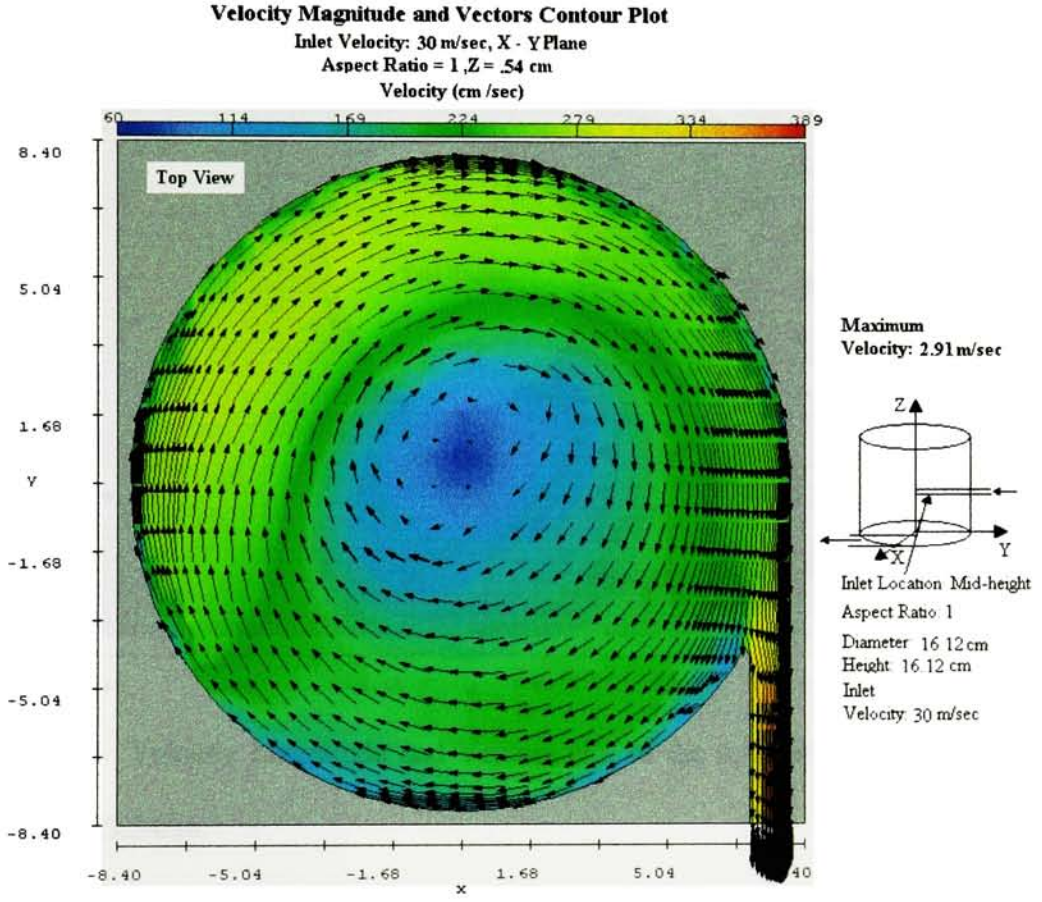

Figure 4.30 Velocity Magnitude and Vectors plot at the bottom of the optimized vortex chamber.

Figure 4.31 below is a velocity magnitude and vectors plot of the optimized vortex chamber at an elevation of 3.54 cm.

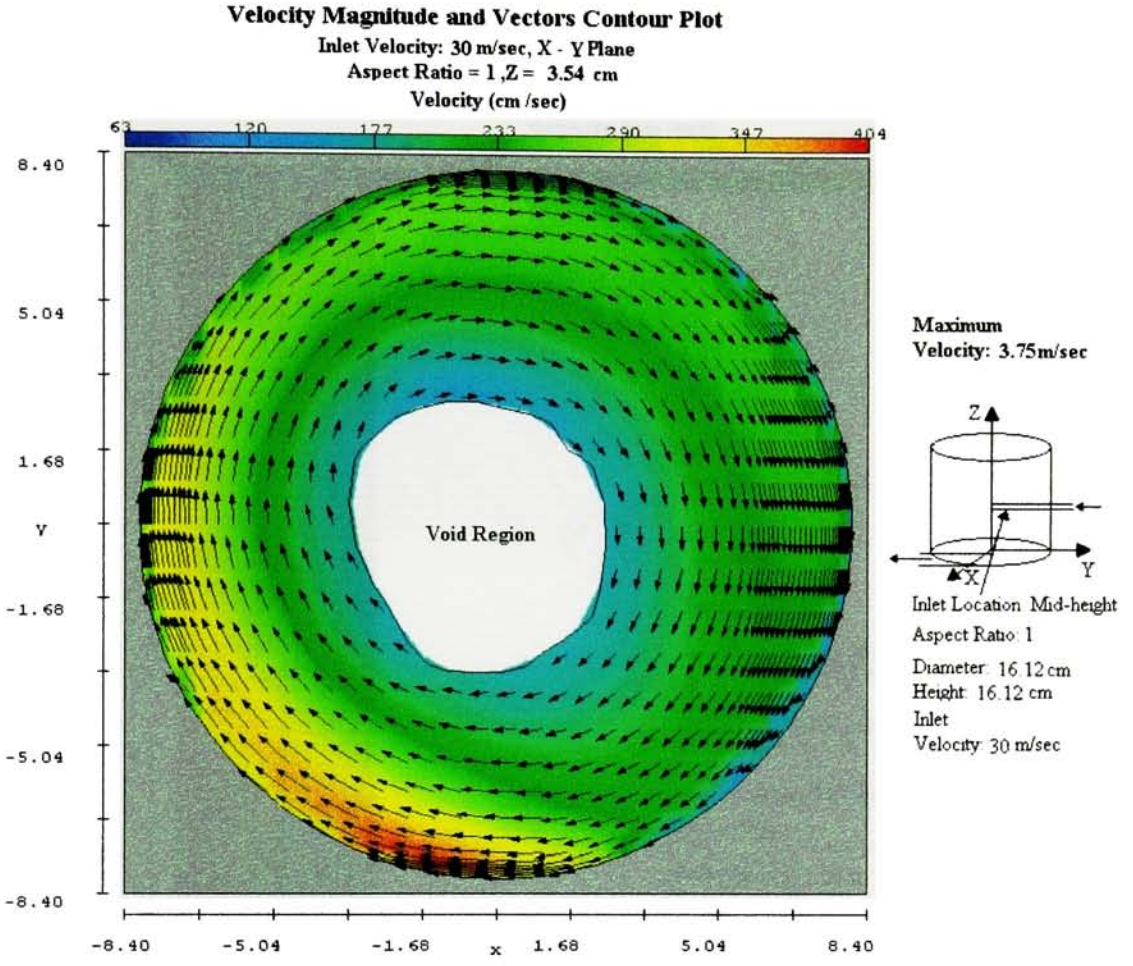

Figure 4.31 Velocity Magnitude and Vectors plot of the optimized vortex chamber at an elevation of 3.54cm.

In figure 4.31 the void region is at the center of the vortex chamber. The tangential velocity increases linearly with increasing in radius up to a critical radius of 7.5 cm. This linear increase in the tangential velocity agrees with the forced vortex flow theory. At a radius bigger than the critical radius, the tangential velocity starts to decrease until it vanishes at the wall. This is the boundary layer region. A detail of the tangential velocity close to the wall is presented in figure 4.32.

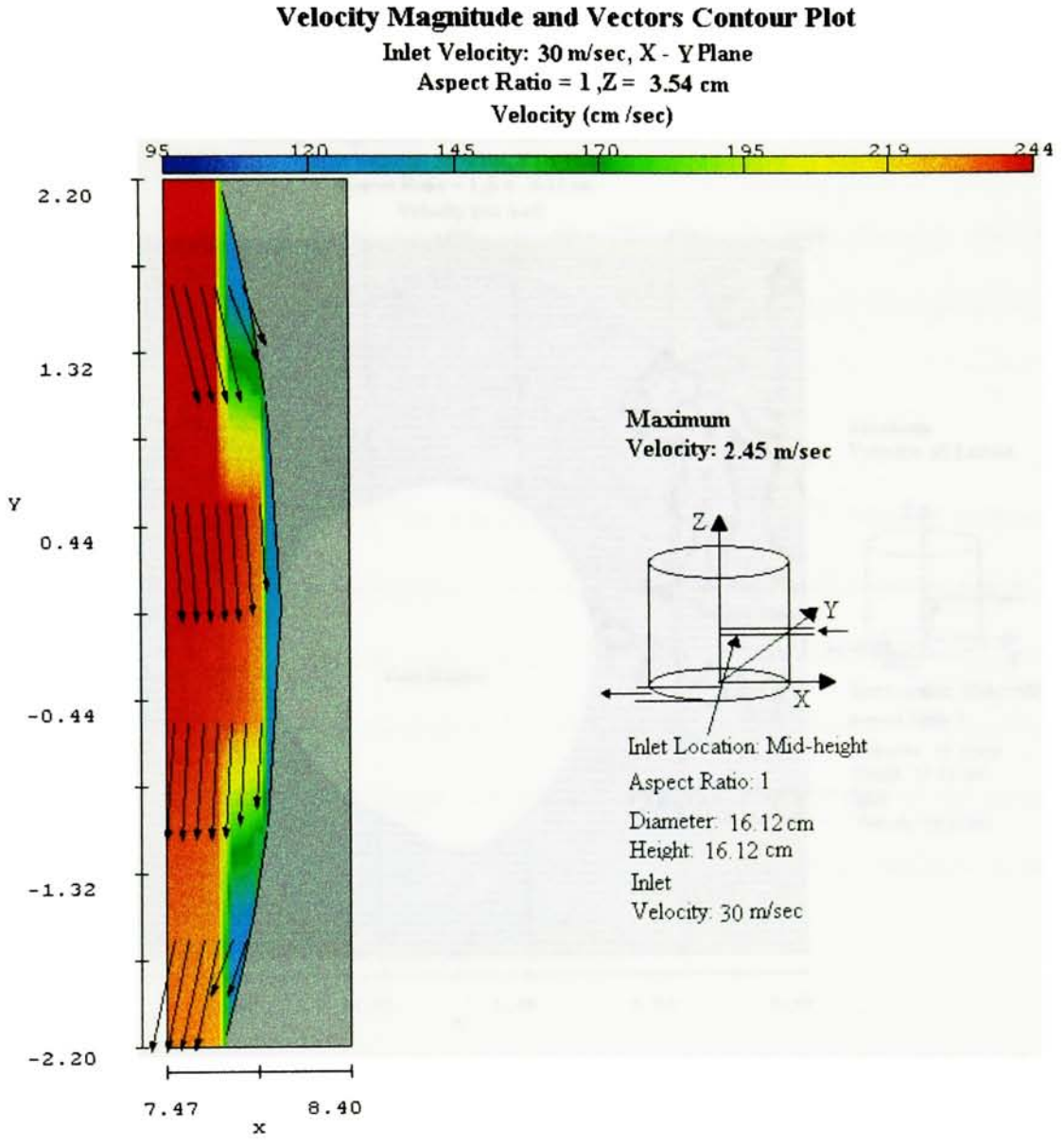

Figure 4.32 Detail of the tangential velocity close to the wall.

Figure 4.32 shows how the tangential velocity of the LiBr-water solution decreases as the fluid particles gets closer to the wall. At the wall the tangential velocity vanishes. This is the boundary layer region.

Figure 4.33 shows a top view of the velocity magnitude and vector contour plot at the mid-height elevation of the optimized vortex chamber.

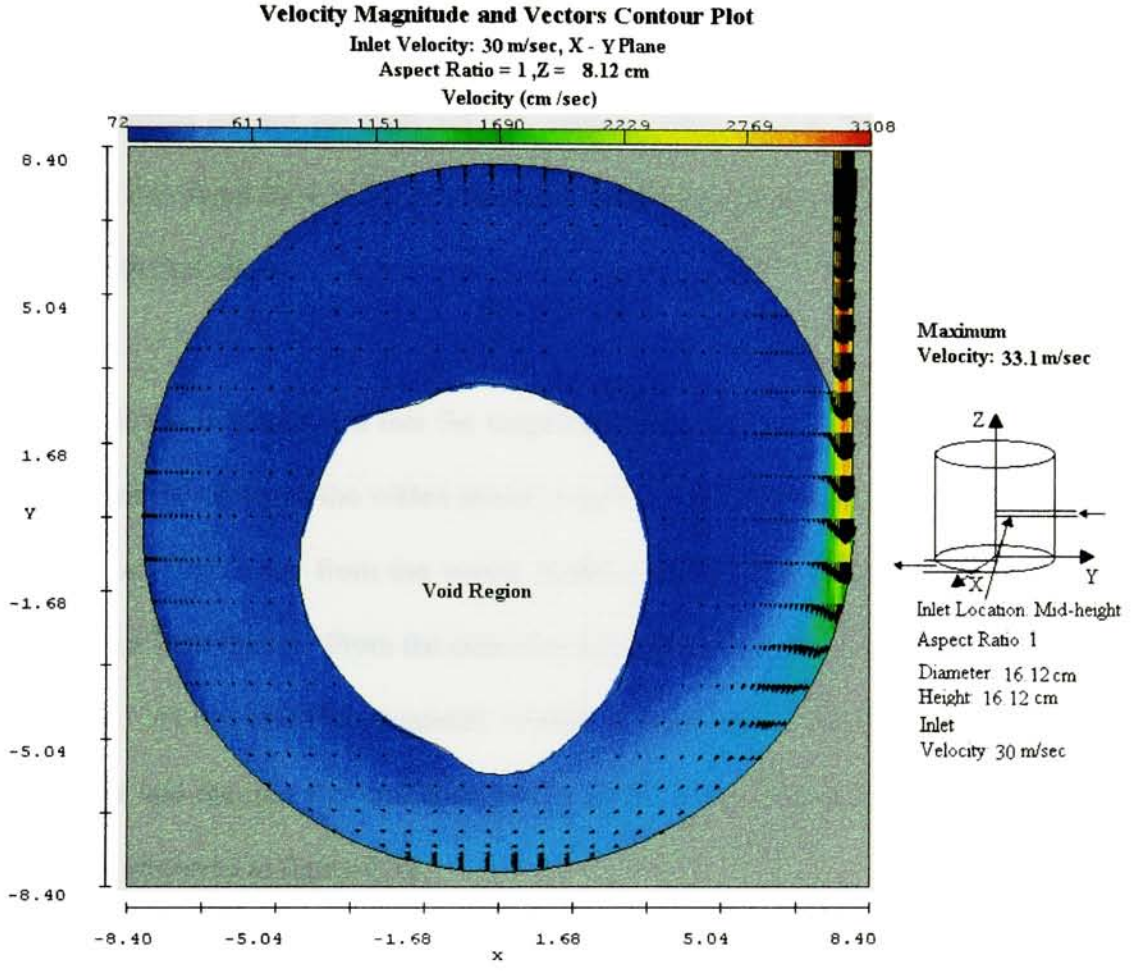

Figure 4.33 Velocity Magnitude and Vectors plot at a mid-height elevation of the optimized vortex chamber.

Figure 4.33 shows how fast the velocity of the incoming solution is reduced when it enters the vortex chamber. At the inlet, the LiBr-water solution is a fully develop flow. Therefore, the velocity profile with the parabolic shape with maximum velocity at the center of the pipe and zero velocity at the walls of the pipe is well defined. The sudden reduction

in the velocity of the fluid particles when it enters the chamber is due to the increase in the area of fluid flow. Due to mass conservation the velocity of the solution entering the vortex chamber has to decrease. Also it can be appreciated from the figure that the void region is shifted toward the high velocity region. This is because in the high velocity region the centrifugal force is higher, therefore the fluid particles are going to remain closer to the wall in that region.

In general it can be concluded that the tangential velocity in the vortex chamber increases linearly from the center of the vortex chamber up to a critical radius. This critical radius is at 7.5 cm or .5 cm away from the vortex chamber wall. This is in accordance with the forced vortex flow theory. From the critical radius to the wall, the tangential velocity starts to decrease. At the wall the tangential velocity is zero m/sec. This is due to the vicous flows effect and the non-slip condition is met at the wall. The non-slip condition at the wall can be observed in figure 4.32.

4.8.3 PRESSURE AND VELOCITY EQUATIONS FOR THE OPTIMIZED VORTEX CHAMBER

PRESSURE

The pressure and tangential and axial velocities in the optimized vortex chamber are function of position in the radial and axial direction. The pressure in the optimized vortex chamber can be predicted by equation 4.1.

$$P(r,z) := \sum_{i=0}^{9} coeffs_i \cdot r^{I_{i,0}} \cdot z^{I_{i,1}} \quad KPa \tag{4.1}$$

where r and z are the respective radius and chamber elevation and are in centimeters. The coefficients for equation 4.1 can be obtained from table 4.7.

$I =$

	0	1
0	1	2
1	0	3
2	0	2
3	0	1
4	1	1
5	2	1
6	0	0
7	1	0
8	2	0
9	3	0

$coeffs =$

	0
0	0.00099458189744
1	-0.003136553487395
2	0.076929146486706
3	-0.4398649751487
4	-0.119653316693047
5	0.009482369892946
6	5.46412716881313
7	0.210769729600339
8	0.109294737402431
9	0.00271378447939

Table 4.7. Table of power for each monomial and coefficients for the pressure equation of the optimized vortex chamber

In table 4.7, the first column of I gives the power of the radius r term of each monomial and the second column gives the corresponding power of the elevation z term. The rows of I and coeffs correspond.

Equation 4.1 was developed using multivariative least square method for polynomial fit curves. The multiple correlation coefficient squared (R^2) for the fitted equation is 0.9937. Figure 4.33 below represents the vortex chamber pressure as a function of radius and elevation. Also shows the corresponding fitted curve.

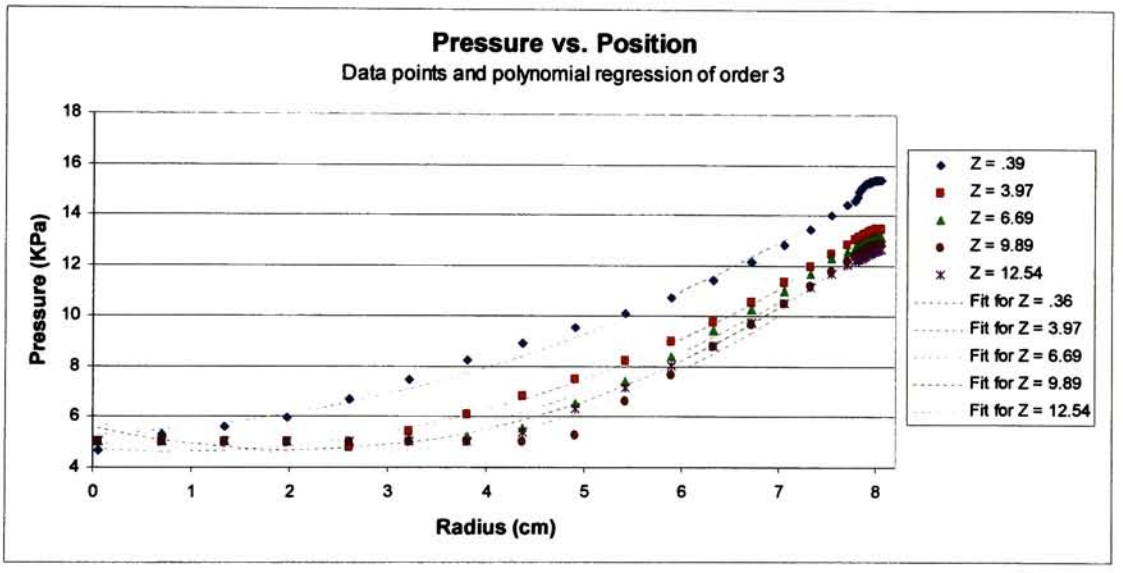

Figure 4.34. Graph of pressure versus position for the optimized vortex chamber.

VELOCITY

Same procedure was used to obtain a suitable curve fit for the tangential and axial velocities. For the tangential velocity, two equation where derived to fit the data. One equation fits the data points of the central portion of the vortex chamber and the other

equation fits the data points close to the vortex chamber wall (the boundary layer). The tangential velocity in the optimized vortex chamber can be predicted by equation 4.2.

$$V_\theta(r,z) := \sum_{i=0}^{14} coeffs_i \cdot r^{I_{i,0}} \cdot z^{I_{i,1}} \quad cm/sec \tag{4.2}$$

where r and z are the respective radius and chamber elevation and are in centimeters. The coefficients for equation 4.2 can be obtained from table 4.8.

I =

	0	1
0	1	3
1	0	4
2	0	3
3	0	2
4	1	2
5	2	2
6	0	1
7	1	1
8	2	1
9	3	1
10	0	0
11	1	0
12	2	0
13	3	0
14	4	0

coeffs =

	For 4 < R < 7.5
	0
0	-0.036343682491699
1	0.033101564288803
2	-0.504948532006731
3	12.1816292308181
4	-2.05316656647552
5	0.140404156384024
6	-316.861947054866
7	111.435042746752
8	-13.9731692845692
9	0.638979967589772
10	-4187.02563310988
11	3261.76512914627
12	-877.711540806701
13	103.151803115783
14	-4.47488311348024

coeffs =

	For 7.5 < R < 8.1
	0
0	-0.271785431629609
1	-0.017976318923379
2	2.74016281681482
3	238.80800147004
4	-69.1194231184806
5	4.81092224781898
6	57592.4914159711
7	-22698.3409142354
8	2986.04903285183
9	-131.022596014987
10	-77501680.5577893
11	40105968.3172743
12	-7781839.65100946
13	670994.005013122
14	-21693.6211527169

Table 4.8. Table of power for each monomial and coefficients for the tangential velocity equation of the optimized vortex chamber.

In table 4.8, the first column of I gives the power of the radius r term of each monomial and the second column gives the corresponding power of the elevation z term. The rows of I and coeffs correspond. Table 4.8 shows two tables for the coefficients of the polynomial fit. The table to use depends on the radius range. For a radius below R = 4 cm, no curve was fitted to the data. The reason for this is because for a radius below R = 4 cm there is

no fluid present. This is the void region. If this region is included in the development of the equation to fit the data, the error will increase. The multiple correlation coefficient squared (R^2) for the fitted equation 4.2 is 0.8995 for a radius within the range of 4 to 7.5 cm, and .8271 for the boundary layer region (R>7.5 cm). Figure 4.34 below represents the vortex chamber tangential velocity as a function of radius and elevation.

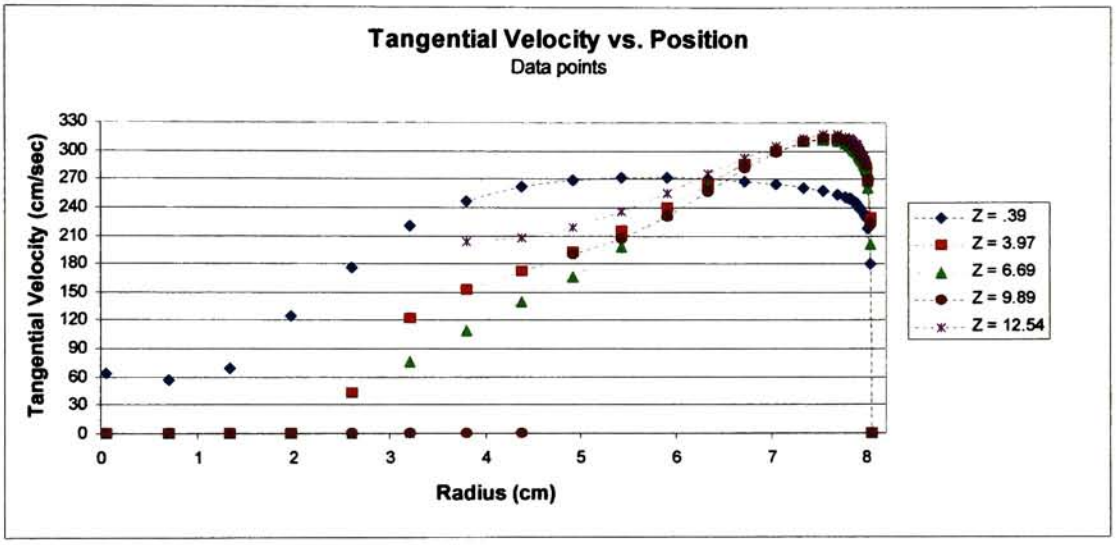

Figure 4.35. Graph of tangential velocity versus position for the optimized vortex chamber.

From figure 4.35 it can be seen how the non-slip condition at the wall is met. For a radius bigger than 7.5 cm, the tangential velocity starts to decrease and at the wall (radius = 8.06 cm) the velocity is zero. This is the boundary layer region and a detail of this region can be seen in figure 4.36. The non-slip condition is met at all the elevations. Figure 4.35 also shows, with the exception of the bottom and top of the vortex chamber, that the tangential velocity has a weak dependence on the elevation of the vortex chamber. At the top and

bottom of the vortex chamber the tangential velocity is smaller because of the wall effects of the top and bottom walls.

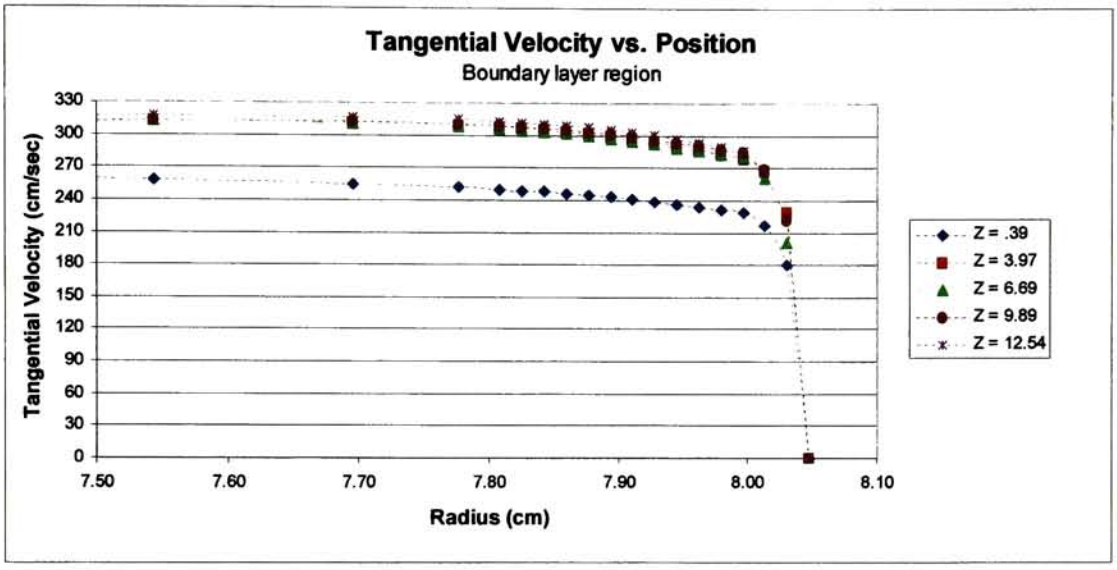

Figure 4.36. Graph of tangential velocity versus position for the optimized vortex chamber at the boundary layer region.

Similar procedure can be use to predict the axial velocity component of the solution within the vortex chamber. The axial velocity in the optimized vortex chamber can be predicted by equation 4.3

$$V_Z(r,z) := \sum_{i=0}^{27} coeffs_i \cdot r^{I_{i,0}} \cdot z^{I_{i,1}} \quad \text{cm/sec} \qquad (4.3)$$

where r and z are the respective radius and chamber elevation and are in centimeters. The coefficients for equation 4.3 can be obtained from table 4.9.

I =

	0	1
0	1	5
1	0	6
2	0	5
3	0	4
4	1	4
5	2	4
6	0	3
7	1	3
8	2	3
9	3	3
10	0	2
11	1	2
12	2	2
13	3	2

	0	1
14	4	2
15	0	1
16	1	1
17	2	1
18	3	1
19	4	1
20	5	1
21	0	0
22	1	0
23	2	0
24	3	0
25	4	0
26	5	0
27	6	0

coeffs =

	0
0	0.000431847866201
1	-0.000014477931407
2	-0.004805419395057
3	-0.479052803177357
4	0.188044357659941
5	-0.014416157344248
6	3.9897358459377
7	0.501474323201657
8	-0.551962109619521
9	0.049552641919227
10	-44.4771658552465
11	19.9314918295351
12	-7.36318529618442
13	1.59773393749025

	0
14	-0.109126177453099
15	8153.78429484149
16	-6809.31671976898
17	2260.84808637315
18	-369.639153880221
19	29.5322173284267
20	-0.919262994821535
21	14676.8308377606
22	-22751.4393437993
23	12877.0097607098
24	-3596.69915435449
25	535.782703622944
26	-40.8950025793878
27	1.25960333000672

Table 4.9. Table of power for each monomial and coefficients for the axial velocity equation of the optimized vortex chamber

In table 4.9, the first column of I gives the power of the radius r term of each monomial and the second column gives the corresponding power of the elevation z term. The rows of I and coeffs correspond.

Equation 4.3 was developed using multivariative least square method for polynomial fit curves. The multiple correlation coefficient squared (R^2) for the fitted equation is 0.9723. Equation 4.3 is valid for R > 4 cm. Figure 4.37 below represents the vortex chamber pressure as a function of radius and elevation. Also shows the corresponding fitted curve.

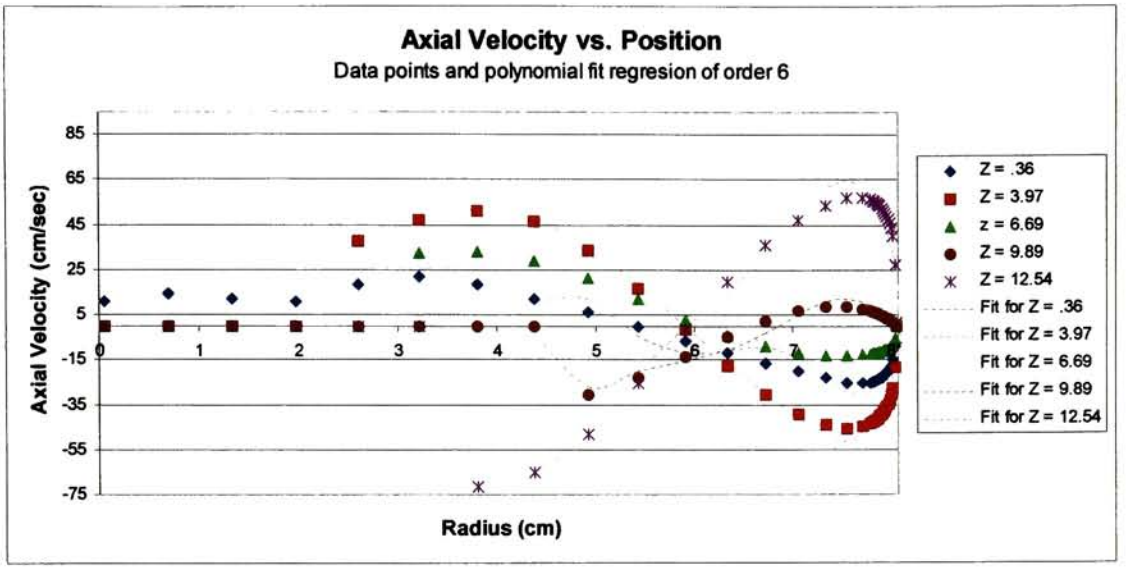

Figure 4.37. Graph of axial velocity versus position for the optimized vortex chamber.

Figure 4.37 shows the axial velocity component vanishing as it approaches to the wall of the vortex chamber. From the graph it can be appreciated that the axial velocity for the fluid adjacent to the wall, points in the negative axial direction if it is below the elevation of the inlet. On the other hand, the axial velocity for the fluid adjacent to the wall, points in the positive axial direction if its above the elevation of the inlet. For both cases, the direction of the axial velocity component is reverse at a radius of approximately 6 cm. This is because the top and bottom walls of the chamber forces the fluid to change its direction.

The procedure that shows the development for the pressure and velocity equations can be found in Appendix D.

CHAPTER

FIVE

CONCLUSIONS

The study performed helps to understand the behavior of the LiBr-Water solution in the vortex chamber. Even the results are not totally accurate due to the limitations of the CFD code utilize, it establishes a clear idea of what is happening inside the vortex chamber. Also helps to investigates the theory of the vortex chamber presented by Dr. Fineblum.

From the study performed the following can be concluded:

1. The flow formed in the chamber is a forced vortex flow.
2. The LiBr-Water solution is a viscous fluid and at the vortex chamber wall the non-slip condition is met.
3. The pressure distribution in the vortex chamber
    A. The pressure decreases toward the center of the vortex chamber.
    B. The pressure increases linearly in the in the axial direction toward the bottom of the vortex chamber.

4. Velocity Distribution

A. Tangential Velocity. The tangential velocity increases linearly with radius up to a certain critical radius. This is the forced vortex flow region. From the critical radius to the vortex chamber wall, the tangential velocity decreases. At the wall, the tangential velocity vanishes. This is the boundary layer region. With the exception of the top and bottom part of the vortex chamber, the tangential velocity is almost constant along the axial axis.

B. Radial Velocity. The radial velocity toward the center of the vortex chamber is more pronounced near the bottom and top wall. The phenomena of the fluid particles moving in the negative radial direction at the bottom of the chamber is called the Eckman layer (Sakai, 1996).

C. Axial Velocity. The axial velocity is more pronounced at the top of the chamber. Due to the loss of centrifugal force, fluid particles falls into the void region.

5. Lithium Bromide - Water solution to Water Vapor free surface area

The free surface area is increased by increasing the inlet velocity and decreasing in aspect ratio. A bigger surface area is obtained if the inlet is placed at the mid-height of the vortex chamber.

6. Optimized Vortex Chamber Design.

The optimized vortex chamber design was selected base on the biggest free surface area of the cases studied. The configuration of the optimized vortex chamber design is as follows:

Aspect Ratio = 1

Diameter = 16.12 cm, Height = 16.12 cm

Inlet Location: Mid-height of the vortex chamber

Inlet Velocity = 30 m/sec

CHAPTER

SIX

RECOMMENDATIONS

Based on the on the results and the limitations found during the study of the vortex chamber, the following is recommended:

1. Bottom Outlet Design

   The bottom outlet diameter should be big enough to achieve a laminar flow and therefore minimize the pressure drop across it. It also should have a valve to control the outflow and avoid the vortex chamber to empty.

2. Inlet Design

   The pressure drop at the inlet is very high. This is due to the high velocity of the fluid particles at the inlet and the small diameter of the pipe in that section. To compensate this big pressure drop at the inlet, a bigger pump will have to be added to the system. To get optimum results of the vortex chamber, a better inlet design will have to be made to reduce the pressure drop across it.

3. Development of new CFD code with evaporation model.

Flow 3D was the CFD code utilize for this investigation. The software was capable to solve the fluid dynamics part of the vortex chamber but was not capable to solve the transition from LiBr-water to water vapor when evaporation was occurring. The reason for this is because FLOW 3D does not have an evaporation model. A CFD code should be develop to model more accurately the vortex chamber. The CFD code should have the following characteristics.

A. It should have an evaporation model. The evaporation model should be base on pressure and not temperature. It should be capable of model transition from LiBr-water to water vapor at the free surface region. Also the evaporation model should consider that only a fraction of the solution is evaporated.

B. The CFD code should be capable of modeling the lower and upper vortex chamber inlet and the condenser together. There is a pressure relation from the lower vortex chamber to the condenser. This relation is not known because there is no knowledge of the behavior of gas dynamics in the upper chamber. What is known is that the condenser operates at the saturation pressure of the solution and this can be use as a boundary condition.

4. Design of a Vortex Chamber with at least two inlet.

Design of a vortex chamber with at least two inlet is recommended to obtain

better symmetry in the fluid flow. These inlets should be placed in opposite sides of the vortex chamber and should be pointing in opposite directions.

REFERENCES

ASHRAE 1983 Equipment Handbook, American Society of Heating, Refrigerating and Air - Conditioning Engineers, Inc. Atlanta, 1993, page 14.1 - 14.6

ASHRAE 1993 Fundamentals Handbook, American Society of Heating, Refrigerating and Air - Conditioning Engineers, Inc. Atlanta, 1993, page 1.22, 1.23, 16.2 ,17.82, 17.83,

Camp, R. Heath, K. , Rosenberg, R. , "Vortex Phase Separator", Technical Report - Senior Design Project, Rochester Institute of Technology, Rochester, NY,1999

Dorgan, C . B., Leight, S. P., Dorgan, C. E., " Application Guide for Absorption Cooling / Refrigeration Using Recovered Heat", ASHRAE, Atlanta 1995, page 3, 18

Fineblum, S., "An Improved Absorption Generator for Solar-Thermal Powered Heat Pumps - Part 1", Megadyne Incorporated, Rochester, NY

Fineblum, S., "An Improved Absorption Generator for Solar-Thermal Powered Heat Pumps - Part 2", Megadyne Incorporated, Rochester, NY

Fineblum, S., "Feasibility Analysis of a Vortex Generator for Absorption Heat Pumps", ASME Advance Energy System Div., AES vol. 36 , ASME, NY, 1996, page 395-412

Flow Science, Inc, "Flow-3D Users Manual", Flow Science, Inc. 1999

Fluent, Inc., "Fluent - Users Manual", Fluent, Inc, March 1996, page 13.2-13.22

Gerhart P. , Gross R., Hochstein J.,"Fundamentals of Fluid Mechanics", 2nd ed., Addison-Wesley 1992, page 311-386

Granger, Robert A. , " A Forced Vortex Flow", Ph.D. Thesis,University of Michigan, College Park, 1978.

Guyer, E., " Handbook of Applied ThermalDesign", McGraw - Hill, NY, 1988, page 9.33 - 9.39

Herold, K. "Absorption Chillers and Heat Pumps" , 1996, page 32, 33, 63 - 143

Herold, Keith, " Design Challenge in Absorption Chillers", ASME, Advance Energy Systems Division, October 1995, page 80-83

Hirt, C.W., Harper,R.P., "Flow in a Vortex Chamber", Flow Science, Inc., May 1998

Hodge, B., "Analysis and Design of Energy Systems", Prentice Hall, 1990, page 1- 19

King, M. , Rothfus, R., Kermode R., " Static Pressure and Velocity Profiles in Swirling Incompressible Tube Flow" AIChE Journal, Vol. 15, No. 36, 1996, page 837-842

MacNeil, R. , Mizo, V. , " CFD Analysis of Vortex Chamber Generator", Technical Report Rochester Institute of Technology, Rochester, NY, Spring 1995

Sakai S. , Madarame H. , Okamoto K., " Gas Core Shape and Velocity Distribution around a Bathtub Vortex", 1996 Fluids Engineering Division Conference, Volume 3, ASME 1996

Swokowski E., Olinik M., Pence D., " Calculus", PWS Publishing Company, Boston, MA, 1994, page 468 - 477

APPENDIXES

APPENDIX A. Example of Calculation for the Pressure Drop at the Vortex Chamber Inlet

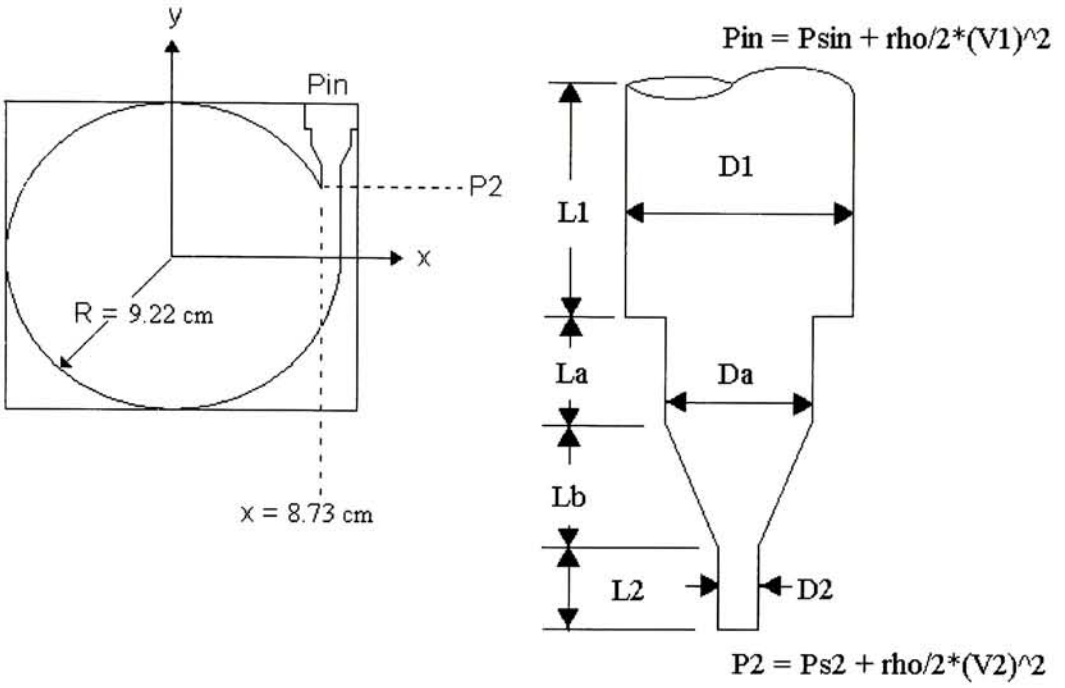

Inputs:

Length	Diameter	Chamber Radius	LiBr-Water Properties
$L_1 := 2.54cm$	$D_1 := 1.27cm$	$R := 10.16cm$	$\rho := 1670\frac{kg}{m^3}$
$L_a := 1.27cm$	$D_a := .927cm$		$\mu := .0029\frac{kg}{m \cdot s}$
$L_b := 1.27cm$	$D_2 := .485cm$		

L_2 varies with the chamber radius

$$L_2 := R - L_1 - L_a - L_b - \sqrt{R^2 - (R - D_2)^2} \qquad L_2 = 1.978cm$$

Inlet Velocity	Pipe Roughness
$V_2 := 30\frac{m}{s}$	$\varepsilon := .000046m$

Calculation of Velocities Va and V1

$$V_a := V_2 \cdot \left(\frac{D_2}{D_a}\right)^2 \qquad V_a = 8.212\frac{m}{s}$$

$$V_1 := V_2 \cdot \left(\frac{D_2}{D_1}\right)^2 \qquad V_1 = 4.375\frac{m}{s}$$

Calculation of Reynolds Number

$$Re_1 := \frac{\rho \cdot V_1 \cdot D_1}{\mu} \qquad Re_1 = 3.2 \times 10^4$$

$$Re_a := \frac{\rho \cdot V_a \cdot D_a}{\mu} \qquad Re_a = 4.384 \times 10^4$$

$$Re_2 := \frac{\rho \cdot V_2 \cdot D_2}{\mu} \qquad Re_2 = 8.379 \times 10^4$$

Calculation of friction factor and contraction coefficients

Guess

$f_1 := .026 \qquad f_a := .026 \qquad f_2 := .026$

Given

$$f_1 = \frac{.25}{\left[\log\left[\left(\frac{\varepsilon}{3.7 \cdot D_1}\right) + \frac{2.51}{Re_1 \cdot \sqrt{f_1}}\right]\right]^2}$$

$f_1 := \text{Find}(f_1)$

$f_1 = 0.031$

Given

$$f_a = \frac{.25}{\left[\log\left[\left(\frac{\varepsilon}{3.7 \cdot D_a}\right) + \frac{2.51}{Re_a \cdot \sqrt{f_a}}\right]\right]^2}$$

$f_a := \text{Find}(f_a)$

$f_a = 0.032$

Given

$$f_2 = \frac{.25}{\left[\log\left[\left(\frac{\varepsilon}{3.7 \cdot D_2}\right) + \frac{2.51}{Re_2 \cdot \sqrt{f_2}}\right]\right]^2}$$

$f_2 := \text{Find}(f_2)$

$f_2 = 0.038$

$$K_c := .42 \cdot \left[1 - \left(\frac{D_a}{D_1}\right)^2\right] \qquad K_c = 0.196$$

$K_n := .1$

Pressure drop at the inlet

$$\Delta P_{inlet} := \frac{\rho \cdot V_2^2}{2} + f_1 \cdot \left(\frac{L_1}{D_1}\right) \cdot \frac{\rho \cdot V_1^2}{2} + f_a \cdot \left(\frac{L_a}{D_a}\right) \cdot \frac{\rho \cdot V_a^2}{2} + f_2 \cdot \left(\frac{L_2}{D_2}\right) \cdot \frac{\rho \cdot V_2^2}{2} \ldots + K_c \cdot \frac{\rho \cdot V_a^2}{2} + K_n \cdot \frac{\rho \cdot V_a^2}{2} - \frac{\rho \cdot V_1^2}{2}$$

$\Delta P_{inlet} = 872.081 \text{KPa}$

$\Delta P_{inlet} = 126.485 \text{psi}$

APPENDIX B. Example of Calculation for the Pressure Drop at the Vortex Chamber Outlet

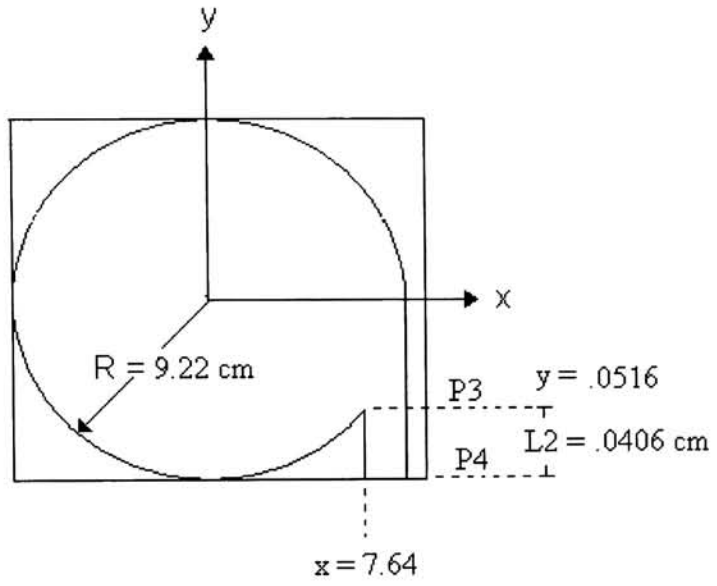

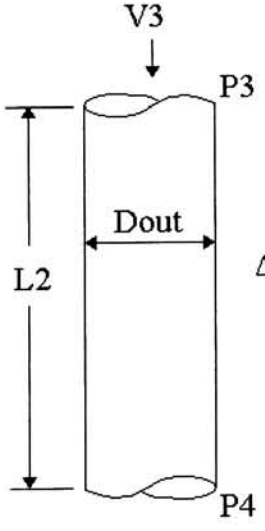

$$\Delta P = P3 - P4 = f\left(\frac{L2}{Dout}\right)\left(rho * \frac{V3^2}{2}\right)$$

Inputs:

Diameter: $D_{out} := 1.6cm$

Chamber Radius: $R := 10.16cm$

Length: L_2 varies with the chamber radius

$$L_2 := R - \sqrt{R^2 - (R - D_{out})^2}$$

$L_2 = 4.687cm$

LiBr-Water Properties

$\rho := 1670\frac{kg}{m^3}$

$\mu := .0029\frac{kg}{m \cdot s}$

Outet Velocity

$V_3 := 3\frac{m}{s}$

Pipe Roughness

$\varepsilon := .000046m$

Calculation of Reynolds Number

$$Re_{out} := \frac{\rho \cdot V_3 \cdot D_{out}}{\mu}$$

$Re_{out} = 2.764 \times 10^4$

Calculation of friction factor and contraction coefficients

Guess

$f_{out} := .026$

Given

$$f_{out} = \frac{.25}{\left[\log\left[\left(\frac{\varepsilon}{3.7 \cdot D_{out}}\right) + \frac{2.51}{Re_{out} \cdot \sqrt{f_{out}}}\right]\right]^2}$$

$f_{out} := \text{Find}(f_{out})$

$f_{out} = 0.03$

Pressure drop at the inlet

$$\Delta P_{outlet} := f_{out} \cdot \left(\frac{L_2}{D_{out}}\right) \cdot \frac{\rho \cdot V_3^{\,2}}{2}$$

$\Delta P_{outlet} = 0.661KPa$

$\Delta P_{outlet} = 0.096psi$

Example of Calculation of Surface Area:

Aspect Ratio: 1
Inlet Velocity: 30m/s
Inlet Location: Center

Surface Function:

The surface function from the vortex chamber is approximated from the results obtained from Flow 3D.

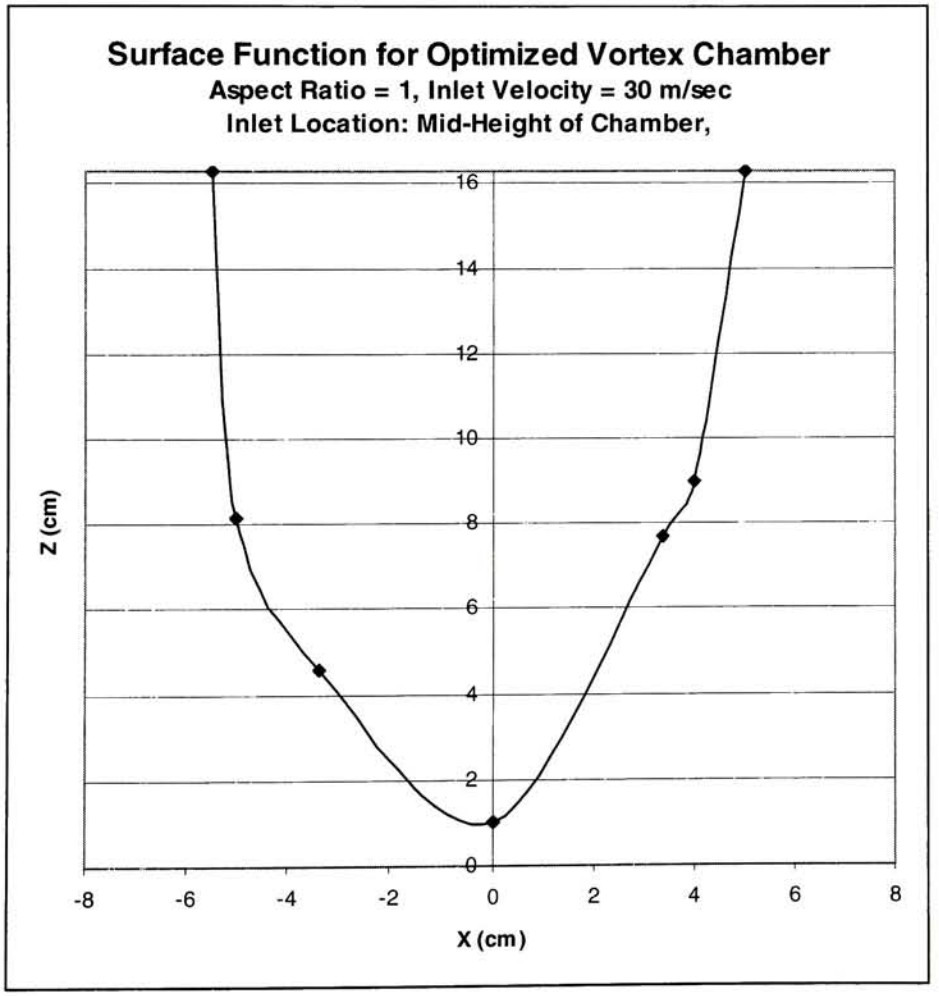

The surface function for the optimized vortex chamber is:

$$Z(x) = 0.012x^4 + 0.0003x^3 + 0.167x^2 + 0.5363x + 1.6008$$

Surface Area:

The solid of revolution technique was used to calculate the vortex chamber free surface area. To applied solid of revolution around the Z axis, the surface function has to be isolated for Z. This is not possible. The surface function was break and redefine in two functions new functions. One function corespond to the negative values of X and the other one corresponds to the positive values of X.

$f1(x) := .167 + 2.07 \cdot \ln(x)$

$f2(x) := -.0368 + 1.79 \cdot \ln(x)$

$$\text{SurfaceArea} := \pi \cdot \int_{1}^{16.3} f1(x) \cdot \sqrt{1 + \left(\frac{d}{dx} f1(x)\right)^2} + f2(x) \cdot \sqrt{1 + \left(\frac{d}{dx} f1(x)\right)^2}\, dx$$

$\text{SurfaceArea} = 391.072\ \text{cm}^2$

APPENDIX D. Procedure of Polynomial Regresion fit using Least Square method to determine the Pressure and Velocities as a function of Radius and Elevation

Enter the data as vectors. Each vector represents an independent variables or the dependent variable. In this case, the independent variables are Vortex Chamber Radius (R) and Vortex Chamber Elevetation. The dependent variable are pressure, tangential velocity and axial velocity. This example shows the procedure used to develop the pressure equation that best fit the pressure data. Same procedure is applied for the axial and tangential velocities.

Independent Variables		**Dependent Variable**
Radius (R)	Elevetion (Z)	Tangential Velocity Axial Velocity Pressure

- Create a real array, M. Each column in M represents data corresponding to one of the independent variables (Radius and Elevetion).

$$M := \text{augment}(R, Z)$$

- Create a real vector, Variable, that represents the data for the dependent variable

$$\text{Variable}$$

- A positive integer, n, specifying the degree of the polynomial function to which the data will be fit.

$$n := 4$$

- Define the regress function. The regress(M,Variable,n) returns a vector which interp uses to find the nth order polynomial curve that best fits the values for the dependent variable as a function of radius and elevation.

$$A := \text{regress}(M, \text{Variable}, n)$$

$A =$

	0
0	3
1	3
2	4
3	-0.0000589
4	0.000064
5	-0.0017831
6	0.0004116
7	0.0214497
8	-0.0021113
9	0.2103453
10	-0.3671523
11	0.0377152
12	-0.0002274
13	4.1345294
14	1.8836018
15	-0.6971749

- Use the interp function to define a two-variable polynomial function (Radius and Elevation) which uses the coefficients generated by regress

$$f(r,z) := \text{interp}\left[A, M, \text{Variable}, \begin{pmatrix} r \\ z \end{pmatrix}\right]$$

$r := 8.2279997$ cm

$z := 0.38636363$ cm

r and z radius and elevation of the vortex chamber and are used to define position within the chamber

$f(r,z) = 15.081$ KPa

- The program below is used to extract the specific coefficients associated with individual monomial terms in the model function.

A polynomial of nvar independent variables of degree deg has a number of terms given by the function Nterms:

$$\text{Nterms}(nvar, deg) := \frac{(nvar + deg)!}{deg! \cdot nvar!}$$

The number of variables of the polynomial is: $Nvars := \text{cols}(M)$

The number of data points is: $Ndata := \text{rows}(M)$

The degree of the fitting function: $deg := n$

Here are the two programs that extract the coefficients.

```
Step(v, Nvar, deg) := | for i ∈ 0..deg    if Nvar = 1
                      |   v_{i,0} ← v_{i,0} + i
                      | for i ∈ 0..Nvar − 1  if deg = 1
                      |   v_{i,i} ← v_{i,i} + 1
                      | otherwise
                      |   | inc ← Nterms(Nvar, deg − 1)
                      |   | for i ∈ 0..inc − 1
                      |   |   v_{i,Nvar−1} ← v_{i,Nvar−1} + 1
                      |   | v ← stack(Step(submatrix(v, 0, inc − 1, 0, cols(v) − 1), Nvar, deg − 1), Step(submatrix(v, inc, rows(v) − 1, 0, cols(v) − 1), Nvar − 1, deg))
                      | v
```

$$\text{COrder}(\text{Nvar},\text{deg}) := \left| \begin{array}{l} v_{\text{Nterms}(\text{Nvar},\text{deg})-1,\ \text{Nvar}-1} \leftarrow 0 \\ \text{Step}(v,\text{Nvar},\text{deg}) \end{array} \right.$$

Call the program $\text{COrder}(\text{Nvars},\text{deg})$ using the definitions above, and strip the vector, A, of its first three terms.

$I := \text{COrder}(\text{Nvars},\text{deg})$ $\quad$ $\text{coeffs} := \text{submatrix}(A,3,\text{rows}(A)-1,0,0)$

$I =$

	0	1
0	1	3
1	0	4
2	0	3
3	0	2
4	1	2
5	2	2
6	0	1
7	1	1
8	2	1
9	3	1
10	0	0
11	1	0
12	2	0
13	3	0
14	4	0

coeffs =

	0
0	-0.000058853692251
1	0.00006404836485
2	-0.001783086836817
3	0.00041158316267
4	0.021449711076713
5	-0.002111312165314
6	0.210345309725764
7	-0.36715229601116
8	0.037715210907945
9	-0.000227449693703
10	4.1345294358026
11	1.88360179131188
12	-0.697174935718835
13	0.152750647383632
14	-0.009228674558432

The first column of I gives the power of the R term of each monomial corresponding to the power of the Z term given in the second column. The rows of I and coeffs correspond. Therefore, we can define the model function using the following summation.

$$F(r,z) := \sum_{i=0}^{\text{last}(\text{coeffs})} \text{coeffs}_i \cdot r^{I_{i,0}} \cdot z^{I_{i,1}}$$

Comparing:

$F(r,z) = 15.081$ KPa $\qquad$ $f(r,z) = 15.081$ KPa

$r := 0, .1 .. 8$

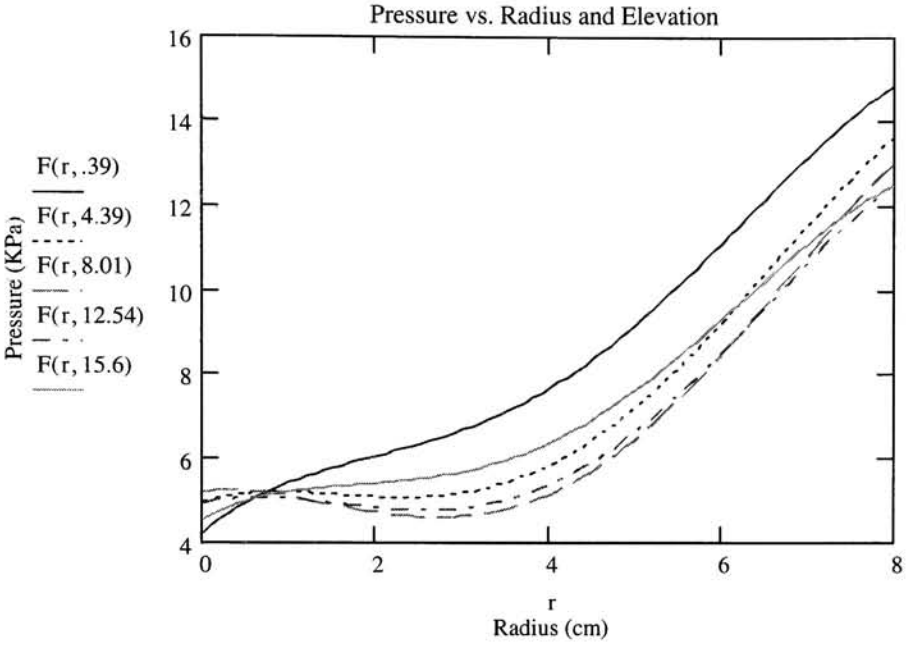

- Calculation of the Correlation coefficient squared (R^2).

Number of elements in vector Variable: $L := \text{length}(\text{Variable})$ $L = 184$

Mean of the dependent variable (Variable):

$$\text{Variable}_{avg} := \frac{\sum_{j=0}^{L-1} \left(\text{Variable}_j\right)}{L} \qquad \text{Variable}_{avg} = 9.856$$

The residual sum of the squares: $Sr := \sum_{j=0}^{L-1} \left(\text{Variable}_j - F\left(R_j, Z_j\right)\right)^2$ $Sr = 7.9388$

The total sum of the squares:

$$St := \sum_{j=0}^{L-1} \left(\text{Variable}_j - \text{Variable}_{avg}\right)^2 \qquad St = 1.923 \times 10^3$$

$$Rsquared := 1 - \frac{Sr}{St} \qquad Rsquared = 0.9959$$

APPENDIX E. Equilibrium Chart for Aqueous Lithium Bromide Solutions

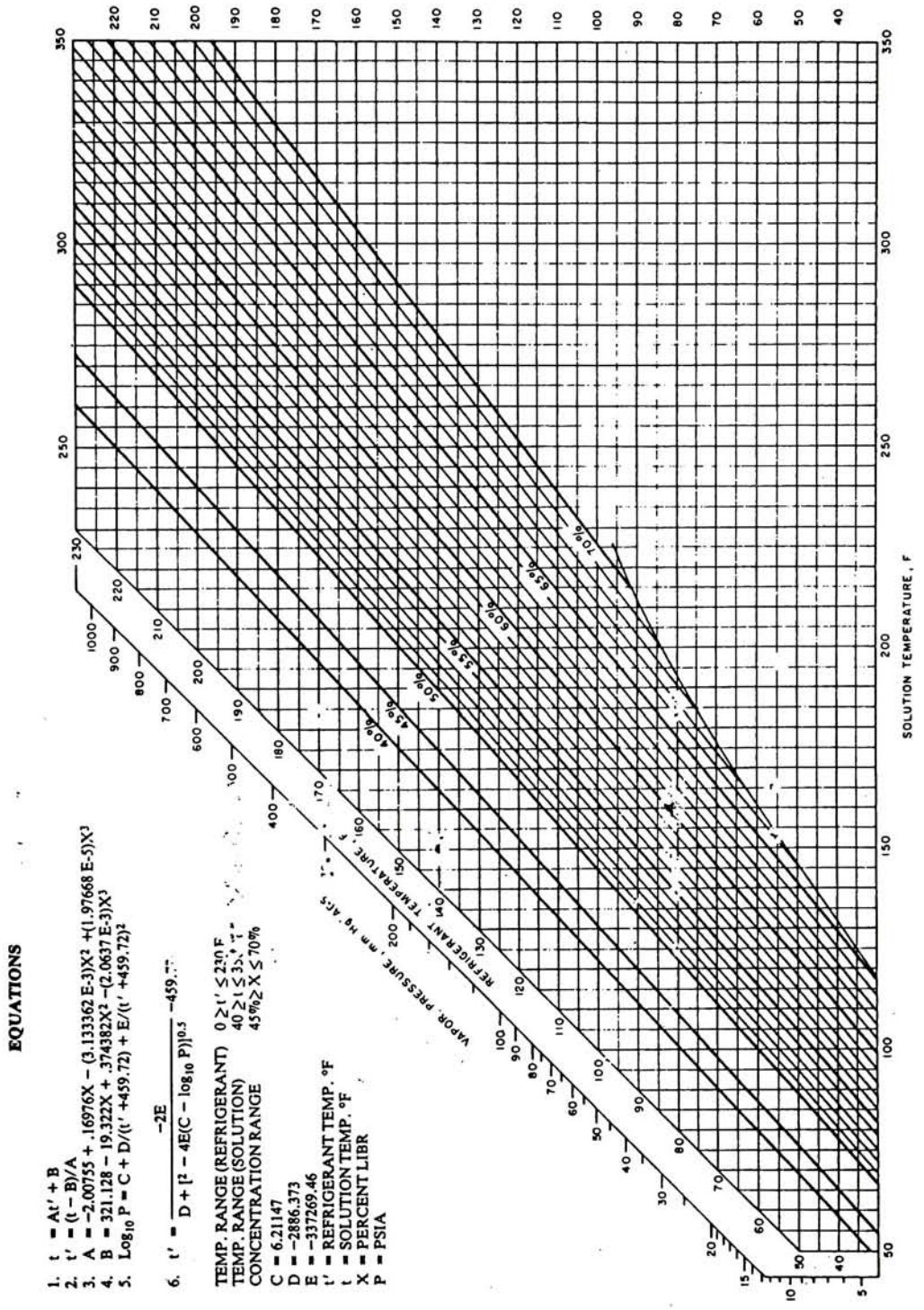

Figure E.1 Equilibrium Chart for Aqueous Lithium Bromide Solutions

APPENDIX F. Specific Gravity of Aqueous Solutions of Lithium Bromide

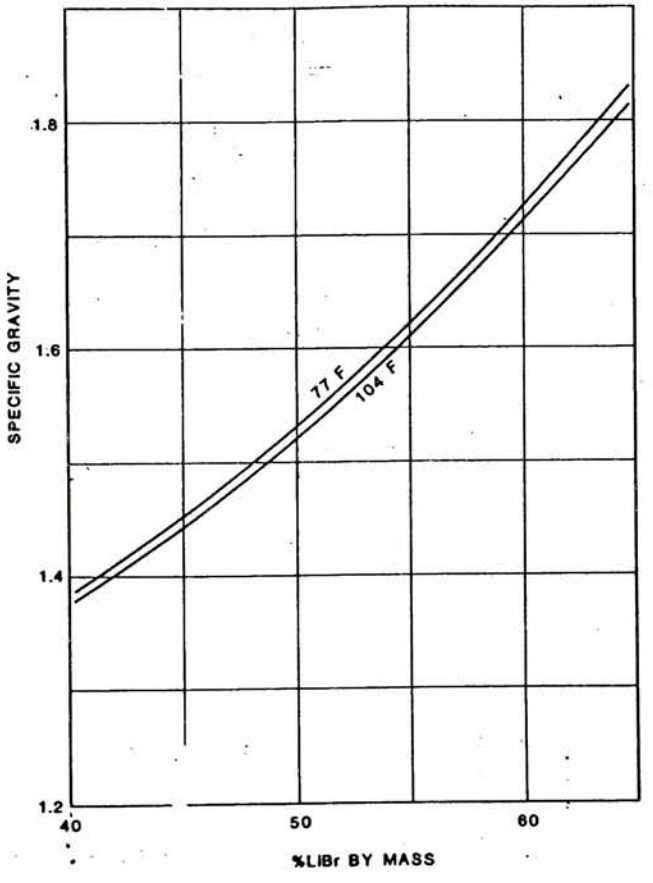

Figure F.1 Specific Gravity of Aqueous Solutions of Lithium Bromide

APPENDIX G. Viscosities of Aqueous Solutions of Lithium Bromide

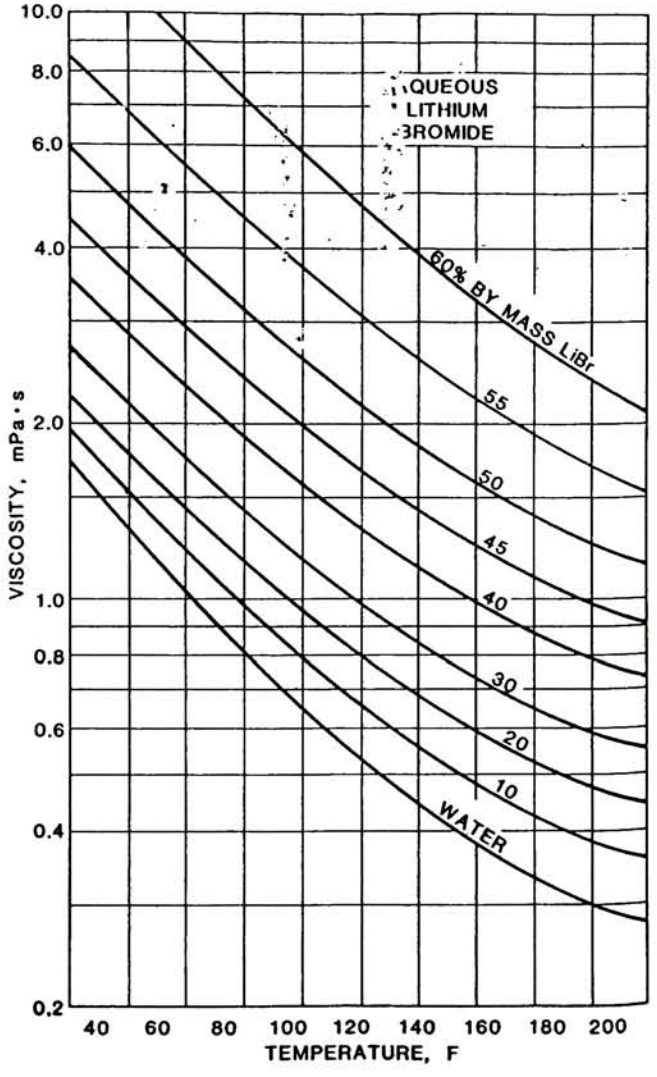

Figure G.1 Viscosities of Aqueous Solutions of Lithium Bromide

APPENDIX H. Specific Heat of Aqueous Lithium Bromide Solutions

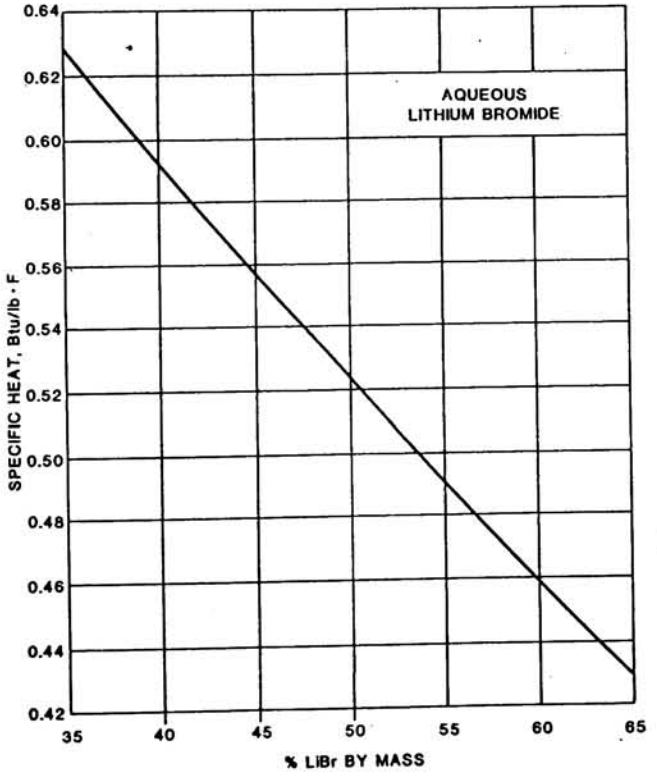

Figure H.1 Specific Heat of Aqueous Lithium Bromide Solutions

APPENDIX I. Enthalpy-Concentration Diagram for Aqueous Lithium Bromide Solutions

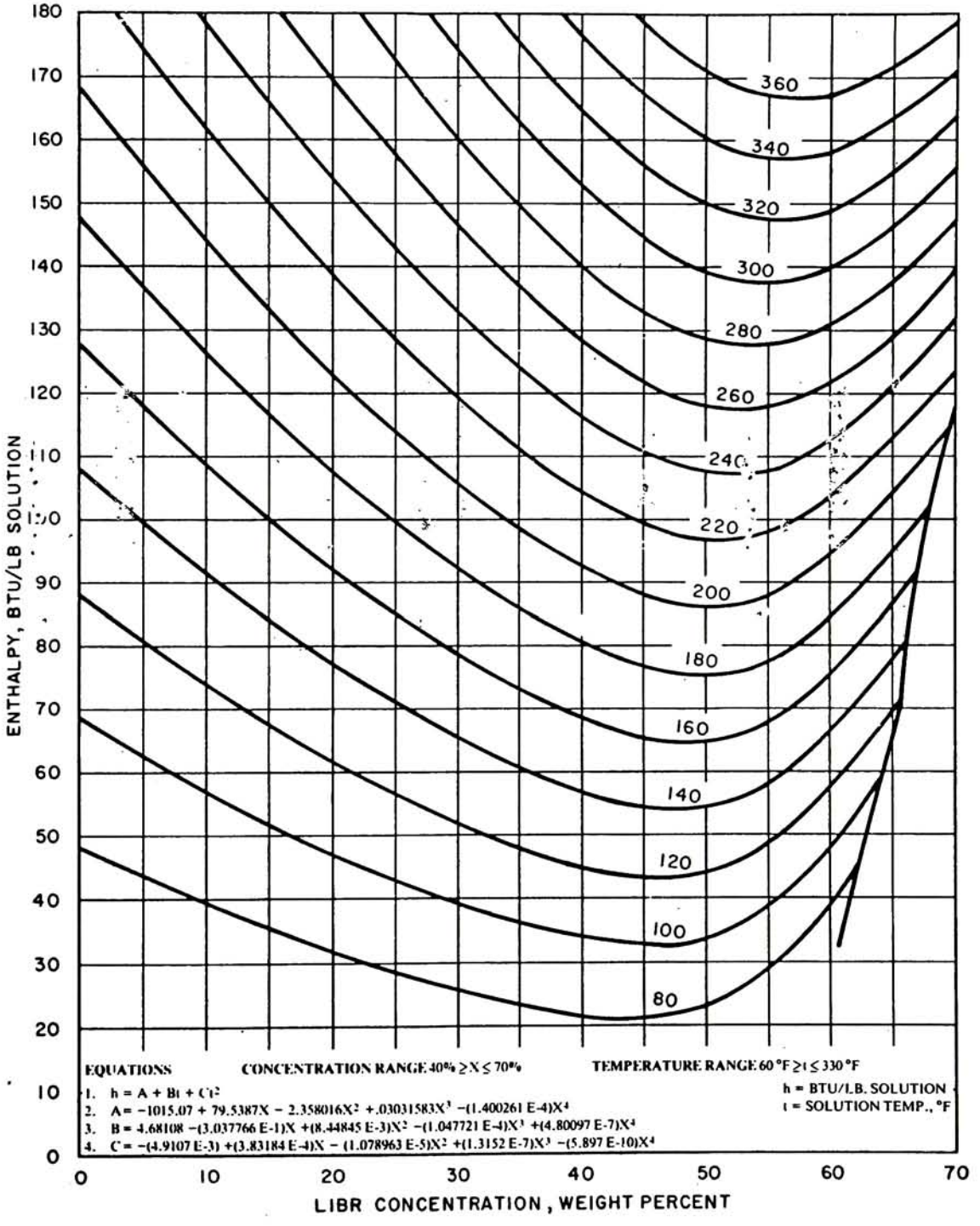

Figure I.1 Enthalpy-Concentration Diagram for Aqueous Lithium Bromide Solutions

APPENDIX J. The Moody Diagram for Friction Factor

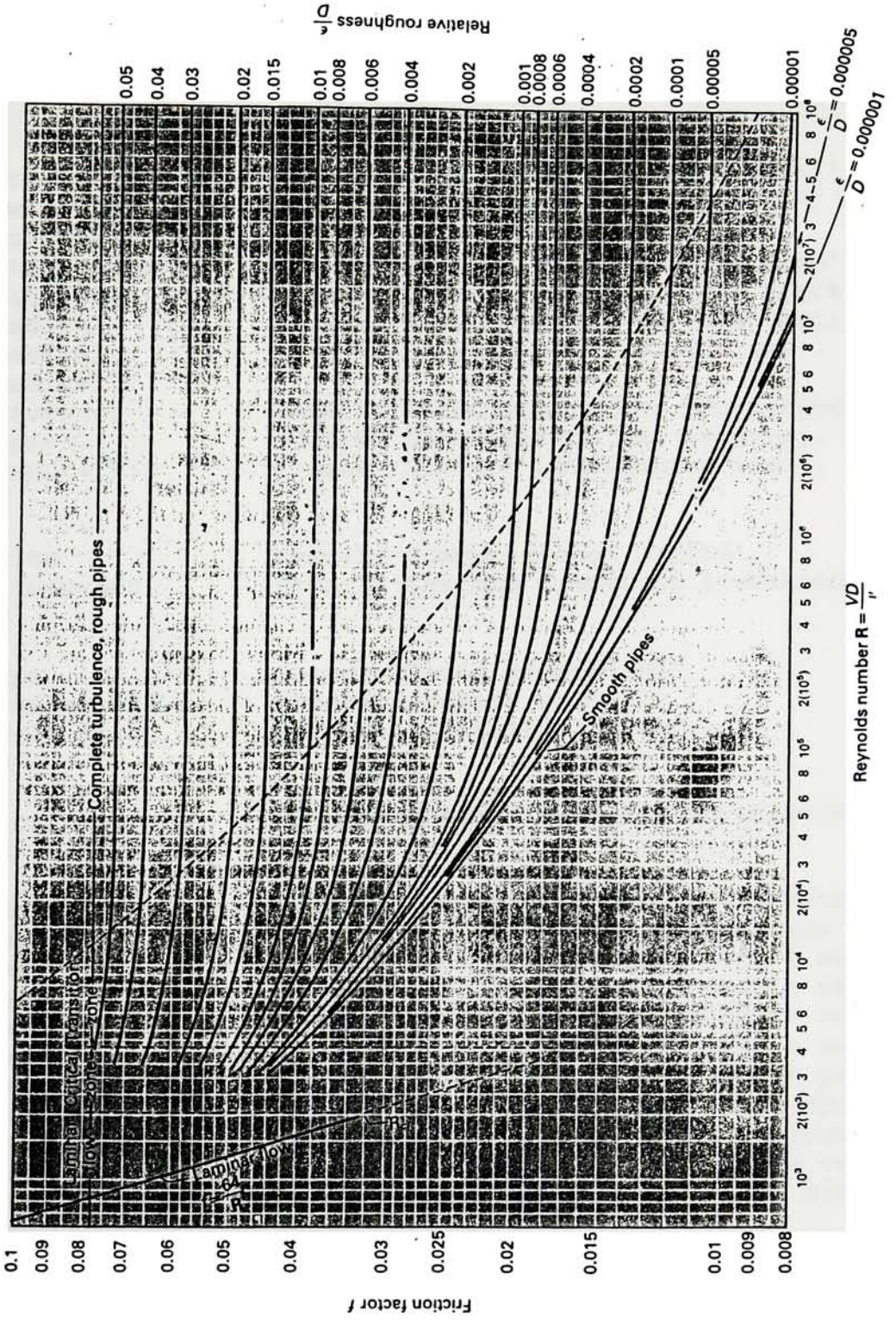

Figure J.1 The Moody Diagram for Friction Factor

APPENDIX K. Example of FLOW-3D Input file

```
Title Lower Chamber

$xput                  remark='Computational parameters and general
                       remark='description of problem',
                       remark='units are CGS',
   itb=1,              remark='Turn on Free Surface model',
   twfin=30.,          remark='Finishing time (seconds)',
   gz=-981.,           remark='Gravity  (cm/s^2)',
   dtmin=1.0e-8,       remark='Minimum permited time step',
   pltdt=2.5,          remark='Time interval between plots',
   iadix=1,            remark='Solve implicit method (ADI)
   iadiy=1,            remark='in x, y and z directions',
   iadiz=1,
   ifvis=4,            remark='Turbulence model RNG activated',
   lpr=3,              remark='Debug prints and outputs',
   trest=15.,          remark='Restart calculation time',
$end

$limits                remark='Computational limits',
   itmax=500,          remark='Maximum number of iterations',
$end

$props                 remark='Fluid properties',
   rhof=1.670,         remark='density gm/cm^3',
   mu1=.0145,          remark='viscosity  gm/cm/s',
$end

$scalar                remark='Scalar Transport Parameters',
$end

$bcdata                remark='Boundary Condition Parameters',
   pbctyp=0.,          remark='Static pressure boundaries',
   wl=2,               remark='BC's at minimum x side = wall',
   wr=2,               remark='BC's at maximum x side = wall',
   wb=2,               remark='BC's at minimum z side = wall',
   wt=2,               remark='BC's at minimum z side = wall',
   wf=5,               remark='BC's at minimum y side = pressure',
   pbc(3)=45000.,      remark='Pressure boundary = 4.5 KPa',
   fbc(3)=0.,          remark='Fluid fraction at mesh boundary',
   wbk=6,              remark='BC's at maximum y side = velocity',
   vbc(4)=-3000.,      remark='velocity boundary = -30 m/sec',
$end

$mesh                  remark='Mesh Generator',
 nxcelt=23,            remark='Number of cells in x direction',
  px(1)=-10.5,       px(2)=-10.16,    px(3)=8.54,
  px(4)=9.652,       px(5)=10.16,     px(6)=10.5,
```

```
  nxcell(3)=4,     nxcell(4)=3,
 nycelt=20,          remark='Number of cells in y direction',
  py(1)=-10.5,     py(2)=10.5,
 nzcelt=20,          remark='Number of cells in z direction',
  pz(1)=0.,        pz(2)=.9779,    pz(3)=9.652,
  pz(4)=10.16,     pz(5)=10.3810,
  nzcell(1)=3,     nzcell(3)=3,
$end

$obs                remark='Obstacle Setup',
 avrck=-2.1,
 nobs=1,            remark='Number of obstacle',
 remark='Vortex Chamber',
  ral(1)=10.16,     remark='Vortex Chamber Radius',
 remark='Top outlet',
  iob(2)=1,
  ral(2)=1.35,      remark='Top outlet radius',
  zl(2)=10.16,      remark='Top outlet location',
 Remark='Inlet D=.191 in',
  iob(3)=1,
  ioh(3)=0,
  rah(3)=.254,      remark='Inlet radius',
  rotx(3)=-90.,     remark='Rotation around x axis',
  zl(3)=0.,         remark='Location of inlet',
  trnz(3)=9.9066,
  trnx(3)=9.9066,
 remark='Bottom outlet',
  iob(4)=1,
  ioh(4)=0,
  rah(4)=.8,        remark='Bottom outlet radius'
  rotx(4)=90.,      remark='Rotation around x axis',
  zl(4)=0.,         remark='Location of bottom outlet',
  trnx(4)=9.36,
  trnz(4)=.8,

$end

$fl                 remark='Initial Fluid Conditions',
                    remark='Solution LiBr-water',
   presi=60000.,    remark='Initial fluid pressure',
   pvoid=50000.,    remark='Void pressure',
   nfls=3,          remark='Number of fluid regions',
   fral(1)=3.5,     remark='Creation of fluid regions',
   ifdis(2)=4,
   fcy(2)=98.45
   frah(2)=10.16,
   ifdis(3)=5,
   fcx(3)=-98.45,
   frah(3)=10.16,
$end
```

```
$bf             remark='Baffle regions',
$end

$temp           remark='Inital fluid and solid temperatures
$end

$motn           remark='Non-inertial referance frame',
$end

$grafic         remark='Graphic Outpur',
 nvplts=1,      contpv(1)='p',   yv1(1)=0.0,     yv2(1)=0.0
 nsplts=0,      contps(1)='f',   clrtps(1)='p',
 xloc(1)=0.0,   yloc(1)=0.0,     zloc(1)=0.0,
 nwinf=1,
$end

$parts
$end
```

APPENDIX K. Data used for Development of Pressure and Velocity Equations

Position		Velocity Components (cm/sec)			Pressure
X (cm)	Z (cm)	U	V	W	P (KPa)
8.04747	0.36000	-0.00398	0.00000	-0.00841	15.40603
8.03040	0.36000	0.29684	179.67958	-9.20000	15.41444
8.01333	0.36000	0.89210	217.25313	-15.09022	15.40844
7.99627	0.36000	1.50935	229.39745	-17.45909	15.39985
7.97920	0.36000	2.19758	231.89486	-18.97431	15.38745
7.96213	0.36000	2.94792	234.30915	-20.04642	15.37022
7.94507	0.36000	3.74625	236.64468	-20.86536	15.34733
7.92800	0.36000	4.57868	239.02170	-21.54133	15.31818
7.91093	0.36000	5.43176	241.37239	-22.14803	15.28237
7.89387	0.36000	6.30075	243.22621	-22.76205	15.24044
7.87680	0.36000	7.18773	244.88466	-23.35153	15.19231
7.85973	0.36000	8.09198	246.35438	-23.87233	15.13773
7.84267	0.36000	9.01759	247.64037	-24.30367	15.07310
7.82560	0.36000	9.96951	248.73650	-24.64610	14.95343
7.80853	0.36000	10.89311	249.69373	-24.90347	14.74228
7.77718	0.36000	12.57378	251.20190	-25.22881	14.59843
7.69538	0.36000	17.05619	253.84152	-25.45323	14.44171
7.54361	0.36000	25.39429	256.70798	-25.11927	14.00837
7.32655	0.36000	37.15272	258.31525	-22.93992	13.43919
7.04890	0.36000	51.35735	259.18262	-20.08493	12.80591
6.71533	0.36000	66.41724	258.83936	-16.30278	12.12103
6.33054	0.36000	80.49100	257.71216	-11.66422	11.42165
5.89921	0.36000	91.52393	256.12296	-6.40408	10.74459
5.42602	0.36000	96.98306	254.10269	-0.44794	10.11475
4.91567	0.36000	94.21323	251.78526	5.96187	9.52730
4.37283	0.36000	81.61928	248.50345	12.23714	8.93642
3.80220	0.36000	59.00536	240.20343	18.30449	8.26749
3.20846	0.36000	29.04128	218.67445	21.84387	7.48435
2.59630	0.36000	-5.22882	176.15012	18.40770	6.67375
1.97040	0.36000	-35.09212	119.72822	11.11931	5.96264
1.33544	0.36000	-49.97903	48.55722	12.28356	5.59757
0.69613	0.36000	-55.07414	12.21505	14.30663	5.27244
0.05714	0.36000	-63.18361	-0.03307	11.12482	4.66189
8.04747	2.35817	0.00023	0.00000	-0.75734	13.85366
8.03040	2.35817	0.12170	193.47173	-25.36715	13.85319
8.01333	2.35817	0.33046	250.39718	-38.60098	13.83758
7.99627	2.35817	0.50632	269.32523	-42.68640	13.81838
7.97920	2.35817	0.68712	272.69556	-45.42905	13.79624
7.96213	2.35817	0.87419	275.80551	-47.47395	13.77140
7.94507	2.35817	1.06232	278.73361	-49.12328	13.74401
7.92800	2.35817	1.24372	281.65717	-50.55753	13.71424
7.91093	2.35817	1.40926	284.50626	-51.89892	13.68225
7.89387	2.35817	1.55533	286.74582	-53.27748	13.64951

Position		Velocity Components (cm/sec)			Pressure
X (cm)	Z (cm)	U	V	W	P (KPa)
7.87680	2.35817	1.68392	288.74435	-54.58481	13.61626
7.85973	2.35817	1.79637	290.51096	-55.72075	13.58254
7.84267	2.35817	1.89388	292.05356	-56.65714	13.54838
7.82560	2.35817	1.97805	293.38306	-57.40971	13.51252
7.80853	2.35817	2.05002	294.51025	-58.00875	13.47331
7.77718	2.35817	2.14729	296.21884	-58.88306	13.39811
7.69538	2.35817	2.28917	298.94418	-60.16571	13.20905
7.54361	2.35817	2.40553	300.63528	-60.85123	12.88450
7.32655	2.35817	2.45203	299.17239	-58.53666	12.44602
7.04890	2.35817	2.46641	293.88864	-53.08281	11.88359
6.71533	2.35817	2.46964	284.50296	-43.40587	11.20145
6.33054	2.35817	2.35523	271.25525	-29.37482	10.43816
5.89921	2.35817	1.90085	255.50717	-11.23873	9.64186
5.42602	2.35817	0.98731	238.78333	9.98234	8.84423
4.91567	2.35817	-0.41799	222.45128	30.80224	8.06594
4.37283	2.35817	-2.49347	205.64096	46.62645	7.29933
3.80220	2.35817	-5.47860	185.28143	52.94898	6.51624
3.20846	2.35817	-9.26552	159.78543	49.24340	5.69685
2.59630	2.35817	-13.59405	130.86194	39.64993	4.94883
1.97040	2.35817	-22.73116	99.48251	29.96234	4.49950
1.33544	2.35817	-40.99761	65.12968	25.54269	5.16435
0.69613	2.35817	-52.46837	49.48513	8.02449	5.10036
0.05714	2.35817	-26.26170	0.00000	-11.51655	5.02036
8.04747	3.97140	-0.00023	0.00000	-0.45994	13.51011
8.03040	3.97140	0.03042	229.14050	-18.12073	13.51002
8.01333	3.97140	0.08663	267.31519	-27.93675	13.49431
7.99627	3.97140	0.13679	279.24490	-30.80030	13.47437
7.97920	3.97140	0.18641	283.69128	-32.83382	13.45119
7.96213	3.97140	0.23403	287.49728	-34.40926	13.42513
7.94507	3.97140	0.27492	290.90494	-35.71787	13.39639
7.92800	3.97140	0.30224	294.18143	-36.87791	13.36518
7.91093	3.97140	0.30778	297.27768	-37.96890	13.33170
7.89387	3.97140	0.28851	299.67245	-39.08092	13.29757
7.87680	3.97140	0.24681	301.78439	-40.13044	13.26303
7.85973	3.97140	0.18478	303.62598	-41.04215	13.22810
7.84267	3.97140	0.10436	305.20947	-41.79812	13.19281
7.82560	3.97140	0.00782	306.55093	-42.41391	13.15691
7.80853	3.97140	-0.10247	307.66611	-42.91467	13.12000
7.77718	3.97140	-0.34136	309.31604	-43.66718	13.05070
7.69538	3.97140	-1.07898	311.74512	-44.87751	12.86573
7.54361	3.97140	-2.59859	312.44388	-45.61785	12.51126
7.32655	3.97140	-4.84396	308.89691	-43.93824	11.99625
7.04890	3.97140	-7.57256	299.92090	-39.34535	11.34882
6.71533	3.97140	-10.40578	284.96347	-30.73272	10.61000
6.33054	3.97140	-12.89396	264.15366	-17.86681	9.82384
5.89921	3.97140	-14.55701	239.65439	-1.37877	9.02907
5.42602	3.97140	-14.92205	214.44014	16.82136	8.25969
4.91567	3.97140	-13.92576	191.71408	33.91886	7.53985
4.37283	3.97140	-11.97295	171.50011	46.41440	6.84434
3.80220	3.97140	-9.53873	151.94409	50.97339	6.13087

Position		Velocity Components (cm/sec)			Pressure
X (cm)	Z (cm)	U	V	W	P (KPa)
3.20846	3.97140	-6.91295	121.87097	46.97762	5.43035
2.59630	3.97140	-4.05626	42.58958	37.54044	4.81692
1.97040	3.97140	0.00000	0.00000	0.00000	5.02036
1.33544	3.97140	0.00000	0.00000	0.00000	5.02036
0.69613	3.97140	0.00000	0.00000	0.00000	5.02036
0.05714	3.97140	0.00000	0.00000	0.00000	5.02036
8.04747	6.69309	0.00010	0.00000	-0.20746	13.13055
8.03040	6.69309	0.13220	200.39466	-5.50800	13.13053
8.01333	6.69309	0.34729	260.57007	-8.23289	13.11446
7.99627	6.69309	0.51645	279.88071	-9.05681	13.09516
7.97920	6.69309	0.69443	283.10773	-9.59783	13.07315
7.96213	6.69309	0.88154	286.20081	-9.99733	13.04867
7.94507	6.69309	1.07157	289.18381	-10.31902	13.02183
7.92800	6.69309	1.25584	292.21246	-10.60075	12.99280
7.91093	6.69309	1.42437	295.18295	-10.86833	12.96177
7.89387	6.69309	1.57225	297.51990	-11.14990	12.93029
7.87680	6.69309	1.70053	299.62143	-11.42331	12.89867
7.85973	6.69309	1.81040	301.49185	-11.66659	12.86693
7.84267	6.69309	1.90272	303.13516	-11.87268	12.83512
7.82560	6.69309	1.97868	304.55988	-12.04396	12.80354
7.80853	6.69309	2.04007	305.77548	-12.18602	12.77268
7.77718	6.69309	2.11293	307.63107	-12.40387	12.71713
7.69538	6.69309	2.15713	310.64664	-12.77846	12.57393
7.54361	6.69309	1.99666	312.40414	-13.10873	12.31408
7.32655	6.69309	1.52045	310.13098	-12.89945	11.67467
7.04890	6.69309	0.86064	302.08844	-11.75445	10.99564
6.71533	6.69309	0.41706	286.91458	-9.04452	10.29536
6.33054	6.69309	0.76057	263.44427	-4.20213	9.42094
5.89921	6.69309	2.42645	232.81210	2.94819	8.38437
5.42602	6.69309	5.67498	198.83862	11.98602	7.44457
4.91567	6.69309	10.22094	166.13585	21.49335	6.52882
4.37283	6.69309	15.23435	138.84274	29.22024	5.57624
3.80220	6.69309	19.85152	107.75518	33.04212	5.22185
3.20846	6.69309	23.96929	71.67766	32.33163	5.12036
2.59630	6.69309	0.00000	0.00000	0.00000	5.02036
1.97040	6.69309	0.00000	0.00000	0.00000	5.02036
1.33544	6.69309	0.00000	0.00000	0.00000	5.02036
0.69613	6.69309	0.00000	0.00000	0.00000	5.02036
0.05714	6.69309	0.00000	0.00000	0.00000	5.02036
8.04747	7.92750	-0.01125	0.00000	0.04348	13.01590
8.03040	7.92750	0.06134	237.38666	-1.14912	13.01045
8.01333	7.92750	0.18765	270.89984	-1.97108	13.04675
7.99627	7.92750	0.27639	281.48355	-2.25776	13.01244
7.97920	7.92750	0.37598	284.88519	-2.47181	12.99620
7.96213	7.92750	0.48770	288.09164	-2.64735	12.99074
7.94507	7.92750	0.60595	291.15466	-2.80011	12.98628
7.92800	7.92750	0.72238	294.24445	-2.93992	12.98295
7.91093	7.92750	0.82707	297.25961	-3.07388	12.97950
7.89387	7.92750	0.91526	299.62823	-3.21093	12.97610
7.87680	7.92750	0.98804	301.75800	-3.34477	12.96492

Position		Velocity Components (cm/sec)			Pressure
X (cm)	Z (cm)	U	V	W	P (KPa)
7.85973	7.92750	1.04701	303.65323	-3.46842	12.93565
7.84267	7.92750	1.08285	305.31830	-3.57949	12.90483
7.82560	7.92750	1.09866	306.76276	-3.68080	12.87983
7.80853	7.92750	1.12898	307.99719	-3.77306	12.82040
7.77718	7.92750	1.16188	309.88889	-3.91884	12.79290
7.69538	7.92750	1.11003	313.02472	-4.22292	12.54670
7.54361	7.92750	0.89544	315.15350	-4.65717	12.29810
7.32655	7.92750	0.52372	313.70493	-5.12009	11.64230
7.04890	7.92750	0.12704	307.18417	-5.53126	11.02570
6.71533	7.92750	0.03909	294.34753	-5.83296	10.19691
6.33054	7.92750	0.88154	274.12326	-5.92607	9.38640
5.89921	7.92750	3.63149	247.63092	-5.53421	8.13391
5.42602	7.92750	9.41892	217.58690	-3.85484	6.77280
4.91567	7.92750	18.58979	186.54158	0.57112	5.67090
4.37283	7.92750	29.42391	157.66016	9.22845	5.02036
3.80220	7.92750	38.01573	133.27370	21.27495	5.02036
3.20846	7.92750	40.42607	46.52360	32.03403	5.02036
2.59630	7.92750	0.00000	0.00000	0.00000	5.02036
1.97040	7.92750	0.00000	0.00000	0.00000	5.02036
1.33544	7.92750	0.00000	0.00000	0.00000	5.02036
0.69613	7.92750	0.00000	0.00000	0.00000	5.02036
0.05714	7.92750	0.00000	0.00000	0.00000	5.02036
8.04747	9.89888	0.00000	0.00000	-0.27265	12.87951
8.03040	9.89888	0.08889	221.90598	0.48614	12.87939
8.01333	9.89888	0.20606	268.82992	1.67875	12.86205
7.99627	9.89888	0.26012	284.45966	2.20619	12.84103
7.97920	9.89888	0.31301	287.66574	2.67638	12.81696
7.96213	9.89888	0.36696	290.67957	3.11272	12.79009
7.94507	9.89888	0.41719	293.55151	3.52548	12.76056
7.92800	9.89888	0.45612	296.45102	3.92058	12.72855
7.91093	9.89888	0.47468	299.29102	4.30044	12.69424
7.89387	9.89888	0.46907	301.49591	4.67623	12.65921
7.87680	9.89888	0.44122	303.45471	5.03777	12.62372
7.85973	9.89888	0.39304	305.17300	5.37127	12.58778
7.84267	9.89888	0.32630	306.65668	5.67202	12.55142
7.82560	9.89888	0.24311	307.91675	5.94185	12.51411
7.80853	9.89888	0.14570	308.96524	6.18490	12.47505
7.77718	9.89888	-0.07145	310.51404	6.59016	12.40011
7.69538	9.89888	-0.76515	312.75549	7.43102	12.19443
7.54361	9.89888	-2.23372	313.13745	8.31633	11.79292
7.32655	9.89888	-4.45321	308.91763	8.27716	11.21543
7.04890	9.89888	-7.18083	298.45920	6.54735	10.50760
6.71533	9.89888	-9.96319	280.91879	2.30212	9.71420
6.33054	9.89888	-12.19730	256.71506	-4.68342	8.82469
5.89921	9.89888	-13.21493	230.05063	-13.58667	7.68382
5.42602	9.89888	-12.05753	206.55183	-23.06809	6.66589
4.91567	9.89888	-6.54599	190.45232	-30.83245	5.32036
4.37283	9.89888	0.00000	0.00000	0.00000	5.02036
3.80220	9.89888	0.00000	0.00000	0.00000	5.02036
3.20846	9.89888	0.00000	0.00000	0.00000	5.02036

Position		Velocity Components (cm/sec)			Pressure
X (cm)	Z (cm)	U	V	W	P (KPa)
2.59630	9.89888	0.00000	0.00000	0.00000	5.02036
1.97040	9.89888	0.00000	0.00000	0.00000	5.02036
1.33544	9.89888	0.00000	0.00000	0.00000	5.02036
0.69613	9.89888	0.00000	0.00000	0.00000	5.02036
0.05714	9.89888	0.00000	0.00000	0.00000	5.02036
8.04747	12.54200	-0.00038	0.00000	1.29546	12.64221
8.03040	12.54200	0.02552	225.41760	27.38977	12.64188
8.01333	12.54200	0.05206	265.96250	40.09207	12.62476
7.99627	12.54200	0.04695	285.73816	43.58210	12.60336
7.97920	12.54200	0.03359	290.11395	45.89184	12.57859
7.96213	12.54200	0.01398	293.86288	47.57153	12.55084
7.94507	12.54200	-0.01540	297.20569	48.89511	12.52032
7.92800	12.54200	-0.06070	300.40649	50.03063	12.48724
7.91093	12.54200	-0.12958	303.42682	51.09359	12.45180
7.89387	12.54200	-0.22421	305.75272	52.19988	12.41565
7.87680	12.54200	-0.34147	307.79297	53.23946	12.37901
7.85973	12.54200	-0.47905	309.56085	54.12098	12.34191
7.84267	12.54200	-0.63461	311.06940	54.82419	12.30436
7.82560	12.54200	-0.80544	312.33539	55.36831	12.26564
7.80853	12.54200	-0.98944	313.37555	55.78288	12.22477
7.77718	12.54200	-1.36219	314.89105	56.35822	12.21724
7.69538	12.54200	-2.43053	317.00818	57.03823	12.04157
7.54361	12.54200	-4.50060	317.36987	56.80392	11.64923
7.32655	12.54200	-7.40255	313.78424	53.64320	11.17729
7.04890	12.54200	-10.78199	305.50870	47.02897	10.54293
6.71533	12.54200	-14.20020	292.40909	35.76767	9.77301
6.33054	12.54200	-17.26894	274.97247	19.46310	8.84391
5.89921	12.54200	-19.77679	254.99539	-1.60481	8.01884
5.42602	12.54200	-21.70661	234.67999	-25.46404	7.17989
4.91567	12.54200	-23.86886	217.39908	-48.35497	6.35650
4.37283	12.54200	-28.34200	205.36313	-64.93797	5.38293
3.80220	12.54200	-36.13580	200.49071	-71.25113	5.02036
3.20846	12.54200	0.00000	0.00000	0.00000	5.02036
2.59630	12.54200	0.00000	0.00000	0.00000	5.02036
1.97040	12.54200	0.00000	0.00000	0.00000	5.02036
1.33544	12.54200	0.00000	0.00000	0.00000	5.02036
0.69613	12.54200	0.00000	0.00000	0.00000	5.02036
0.05714	12.54200	0.00000	0.00000	0.00000	5.02036